AN ABSTRACT OF THE DISSERTATION OF

Stephany S. Chacon for the degree of Doctor of Philosophy in Soil Science presented on December 3, 2018.

Title: Mineral Surfaces As Agents of Environmental Proteolysis: Mechanisms and Controls

Abstract approved: _____

Markus Kleber

The bottleneck in the turnover of soil organic matter (SOM) is the conversion of large molecular compounds into smaller compounds that can be transported through a cell membrane of a microbe for processing. Once inside the cell, organic compounds can be converted into biomass or be respired. The microbial depolymerization of SOM by microbes is catalyzed by extracellular enzymes. SOM is intimately associated with the mineral matrix, which can affect turnover by interfering with the accessibility of OM or the function of extracellular enzymes. Interactions with the mineral matrix have been primarily associated as a protective mechanism of SOM against microbial degradation. But it has been observed that soil minerals can participate in the chemical degradation of organic compounds This dissertation attempts to address whether soil minerals have the capacity to chemically modify or break down proteins in order to infer whether the mineral ma-

trix has the capacity to alter extracellular enzymes in soil. The following research aims to identify what conditions are conducive to protein modifications by mineral interactions. The first research chapter explored how mineral surfaces can switch from sorbents to reactants towards proteins under a gradient of increasing energy similar to fireline intensities experienced in wildfires. The second research chapter observed the mechanisms responsible for proteolysis and the locations of cleavage by minerals. The last research chapter revealed that inserting an amino acid trimer to a model protein was sufficient in altering protein-mineral interactions such as adsorption and fragmentation. Together this work provides evidence to expand the role of protein-mineral interactions to include the degradative functionality of minerals in the cycling of SOM.

Mineral Surfaces As Agents of Environmental Proteolysis: Mechanisms and Controls

by

Stephany S. Chacon

A DISSERTATION

submitted to

Oregon State University

in partial fulfillment of
the requirements for the
degree of

Doctor of Philosophy

Presented December 3, 2018
Commencement June 2019

Doctor of Philosophy dissertation of Stephany S. Chacon presented on December 3, 2018.

APPROVED:

Major Professor, representing Soil Science

Head of the Department of Crop and Soil Science

Dean of the Graduate School

I understand that my dissertation will become part of the permanent collection of Oregon State University libraries. My signature below authorizes release of my dissertation to any reader upon request.

Stephany S. Chacon, Author

ACKNOWLEDGEMENTS

I would like to acknowledge my advisor Dr. Markus Kleber for his support and guidance in my Ph.D. studies. I special thank you to my collaborators Dr Suet Yi Liu, Dr. Musahid Ahmed, Dr. Nancy Washton, Dr. Patrick Reardon, Dr Eric Walter, Samuel Purvine, and Dr. Mary Lipton, who had the patience to walk me through cutting edge and expensive equipment in order to answer my research questions. Their willingness to bridge the world of physical chemistry and spectrometry to soil science was instrumental in completing my work I'd like to thank my committee Dr. David Myrold, Dr. Peter Bottomley, Dr. Maria Dragila and Dr. Daniel Luoma for their help and encouragement throughout the years. I am in debt with the researchers at Oregon State University, Lawrence Berkeley National Lab and Pacific Northwest National Laboratory for their support in finishing my research and studies.

Personally, I could not have completed my Ph.D without the camaraderie of the soils graduate students these past years. To my partners in crime and coffee aficionados : Vance Almquist, Kris Osterloh, Burl Carpenter, Adrian Gallo, and Clara Weidman (+Roan and Riff). To my fellow soils nerds Ruben Aleman, Shannon Cappellazzi (+Jed), Gloria Ambrowiak, Chris Burgess, Marci Burton, Stephen Clarke, Aimee Clark, Brian Hill, Sarah Light, Pedro Martinez,Jade Marks, Amy Mayedo, Trang Nguyen Thi Huyen, Danielle Runion, Ashley Waggoner(+Emma), and many many more!

To Benjamin Lewis for his companionship, love, and daily support. To my

amazing triphis Cathereen Lim, Sunny Patel, Linda Chung and Jerome Gonzales who inspired me to explore the world. Most importantly, to my loving familia: Mama, Papa, Maria, Lalo, Nataly, Brett, Marshall, Jonah, and Brandie. You have supported my selfish journey to satisfy my curiosity of the natural world.

CONTRIBUTION OF AUTHORS

S.Y. Liu assisted with the laser desorption post ionization analyses in chapter one. M. Ahmed, M.Jaramillo and M. Kleber contributed to the writing of chapter one publication. R. Chu and T.H. Clauss ran the liquid chromatography tandem mass spectrometer for chapter 2 and 3. S. Purvine ran the SEQUEST analysis for chapter 2 and 3. C. Burgess co-wrote the code to for DECON routine in chapter 2 and 3. P. Reardon assisted with the NMR analysis and data processing. P. Reardon, R. Chu, T.H Clauss, S. Purvine, C. Burgess, D. Myrold, N. Washton and M. Kleber contributed to the writing of the submitted manuscript for chapter 2.

TABLE OF CONTENTS

Page

1 Introduction 1

2 Differential capacity of kaolinite and birnessite to protect surface associated proteins against thermal degradation 6

2.1 Abstract 7

2.2 Introduction 8

2.3 Materials and Methods 13

2.3.1 Materials 13

2.3.2 Development of a variable to quantify the extent of electrostatic attraction 15

2.3.3 Development of a variable to estimate potential contribution of conformational change to protein adsorption 18

2.3.4 Protein adsorption to mineral surfaces 18

2.3.5 Laser desorption post ionization mass spectrometry of protein-mineral samples 20

2.4 Results 22

2.4.1 Protein adsorption as a function of charge overlap and conformational change 22

2.4.2 Total ion counts and mass spectra include signals from buffer and birnessite 23

2.4.3 The abundance of fragmentation products as a function of energy applied 26

2.4.4 Protein fragmentation patterns differ between mineral surfaces 27

2.4.5 Fragmentation does not depend on protein size 27

2.4.6 pH dependence of protein fragmentation 30

2.4.7 Total ion counts as a function of power density 30

2.5 Discussion 32

2.5.1 Adsorption mechanisms and protein fragmentation are mineral dependent 32

2.5.2 Birnessite is more susceptible to disintegration than kaolinite 34

2.5.3 Energy dependence of fragmentation shows a threshold . . . 35

2.5.4 The dominant protein fragmentation mechanism shifts away from hydrolysis 36

2.5.5 Greater protein size does not lead to more fragmentation products 37

TABLE OF CONTENTS (Continued)

Page

2.5.6 Acidic pH enhances fragmentation of BG by birnessite . . . 38
2.6 Conclusions . . . 38
2.7 References . . . 40
2.8 Appendix for Chapter 2 . . . 47
2.8.1 Schematic of LDPI-MS Setup at 9.0.2 Beamline of the Advanced Light Source . . . 47
2.8.2 Laser Application of Protein-Mineral Samples . . . 48
2.8.3 Prolonged Salt Titration (PST) Method for Determining Point of Zero Charge (PZC) . . . 49
2.8.4 Adsorption of proteins on birnessite and kaolinite . . . 51
2.8.5 Total Ion Counts as a function of energy applied for mineral-buffer samples and protein-mineral samples . . . 52
2.8.6 Multivariable linear regression analysis results for protein adsorption . . . 53
2.8.7 Presence of large masses for birnessite-buffer samples . . . 55

3 Mineral Surfaces As Agents of Environmental Proteolysis: Mechanisms and Controls . . . 60
3.1 Abstract . . . 61
3.2 Introduction . . . 62
3.3 Materials and Methods . . . 65
3.4 Results and Discussion . . . 68
3.4.1 All minerals induce protein fragmentation . . . 68
3.4.2 Fragmentation patterns are not entirely random . . . 70
3.4.3 Cleavage is not restricted to acidic pH . . . 73
3.4.4 Protein fragmentation changes with exposure time . . . 74
3.5 Discussion . . . 75
3.6 Significance and Implications . . . 80
3.6.1 Acknowledgements . . . 82
3.7 References . . . 83
3.8 Appendix for Chapter 3 . . . 88
3.8.1 Preparation of Protein-Mineral Samples . . . 88

TABLE OF CONTENTS (Continued)

Page

3.8.2 Differentiation between products of hydrolysis and products of oxidation . . . 89
3.8.3 Parameterizing electrostatic attraction and conformational change . . . 114

4 Insertion of an amino acid trimer modifies the outcome of protein-mineral interactions . . . 127
4.1 Abstract . . . 128
4.2 Introduction . . . 129
4.3 Materials and Methods . . . 134
4.3.1 Expression and purification of the His-tagged loop variants . 134
4.3.2 Preparation of Minerals . . . 136
4.3.3 Adsorption of Modified Proteins to Minerals . . . 136
4.3.4 NMR Analysis of supernatant samples . . . 137
4.3.5 Tandem Mass Spectrometry Analysis . . . 138
4.4 Results and Discussion . . . 139
4.4.1 Adsorption of GB1 to mineral surfaces was be affected by the addition of three amino acids into one of its loop regions. 139
4.4.2 Insertion of three amino acids in the loop region did change the incidence of cleavage through hydrolysis or oxidation by minerals . . . 145
4.4.3 The location of cleavage points did not remain constant regardless of the specific charge characteristics of the inserted trimer . . . 147
4.4.4 The number of unique peptides did not remain constant independent of the charge characteristics of the inserted trimer. 150
4.5 Conclusion . . . 153
4.6 Acknowledgements . . . 154
4.7 References . . . 154
4.8 Appendix Chapter 4 . . . 160
4.8.1 Transformation of E.coli cells with Plasmid DNA encoding Loop Mutants . . . 160
4.8.2 Nickel (Ni-NTA) affinity chromatography purification . . . 161
4.8.3 Thrombin Cleavage Reaction . . . 161

TABLE OF CONTENTS (Continued)

Page

4.8.4 Time series of Modified Proteins interacting with Birnessite . 164

5 Conclusion 166

6 Bibliography For Introduction and Conclusion 170

LIST OF FIGURES

Figure Page

1.1 General view of the outcomes of protein-mineral interactions. A protein (black) has an initial adsorption step to a mineral surface (sorbent) The protein can (1) rearrange the mode of attachment to create greater points of contact to the surface, or (2) undergo minor or extensive conformational changes. The protein can also be released back into the solution without any or extensive changes to the original protein structure 3

2.1 Charge overlap for combinations of two proteins Beta-Glucosidase (BG) and Bovine Serum Albumin (BSA) with two minerals (kaolinite and birnessite) at pH 5 and 7. High alpha values indicate high potential for attractive electrostatic interactions between proteins and minerals at pH 5 and pH 7. Light grey indicates proportion of surface that has positive charge (+). Dark grey indicates proportion of surface with has negative charge (-).The proportion of surface charge was calculated using equations 1 and 2. 14

2.2 Charge overlap for combinations of two proteins Beta-Glucosidase (BG) and Bovine Serum Albumin (BSA) with two minerals (kaolinite and birnessite) at pH 5 and 7.High alpha values indicate high potential for attractive electrostatic interactions between proteins and minerals at pH 5 and pH 7. Light grey indicates proportion of surface that has positive charge (+). Dark grey indicates proportion of surface with has negative charge (-).The proportion of surface charge was calculated using equations 1 and 2. 24

2.3 Mass spectra from birnessite+buffer samples (A-D) were compared to protein+birnessite+buffer samples (E-L) to identify the presence of peaks only found in protein containing samples between 200-800 mass per charge (m/z). Spectra were annotated with the pH on the left side in the brackets and the energy applied at the right side. For example, samples with pH 5 at energy applied 1.27 $MWcm^{-2}$ are designated [5/1.27]. Peaks highlighted in birnessite samples containing Bovine Serum Albumin (BSA) and Beta-Glucosidase (BG) are unique peaks that are not found in birnessite buffer samples or have higher signal intensity than birnessite-buffer peaks. Peaks from birnessite buffer samples were underlined. Mass spectra shown here are from the two highest energy applications 25

LIST OF FIGURES (Continued)

Figure | Page

2.4 Comparison between mass spectra from Beta-Glucosidase (BG) and Bovine Serum Albumin (BSA) desorbed off Birnessite (top), Kaolinite (center) and Si wafer (bottom) at pH 5 and pH 7. Energy applied to all samples was 1.84 $MWcm^{-2}$. Breaks were at added at 85 percent of the scale to focus on peaks not from the buffers. The x-axis includes data from 0-800 m/z. 29

2.5 Total Ion counts of samples on birnessite (left), kaolinite (middle), and Si wafer (right). Mineral samples (square) indicate either birnessite, or kaolinite with only buffer at pH 5 (closed) and pH 7 (open). X-axis arranged to show increasing application of energy towards the right. TIC below energy threshold show linear trend on log10 y-axis. After 0.2 $MWcm^{-2}$, exponential increase of TIC observed. 32

2.6 The Laser Desorption Post Ionization Set up at the 9.0.2 Beamline uses a laser to desorb a sample from the surface (green arrow). The desorbed sample is ionized using tunable synchrotron vacuum ultraviolet (VUV) radiation and detected with a mass spectrometer. 47

2.7 Laser energies on the protein-mineral sample was applied by rastering the laser across the sample and ionizing the compounds desorbed. Once the ions were desorbed and detected, the next energy application followed below the previous laser raster. The energy increased from top to bottom 48

2.8 Point of zero charge was determined for acid birnessite by fitting a polynomial curve (red) and determining when Delta pH was equal to zero. 50

2.9 Amount of Bovine Serum Albumin (BSA) and Beta-Glucosidase (BG) adsorbed onto Birnessite and Kaolinite. The adsorption conditions were 100 mM sodium acetate pH 5 (black) and 100 mM Tris pH 7 (grey). 51

LIST OF FIGURES (Continued)

Figure | Page

2.10 Comparison of total ion counts (TIC) as a function of energy. The X-axis was not modified as in Figure 5, which condenses low energy application and emphasizes higher energies. The TIC detected as a function of laser energy applied or power density to Birnessite (left), Kaolinite (middle) and Si wafer (right). Squares represent mineral with just buffer. Samples with BG and buffer are circles, and BSA with buffer is represented with triangles. Closed symbols are pH 5 and open symbols are pH 7. 52

3.1 The sequence of events leading to the identification of protein fragments generated by hydrolysis and oxidation reactions. Experimental measurements are represented in black, the SEQUEST analysis for the identification of hydrolysis products is represented in blue and the DECON-Routine for the identification of oxidation products in red. Note that the DECON-Routine is applied to MS1 data after filtering out any hydrolysis products identified by the SEQUEST algorithm. Because it does not process MS2 data, the DECON - Routine for the identification of oxidation products does not take full advantage of the MS/MS approach and may return false positives. 67

3.2 The cleavage sites on GB1 as a function of mineral exposure. The minerals tested are identified on the left, next to a schematic of the GB1. The top row has the one letter amino acid sequence of GB1. Below the sequence is the amino acid residue number. Letters and circles colored green designate amino acids within the beta sheets. The brown colored letters and circles designate amino acids within the alpha helix. Letters and circles in black and grey designate amino acids that are unassigned or in a loop region. Blue arrows indicate the location of hydrolytic cleavage sites, red arrows indicate the location of oxidative cleavage. 69

3.3 Heat map of the sums of ion counts for each mineral treatment (n=12). Fragment numbers refer to table 1 with items below the bold line representing products of fragmentation. Color gradient spans from white to black and covers 10 orders of magnitude. 72

LIST OF FIGURES (Continued)

Figure | Page

3.4 The number of unique peptides observed, accumulated over four time points. Error bars indicate variability expressed as standard deviations across replicates and time points (n = 12). Data are organized by cleavage mechanism, pH and mineral surface type. . . 74

3.5 The effect of exposure time on the number of unique peptides generated by hydrolysis and oxidation at two pH values. Symbols represent mean values among three replicate samples, with error bars indicating the corresponding standard deviation. Closed symbols and straight lines are pH 5, open signals and dotted lines are respective values at pH 7. 75

3.6 Rationale for differentiation between products of hydrolysis and oxidation. For the same hypothetical peptide, reaction pathways involving hydrolysis (Reaction 1) and Oxidation (Reaction 2) are presented, together with the fragmentation products and their corresponding monoisotopic masses. Masses produced (1, 2 for hydrolysis and and I through IV for oxidation) are generally a function of cleavage site indicated by dotted lines. The oxidative cleavage of a peptide (Reaction 2) occurs in several steps according to Berlett and Stadtman (1997). An oxidant (such as reactive oxygen species) reacts with the peptide and transforms the alpha carbon into a radical. Subsequently, an oxygen molecule may attach at this position and cleave the alpha bond. If cleavage were to occur on the left side of the alpha carbon (A), we would observe fragments I and II. If fragmentation occurs on the right side of the alpha carbon (B), fragments III and IV are created 113

3.7 Adsorption of Gb1 as a function of potential electrostatic attraction (α, electrostatic attraction increasing with increasing values) for montmorillonite (square), kaolinite (triangle), goethite (circle), and birnessite (gray square). Error bars are standard deviation (n=3). The pH during adsorption is indicated next to the symbol 116

4.1 The fraction of protein adsorbed to four soil minerals at pH 5 and pH 7 (n=3). The unaltered control is cGb1, GLU stands for the EEE-mutant (- patch), LYS for the KKK-mutant (+ patch) and TRP is the WWW-mutant (neutral patch). 142

LIST OF FIGURES (Continued)

Figure Page

4.2 Detection of protein at pH 7 by ^{1}H $-^{15}$ N HSQC NMR analysis. Black spectra represent supernatants after reacting the respective mineral with the cGB1 control. Red spectra are from supernatants of adsorption experiments using the mutant with the EEE-trimer (GLU); green spectra are from the KKK-trimer (LYS) and Magenta is the WWW-mutant (TRP). 143

4.3 Detection of protein at pH 5 by ^{1}H $-^{15}$ N HSQC NMR analysis. Black spectra represent supernatants after reacting the respective mineral with the cGB1 control. Red spectra are from supernatants of adsorption experiments using the mutant with the EEE-trimer (GLU); green spectra are from the KKK-trimer (LYS) and Magenta is the WWW-mutant (TRP). 144

4.4 The cleavage sites on GB1 and loop mutants as a function of mineral exposure. On the left side are the minerals that proteins interacted with, next to a string of circles that represent a schematic of the loop mutants. The top row has the one letter amino acid sequence of the proteins. Letters and circles colored green designate amino acids within the beta sheets. The brown colored letters and circles designate amino acids within the alpha helix. Red circles indicate the added glutamic acid amino acids. Blue circles indicate the added lysine amino acids in the loop region. Purple circles indicate the added tryptophan amino acids. Letters and circles in black and grey designate amino acids that are unassigned or in the loop region. The blue arrows above the string of circles indicate the location of hydrolytic cleavage after interacting with a mineral on the left. The red arrows below the string of circles indicate the location of oxidative cleavage catalyzed by the mineral on the left side. 151

4.5 The number of unique peptides observed in the supernatant of the protein-mineral samples at pH 5 or pH 7. The error bars indicate variability expresses as standard deviation (n=3). Data are organized by cleavage mechanism, pH, protein and mineral surface type. 152

LIST OF FIGURES (Continued)

Figure Page

4.6 The release of peptides from Gb1 control and Gb1 modified proteins varies after interacting with birnessite at pH 7. The $^{1}H-^{15}N$ HSQC NMR spectra indicate the release of peptides into the supernatant. cGb1 indicates the spectra are from Gb1 control. GLU indicates spectra from Gb1 Glutamic acid variant. LYS indicates spectra are from Gb1 lysine mutant. TRP indicates spectra are from Gb1 tryptophan mutant. 164

4.7 The release of peptides from Gb1 control and Gb1 modified proteins varies after interacting with birnessite at pH 5. The $^{1}H-^{15}N$ HSQC NMR spectra indicate the release of peptides into the supernatant. cGb1 indicates the spectra are from Gb1 control. GLU indicates spectra from Gb1 Glutamic acid variant. LYS indicates spectra are from Gb1 lysine mutant. TRP indicates spectra are from Gb1 tryptophan mutant. 165

5.1 An expanded view of the outcomes of protein-mineral interactions with our experimental observations. We expanded to include a protein (black) interacting with a mineral surface that is a reactant. This can generate and release peptides into the soil solution. A protein already attached to a surface of a mineral that experiences a large energy input, such as energies experienced in wildfires, can break the protein and the mineral apart.These interactions are controlled by pH, ionic concentration, mineralogy, energy status, and protein properties, such as amino acid sequence. 168

LIST OF TABLES

Table Page

2.1 Properties of the proteins and minerals used in this experiment. . . 16

2.2 Positive (+) and negative (-) surface charge of protein and mineral surfaces at pH 5 and pH 7 calculated from the point of zero charge (pzc) and the isoelectric point (pI). Values reported as percent total charge and were calculated using equation (1) through (4). 19

2.3 Comparison between total ion counts of Beta-Glucosidase and Bovine Serum Albumin samples detected off Birnessite at pH 5 and pH 7 with increasing energy applied. 28

2.4 Multivariable linear regression models testing protein adsorption (dependent variable) with independent variables parameterizing electrostatic interactions such as opposite charge overlap (α) and conformational change (ν) 54

2.5 Elemental compositions for signals found in birnessite-buffer samples. Elements used 102 in Formula Finder were chosen based of the composition of birnessite and the buffers used.. 55

3.1 The abundance of cleavage sites per structural region of the protein and mineral surface type 71

3.2 Order of sample injection for tandem mass spectrometry. Sample name abbreviations with no protein samples are designated by sample number, a single letter indicating mineral with a replicate number, pH value, and the time point. M stands for montmorillonite, K for kaolinite, G for goethite and B for birnessite. For example, 180_M3_pH5_T4 is sample number 180 containing the third replicate with montmorillonite at pH 5 taken after 168 hours. Samples containing protein have GB1 in the front, with mineral name, pH, time point and replicate number. For example, $GB1\_Kaolinite\_pH\_5\_T1\_R1$ is the first replicate of a GB1 sample that interacted with kaolinite at pH 5 for 1 hour. 92

3.3 Charge Characteristics of Minerals 117

LIST OF TABLES (Continued)

Table | Page

3.4 Sequences of protein and peptides detected in the supernatants along with their monoisotopic mass and fragment label. Fragment labels will be used throughout the figures and text.Bold sequences indicate the fragment was filtered from further analysis because it was detected in the control. Oxidation of the amino acids is indicated to the right of the letter with # (e.g. M# means oxidized methionine). 118

3.5 Sequences of oxidized protein and peptides detected in the supernatants along with their monoisotopic mas and fragment label. Fragment labels will be used throughout the figures and text. Strikeout of a peptide indicates the fragment was filtered from further analysis because it was detected in the controls 119

3.6 The presence or absence of peptides 8H (D.DATKTFTVTE.-) and 8I (D.ATKTFTVTE.-) in blanks, Kaolinite, and Montmorillonite samples. In order to determine that the presence of peptides was not a function of carryover, the blanks preceding and following the phyllosilicate protein samples were analyzed. The correlation score of the peptide detected Is indicated below. n.d. refers to the peptide not detected in the sample. If the Cross correlation (Xcorr) scores are above the threshold define by Smith et al. (2002a), they are in bold and highlighted in grey. Italicized sample names indicate blank samples. Samples were presented in the order they were run. R indicates replicate number (R1=replicate) 124

4.1 The abundance of cleavage sites as a function of the protein and mineral surface type. 146

4.2 The sequence of the GB1 and the GB1 Loop Mutant proteins. The proteins expressed by our transformed E. coli were proteins with a histidine tag, shown in blue. The His-tag was at the beginning of the control and the loop mutants (indicated by the asterisk *). After the reaction with the thrombin enzyme, the resulting proteins still contain GSH from the tag. 163

Chapter 1: Introduction

The decomposability of soil organic matter (SOM) is proposed to be controlled by environmental and biological factors that can affect microbial accessibility of SOM. Unprotected SOM is depolymerized by microbially produced-extracellular enzymes (Sinsabaugh et al., 1991), proteins that catalyze chemical reactions outside the cell, into low molecular weight compounds. This makes organic matter available for uptake by microbes, where it can be respired or become incorporated into microbial biomass. Mineral association removes the SOM from being accessed by the extracellular enzymes or the microbes themselves (Conant et al., 2011). More recently, minerals are being examined as a major factor protecting SOM from decomposition (Schmidt et al., 2011; Dungait et al., 2012; Torn et al., 2013)..

A protein is a polymer of amino acids that can have various functional groups in the side chains. This polymer of amino acids can adopt secondary structures such as alpha helices and beta-sheets. Loops are structures between these secondary structures. Proteins can adopt a three-dimensional structure that is necessary for their function. Adsorption to a mineral surface, through the mechanisms of cation exchange, anion exchange, water bridging, ion-dipole interactions, Van der Waals bonds, and hydrophobic interactions (Craig and Collins, 2002), can have many consequences to the function of a protein. Although some proteins can initially attach to a surface without significant changes to the structure (Arai and Norde,

1990), over time they may reorient to increase the number of attachment points to the surface (Rabe et al., 2007). Additionally, if attachment involves the active site of an enzyme, the catalytic function could be impaired due to steric hinderance (Baron et al., 1999). Another way to alter function is through conformational changes to the protein itself (Quiquampoix and Ratcliffe, 1992; Norde and Giacomelli, 2000; Servagent-Noinville et al., 2000). Protein conformational changes alter the affinity of substrates to an active site or completely unfold the protein itself, making the protein not functional. A general view of protein-mineral interactions is encompassed by an initial sorption and subsequent structural changes (Figure 1.1).

There is a body of literature that provides evidence that some minerals can react with organic compounds and SOM. One group of metal oxides, manganese oxides, are commonly found in soil and have been observed to react with organic compounds and SOM. Manganese (IV) oxides that commonly occur in soil include birnessite, cryptomelane, and pyrosulfite (McKenzie, 1971). They have been observed to transform or degrade organic compounds, such as phenolics, aromatic amines, pesticides, antibiotics, dyes, and explosives, more efficiently than iron, aluminum or silica oxides (Li et al., 2003; Barrett and McBride, 2005; Zhang et al., 2008). The mechanisms involved in the reactions between organic compounds and Mn(IV) oxides are reduction, oxidation, and hydrolysis. Birnessite, the most abundant clay-sized Mn(IV) oxide in soil, has been specifically observed to cleave aromatic rings in phenols, polycyclic aromatic hydrocarbons, and other similar derivatives through oxidation (Stone, 1987; McBride, 1989; Rao et al., 2008; Chang

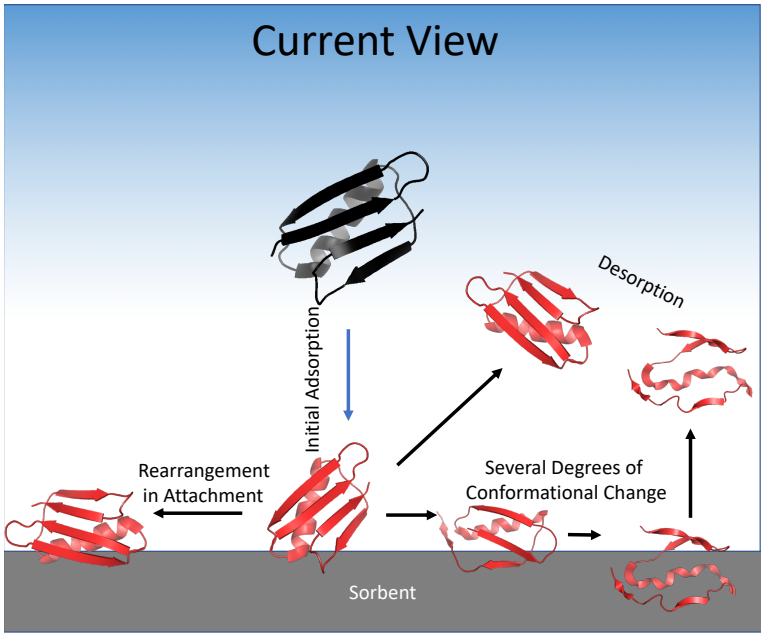

Figure 1.1: General view of the outcomes of protein-mineral interactions. A protein (black) has an initial adsorption step to a mineral surface (sorbent) The protein can (1) rearrange the mode of attachment to create greater points of contact to the surface, or (2) undergo minor or extensive conformational changes. The protein can also be released back into the solution without any or extensive changes to the original protein structure

Chien et al., 2009; Mario et al., 2014) and can transform phenolic compounds by removing halogen, methyl, and carboxylate functional groups (Dec et al., 2001). Biopolymers found in soil, such as prions and dissolved organic matter (DOM) from forest litter, are also susceptible to degradation by birnessite (Chorover and Amistadi, 2001; Russo et al., 2009). Oxidation by birnessite is proposed to be more efficient in terms of yield than enzymes, such as phenol oxidases (Dec et al., 2003).

Phyllosilicates are another group of minerals implicated in protecting organic

matter from decomposition by microorganisms (van Loosdrecht et al., 1990).Phyllosilicates have also been observed to degrade or transform organic compounds, however, not to the same degree as metal oxides. Smectites that are poor in iron have an ability to catalyze the dehydration of glucose molecules (Gonzalez and Laird, 2006). Aromatic amines have been shown to transform into their color derivatives by interaction with clays (Filip et al., 1977). Oxidation sites for phenolic compounds are assumed to be located on the crystal edges of smectites where transition metals within the octahedral layers are exposed (Thompson and Moll, 1973). Oxygen molecules or radicals may also become adsorbed onto a phyllosilicate, facilitating the oxidation of phenolics by concentrating the reactants.

To reconcile the different possible outcomes of mineral interactions with proteins, we propose to conduct experiments that specifically focus on characterizing the ability of minerals to react with model proteins. The first research chapter explores how mineral surfaces can switch from sorbents to reactants towards beta glucosidase and bovine serum albumin under a gradient of increasing energy, (MW cm^{-1}) similar to fire line intensities experienced in wildfires. The second research chapter describes the mechanisms responsible for proteolysis and the sites of cleavage by minerals on a model protein (Beta 1 domain of Protein G; GB1). The third research chapter uses protein engineering to determine if inserting an amino acid trimer to a model protein (GB1) is sufficient to alter protein-mineral interactions such as adsorption and fragmentation. Our approach was to use high-resolution spectrometry to identify chemical modifications of proteins in these experiments. In our first chapter, we took advantage of the synchrotron radiation laser desorp-

tion post-ionization mass spectrometry (LDPI-MS) setup at the 9.0.2 Beamline at the Advance Light Source, to specifically probe proteins sorbed on a mineral surface and subject them to increasing amounts of energy with a laser (MW cm^{-1}). The second chapter took advantage of high-resolution liquid chromatography tandem mass spectrometry (LC-MS/MS) to detect protein fragments in solution at low concentrations and analyze the fragments mass to determine the mechanism of fragmentation. The third chapter used a combination of two-dimensional Nuclear Magnetic Resonance and LC-MS/MS to detect changes in protein-mineral interactions as a result of inserting an amino acid trimer in GB1.

Chapter 2: Differential capacity of kaolinite and birnessite to protect surface associated proteins against thermal degradation

Stephany S. Chacon*,

Manuel Garcia-Jaramillo, Suet Yi Liu, Musahid Ahmed, Markus Kleber

Published In:

Soil Biology and Biochemistry

Elsevier Inc.

1600 John F Kennedy Boulevard Suite 1800 Philadelphia PA 19103-2879, USA

Issue 119, pages 101-109, 2018

2.1 Abstract

It is widely accepted that soil organic carbon cycling depends on the presence and catalytic functionality of extracellular enzymes. Recent reports suggest that combusted and autoclaved soils may have the capacity to degrade organic test substrates to a larger extent than the living, enzyme-bearing soils. In search of the underlying mechanisms, we adsorbed Beta-Glucosidase (BG) and Bovine Serum Albumin (BSA) on the phyllosili- cate kaolinite and the manganese oxide birnessite at pH 5 and pH 7. The protein-mineral samples were then subjected to gradual energy inputs of a magnitude equivalent to naturally occurring wildfire events. The abundance and molecular masses of desorbed organic compounds were recorded after ionization with tunable synchrotron vacuum ultraviolet radiation (VUV). The mechanisms controlling the fate of proteins varied with mineralogy. Kaolinite adsorbed protein largely through hydrophobic interactions and, even at large energy inputs, produced negligible amounts of desorption fragments compared to birnessite. Acid birnessite adsorbed protein through coulombic forces at low energy levels, became a hydrolyzing catalyst at low energies and low pH, and eventually turned into a reactant involving disintegration of both mineral and protein at higher energy inputs. Fragmentation of proteins was energy dependent and did not occur below an energy threshold of 0.20 MW cm^2. Neither signal abundance nor signal intensity were a function of protein size. Above the energy threshold value, BG that had been adsorbed to birnessite at pH 7 showed an increase in signal abundance with increasing energy applications. Signal intensities differed with

adsorption pH for BSA but only at the highest energy level applied. Our results indicate that proteins adsorbed to kaolinite may remain intact after exposure to such energy inputs as can be expected to occur in natural ecosystems. Protein fragmentation and concomitant loss of functionality must be expected in surface soils replete with pedogenic manganese oxides. We conclude that minerals can do both: protect enzymes at high energy intensities in the case of kaolinite and, in the case of birnessite, substitute for and even exceed the oxidative functionality that may have been lost when unprotected oxidative enzymes were denatured at high energy inputs.

2.2 Introduction

The paradigm of mineral control (Torn et al. 1997) posits that the mineral matrix protects soil organic matter (SOM) against microbial decomposition by regulating accessibility and bioavailability of organic substrates through the processes of aggregation and adsorption. Past research into the phenomenon has concentrated on the stabilizing effects of the mineral matrix (Baldock and Skjemstad, 2000; Rasmussen et al., 2006; Basile-Doelsch et al., 2007; Kemmitt et al., 2008; Marin-Spiotta et al., 2008; Schmidt et al., 2011; Dungait et al., 2012; Torn et al., 2013; Doetterl et al., 2015), i.e. the ability of minerals to retard the decomposition of organic substrates. But this research focus is contrasted by long standing evidence for the ability of certain soil minerals to do the exact opposite: promote organic matter degradation by effectively oxidizing (Stone, 1987) and hydrolyzing (Tor-

rents and Stone, 1993) a plethora of organic compounds. Apparently, the mineral matrix has a fundamental capacity to do both: protect organic substrates from decomposition as well as facilitate their disintegration.

Extracellular enzymes depolymerize soil organic matter (SOM) for transport through the cell membrane for full mineralization. To successfully complete their task, EEs must retain activity in soil over reasonable time scales. This means they must survive mineral interactions with minimal impediments to their function. In fact, attachment to mineral surfaces may prove beneficial regarding functionality. Upon adsorption, enzyme activity decreases (Quiquampoix, 2008), but the tradeoff is some degree of protection from microbial predation of the enzyme. An extension of functional life span may result but at a lesser degree of catalytic efficiency than for the free enzyme (Yan et al., 2010). Some noteworthy exceptions where EE have greater reaction rates when adsorbed than free have been observed (Allison, 2006; Fiorito et al., 2008). Given that the mineral phase contributes approximately half the volume of an average surface soil, attachment to mineral surfaces appears to be inevitable for many if not all EE. But what if an EE encounters one of those minerals that have the demonstrated ability (Sunda and Kieber, 1994; Miltner and Zech, 1999) to either oxidize or hydrolyze organic substrates?

Reports of the fate of proteins at oxidizing/hydrolyzing mineral surfaces are scarce but particularly revealing. A prion protein was fully fragmented in soil upon interacting with birnessite in solution at pH 5 (Russo et al., 2009). Protein disintegration after contact with birnessite surfaces was recently confirmed by Reardon et al. (2016) and the mechanism of fragmentation identified as mineral-

catalyzed hydrolysis. The reports of Russo et al. (2009) and Reardon et al. (2016) are in contrast to the work of Naidja et al. (2002), who identified birnessite as a strong adsorbent for protein. If we assume both types of observations to be valid, i.e. when birnessite can act towards protein as both, protective sorbent and fragmenting catalyst, then there is a need to identify mechanisms and circumstances that determine when a mineral surface changes its role.

To constrain this issue it is useful to recall that the main mechanisms of protein mineral interactions include electrostatic attraction and repulsion, hydrogen bonding, hydrophobic interactions, and entropy driven conformational change (Boyd and Mortland, 1990; Craig and Collins, 2002). Among these four mechanisms, electrostatic interactions are the ones that are most susceptible to environmental controls such as soil pH and should therefore receive initial attention. The remaining three factors (hydrophobic interactions, hydrogen bonding and ability to change conformation upon adsorption) are largely determined by protein type and molecular size (Balcke et al., 2002; Sander et al., 2010). We deduced that an attempt to investigate the requirements for an abrupt change in the outcome of mineral organic interactions should include some variation in protein size and in protein responsiveness to electrostatic forces, the former reflected in molecular mass and the latter modified by variation of the isoelectric point of the protein (Quiquampoix et al., 1995; Norde, 2008). We further decided to vary energy input to the system based on a recent observation of temperature-induced variation in the presumably abiotic reactivity of mineral surfaces. This phenomenon was reported by Bach et al. (2013) and Blankinship et al. (2014) who independently performed

measurements of polyphenol oxidase (PPO) and peroxidase (PER) enzyme acitivities in soil samples. In their attempt to quantify any background contribution of the mineral matrix, Bach et al. (2013) and Blankinship et al. (2014) autoclaved and/or combusted their soils to sterilize and completely denature the enzymes and thus supposedly eliminated any enzymatic contribution to their assays. Yet some of the combusted and autoclaved soils degraded the aromatic test substrate (L-DOPA) to a larger extent than the living, enzyme bearing soils, with soils combusted at 500 C showing greater efficacy of oxidation than autoclaved soils. These observations led us to speculate that external energy input, as it occurs in the topsoils of many fireprone ecosystems, may have the potential to enhance the general capacity of the mineral matrix to fragment organic matter and may potentially act to convert sorptive into reactive mineral surfaces.

Consequently, the overarching goal of this research was to contribute to a mechanistic understanding of the dual role of mineral surfaces as both (i) stabilizing agents for soil protein and (ii) catalysts or reactants involved in their abiotic fragmentation. Previous evidence from Russo et al. (2009) and Reardon et al. (2016) looked at the supernatant in their samples, but these studies did not investigate the reactivity of minerals towards proteins in the absence of the aqueous phase, such as in periodically dry topsoils. Hence, our conceptual approach was to document the fate of protein on dry mineral surfaces of different potential surface reactivity while varying four known controls on protein-mineral interactions:

- protein size (measured in kDa)

- mineral surface type (sorbent type versus known catalyst/reactant type mineral)
- surface charge status of proteins and minerals as controlled by soil pH (varying pH as well as the isoelectric point of the proteins and the point of zero charge of the minerals)
- the energy input to the protein-mineral association (subjecting the protein-mineral system to progressively higher inputs of precisely dosed laser energy)

Our experimental design consisted of reacting two types of protein with two kinds of minerals in a slurry at two pH levels bracketing the main pH region for many soils (pH 5 and pH 7). After drying on an inert silica wafer, the protein-mineral mixtures were inserted into a vacuum chamber, subjected to a defined input of laser energy and the abundance and chemical composition of desorbed organic compounds was recorded after Vacuum-Ultraviolet (VUV) photoionization, using a time of flight Mass Spectrometer. To do so, we took advantage of an experimental setup at Beamline 9.0.2 of the Advanced Light Source at Berkeley, CA. Our experimental approach allowed us to test the following hypotheses:

1. The extent of protein adsorption at a mineral surface will be proportional to the extent of attractive electrostatic interactions.
2. With constant protein size and pH, fragmentation is a function of mineralogy, even in the absence of an aqueous phase.
3. The number of peptide signals in the mass spectrum is a function of

a) protein size (constant energy and pH)

b) pH (constant energy and protein size)

c) energy applied (constant protein size and pH)

4. With constant protein size and pH, the intensity of signals in the mass spectrum is a function of energy applied.

2.3 Materials and Methods

We selected the readily available proteins Beta Glucosidase (BG) and Bovine Serum Albumin (BSA) to achieve variation in size and isoelectric point (pI) of the protein. Proteins were adsorbed to acid birnessite (catalyst/reactant type mineral) and kaolinite (sorbent type mineral). The proteins were allowed to interact with the minerals at pH 5 and pH 7 to create variation in the extent of electrostatic attraction and repulsion between constituents (Figure 2.1).

2.3.1 Materials

Beta-glucosidase and bovine serum albumin were obtained from Sigma Aldrich and used directly from their containers. Acid birnessite was synthesized using the protocol described by Villalobos et al. (2003) and purified with a 1000 kDa dialysis tube until conductivity of supernatant was less than 40 S cm-1. The dialyzed birnessite was freeze-dried and stored at room temperature in amber glass bottles. Kaolinite (KGa-1b) was ordered from the Clay Minerals Society Source

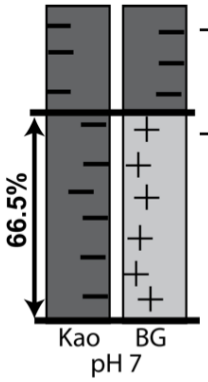

α values for Samples

	BG		BSA	
	pH 5	pH 7	pH 5	pH 7
	% total charge			
Kao	93.5	66.5*	18.1	0.3
Birn	99.4	66.6	23.9	0.3

Figure 2.1: Charge overlap for combinations of two proteins Beta-Glucosidase (BG) and Bovine Serum Albumin (BSA) with two minerals (kaolinite and birnessite) at pH 5 and 7. High alpha values indicate high potential for attractive electrostatic interactions between proteins and minerals at pH 5 and pH 7. Light grey indicates proportion of surface that has positive charge (+). Dark grey indicates proportion of surface with has negative charge (-).The proportion of surface charge was calculated using equations 1 and 2.

Clays Repository and exchanged with sodium chloride to standardize the cation population at the surface. The Na-kaolinite was washed until ionic conductivity was less than 40 Scm^{-1} and freeze-dried. The point of zero charge for birnessite was measured using the Prolonged Salt Titration (PST) method (reported in SI). The general properties of the proteins and minerals are reported in Table 2.1.

2.3.2 Development of a variable to quantify the extent of electrostatic attraction

To assess the dependence of protein adsorption on electrostatic attraction, we developed a simple procedure to estimate the extent of opposite charge overlap between the protein and the mineral (α). The underlying reasoning is as follows. Maximum electrostatic attraction between a protein and a mineral will occur when the total net surface charge of either reaction partner has opposite sign, a situation that we consider as "maximum overlap of opposing charges". At pH ranges typically found in soils, the proteins and minerals chosen for this study will carry variable proportions of both positive and negative charges. In our system, a situation of near total overlap (i.e. one reactant being overwhelmingly positively charged while the other is overwhelmingly negatively charged) occurs at pH 5, where both minerals are negatively charged and beta-glucosidase is positively charged (Figure 2.1). The degree of 'charge overlap' given in Figure 2.1 was calculated as follows: The fraction of positive charge on the protein (YB) was calculated with equation 1 using the proteins isoelectric point (pI).

$$Y_B = Total\,Charge \times \frac{1}{1+10^{(pH-pI)}} \qquad (1)$$

The fraction of positive charge on the mineral (YA) was calculated with equation 2 using the minerals point of zero charge (PZC). The fraction of negative charge on the mineral (XA) was then calculated by subtracting the positive charge from the total charge, which was set at unity (Equation 4). The positive charge of the protein was subtracted from the total charge (also at unity) to yield the frac-

Protein	Isoelectric Point (pH)	Molecular weight (kDa)	Extinction Coefficient
Beta Glucosidase (BG)	7.3[1]	135	43824
Bovine Serum Albumin (BSA)	4.7[2]	66.4[3]	95310[4]

Mineral	Point of Zero Charge (pH)	Cation Exchange capacity ($cmol_c \quad kg^{-1}$)	Surface Area
Kaolinite	3.8	3.0[5]	10.05[6]
Acid Birnessite	4.7[7]	$63 - 240$[8]	40.5[9]

Table 2.1: Properties of the proteins and minerals used in this experiment.

[1] Grover et al. (1977)
[2] Malamud and Drysdale (1978)
[3] Hirayama et al. (1990)
[4] Putnam (1975)
[5] Borden and Giese (2001)
[6] Schroth and Sposito (1997)
[7] Malamud and Drysdale (1978)
[8] Golden et al. (1986)
[9] Mckenzie (1981)

tion of negative charge of the protein (XB) as shown in equation 3. The fractions of charge thus obtained are reported in Table 2.2.

$$Y_A = Total\,Charge \times \frac{1}{1+10^{(}pH-pzc)} \qquad (2)$$

$$X_B = Total\,Charge - Y_B \qquad (3)$$

$$X_A = Total\,Charge - Y_A \qquad (4)$$

These values were used to calculate the extent of opposite charge overlap between protein and minerals (α) at typical soil pH values of 5 and 7, using Equation 5. The overlap of opposite charges can be seen as a coarse proxy for the potential strength of electrostatic attractions between the proteins and the minerals.

$$\alpha = |X_B - X_A| = |Y_B - Y_A| \qquad (5)$$

The values generated in equation 5 are reported for our experimental set up as proportion of total charge and reported as percentages (Figure 1).

2.3.3 Development of a variable to estimate potential contribution of conformational change to protein adsorption

Soft proteins undergo conformational change upon adsorption onto a surface. At the isoelectric point of a protein, volume can shrink in size, which allows more molecules to be packed onto a surface. When electrostatic repulsion increases as the pH moves away from the pI, the protein may spread out on a sorbent surface (Norde 2008). We account for this effect by using the difference between the adsorption pH and the pI as a proxy for eventual conformational change (v). As pH approaches the pI and the value of declines, we expected volume changes caused by conformational change to have a growing influence on the amount of protein adsorbed (q)

$$\upsilon = f|pH_{Adsorption} - pH_{pI}| \qquad (6)$$

2.3.4 Protein adsorption to mineral surfaces

Protein-mineral samples were prepared at pH 5 with a 100 mM sodium acetate buffer and at pH 7 with a 100 mM TRIS buffer. Stock solutions were made by dissolving Beta-Glucosidase (BG) and Bovine Serum Albumin (BSA) into pH 5 and pH 7 buffers at a concentration of 3 mg protein per mL of buffer (Ci), making four stock solutions. Protein-mineral samples were made in triplicate by mixing protein buffer solution at a ratio of 1 mL to 20 mg of kaolinite or birnessite (mmineral). The samples were mixed and allowed to react for 24 hours at 20 C.

Protein	pH 5		pH 7	
	+ Charged Surface (%)	- Charged Surface (%)	+ Charged Surface	- Charged Surface
Beta Glucosidase (BG)	99.50	0.50	66.6	33.40
Bovine Serum Albumin (BSA)	79.92	20.10	3.80	96.20
Mineral	**pH 5**		**pH 7**	
	+ Charged Surface (%)	- Charged Surface (%)	+ Charged Surface	- Charged Surface
Birnessite	0.08	99.9	0.00	100
Kaolinite	5.94	94.10	0.10	99.90

Table 2.2: Positive (+) and negative (-) surface charge of protein and mineral surfaces at pH 5 and pH 7 calculated from the point of zero charge (pzc) and the isoelectric point (pI). Values reported as percent total charge and were calculated using equation (1) through (4).

Unadsorbed protein was removed by centrifuging at 11,700 rcf for 40 minutes and pipetting out the supernatant. The concentration of protein in the supernatant, or the equilibrium concentration (C_eq) was determined using UV-Vis spectroscopy at 280 nm. The protein-mineral pellets were washed with buffer by re-suspending the pellet and centrifuging the samples. The supernatant was removed and the process was repeated once. The amount of protein adsorbed on the mineral surfaces was calculated using equation (7):

$$q = \frac{volume(C_i - C_eq)}{m_mineral} \qquad (7)$$

To test the effects of electrostatic interactions on protein adsorption, we performed linear regression analyses to obtain slopes, coefficients of determination, and P-values for the dependence of q on electrostatic interaction parameters. Multi linear regression analysis was used to test whether there were significant interactions between parameters.

2.3.5 Laser desorption post ionization mass spectrometry of protein-mineral samples

Laser desorption post ionization mass spectrometry (LDPI-MS) setup at the 9.0.2 Beamline at ALS is a combination of three techniques. The setup is a vacuum chamber equipped with a laser with variable energy output, which is used to desorb the sample from a surface. The next setup is the post-ionization technique, once the sample has been desorbed with a laser, it is ionized using tunable synchrotron VUV radiation. After the sample is ionized, it is detected with a mass spectrometer.

The schematic for the LDPI-MS setup is in the supplemental information (Figure S1).

The benefit of LDPI-MS analysis is the minimal fragmentation of organics desorbed from solid phases. Other techniques such as liquid chromatography tandem mass spectrometry and solution state nuclear magnetic resonance (NMR) would require initial extraction and sample preparation before analysis can be conducted. Solid state NMR would only be possible with proteins sorbed on non-paramagnetic minerals. This would limit analysis to only phyllosilicates since birnessite is paramagnetic. Analysis of protein changes with FT-infrared radiation is limited to shifts in secondary structure on a sorbed protein as it does not detect changes to the molecular weight. LDPI-MS has been previously used to detect lignin and its derivatives in soil density fractionation samples (Liu et al., 2013) and melanin constituents in bird feathers (Liu et al., 2014). For these reasons, we decided to use LDPI-MS on our protein-mineral samples. Sample preparation for LDPI-MS was done by suspending the protein-mineral pellets with 1.0 mL MilliQ water. The suspension was transferred to a silicon wafer and allowed to dry in a desiccator for 2 days before analysis. The samples were subsequently placed in the vacuum chamber of the LDPI-MS setup and evacuated. A 349 nm Nd:YLF laser with a focus spot of 15 m was used to irradiate the sample at 8.5 ns pulses using linear raster scanning over 18 mm at a rate of 2 mms^{-1} with the laser at varying energy levels (Figure S2). Expressed in commonly used power density units, the energy applied spanned a range from 0.05 to 1.84 $MWcm^{-2}$. To relate experimental settings to the conditions observed during natural wild fires, power densities were

converted to fire line intensity units (kWm^{-1}) defined as the rate of energy or heat release per unit length of fire front (Byram, 1959). A conversion table is provided in Table S4.

The fragments desorbed by the laser were ionized with VUV radiation at a constant energy of 10.5 eV (Liu et al., 2013). The ions thus generated were detected with a time of flight mass spectrometer at a mass detection limit of 3000 mass per charge (m/z). We used the following parameters to interpret and describe the results from LDPI-MS analysis. The total ion count (TIC) is the sum of peak intensities (unit: total detector counts) of all mass spectral peaks and is used to describe the magnitude of overall signal generation. The signal intensity parameter is the magnitude of a single peak (unit: counts per specific mass), and provides the contribution of a single mass to the mass spectrum. Finally, we use the term signal abundance (unit: number of signals of interest observed) to refer to the number of individual discernible peaks as a proxy for the extent of fragmentation.

2.4 Results

2.4.1 Protein adsorption as a function of charge overlap and conformational change

The amount of protein adsorbed on kaolinite decreased in a strong linear relationship as α increased (Figure 2.2A). This was contrasted by a strong positive linear relationship observed between α and protein adsorption on birnessite. The

relationship between q and α was statistically significant for kaolinite minerals at $p < 0.001$ (Table S1). The influence of ν to protein adsorption is illustrated by plotting q as a function of ν (Figure 2.2B). There was a slight increase in q for kaolinite samples when pH was closer to the pI and the relationship was significant (Figure 2.2C). A similar relationship between q and ν was observed for birnessite samples (Figure 2D). When fitting a linear function, a trend was apparent that was not statistically significant. A multilinear regression model including interactions between opposite charge overlap (α) and conformational change (ν) was able to explain 66 percent of variability for kaolinite samples. The same multilinear regression model for birnessite explained 70 percent of the variability in the data (Table S1).

2.4.2 Total ion counts and mass spectra include signals from buffer and birnessite

Laser application to birnessite control samples (birnessite plus sodium acetate and birnessite plus Tris buffer) released ions with masses greater than 200 Dalton (Figure 2.3) in the absence of protein. Such behavior was not observed on kaolinite samples (Figure S5). Birnessite plus Tris buffer had signals at 355.07, 428.98, 502.95, 552.95 and 626.90 m/z (Figure 2.3A-2.3D). The signals at 552.95 and 626.90 m/z were similarly found on birnessite samples with sodium acetate buffer along with new signals at 405.01 and 479.14 m/z (Figure 2.3C-2.3D). As these signals reached intensities comparable to signal intensities from protein-birnessite

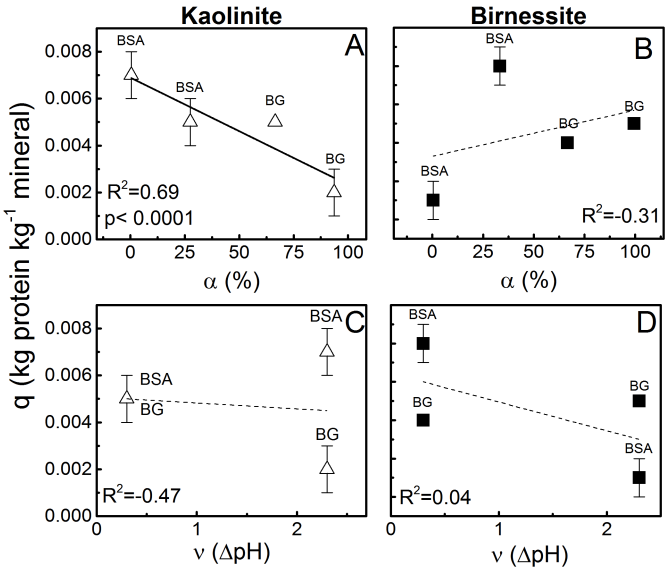

Figure 2.2: Charge overlap for combinations of two proteins Beta-Glucosidase (BG) and Bovine Serum Albumin (BSA) with two minerals (kaolinite and birnessite) at pH 5 and 7.High alpha values indicate high potential for attractive electrostatic interactions between proteins and minerals at pH 5 and pH 7. Light grey indicates proportion of surface that has positive charge (+). Dark grey indicates proportion of surface with has negative charge (-).The proportion of surface charge was calculated using equations 1 and 2.

samples, the mass spectra of protein-mineral samples had to be scrutinized for unique signals that were not present in the mineral-buffer samples and only found in protein-containing samples (Figure 2.3E-2.3L).

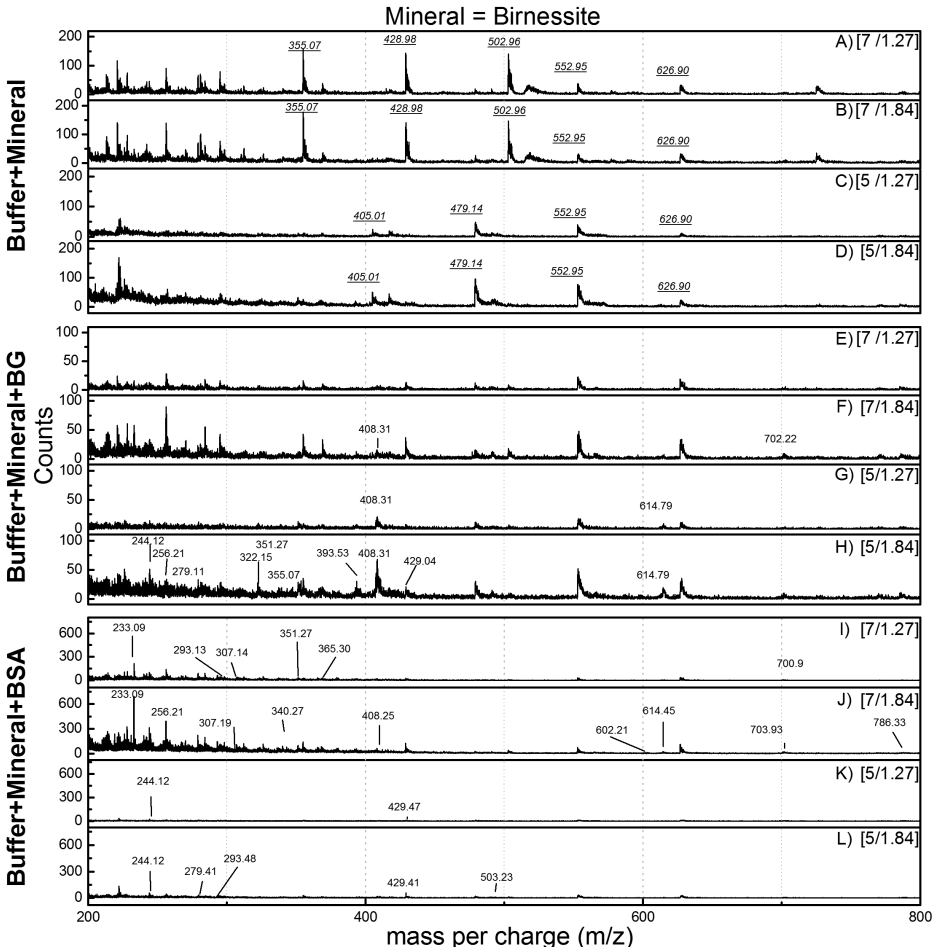

Figure 2.3: Mass spectra from birnessite+buffer samples (A-D) were compared to protein+birnessite+buffer samples (E-L) to identify the presence of peaks only found in protein containing samples between 200-800 mass per charge (m/z). Spectra were annotated with the pH on the left side in the brackets and the energy applied at the right side. For example, samples with pH 5 at energy applied 1.27 $MWcm^{-2}$ are designated [5/1.27]. Peaks highlighted in birnessite samples containing Bovine Serum Albumin (BSA) and Beta-Glucosidase (BG) are unique peaks that are not found in birnessite buffer samples or have higher signal intensity than birnessite-buffer peaks. Peaks from birnessite buffer samples were underlined. Mass spectra shown here are from the two highest energy applications

2.4.3 The abundance of fragmentation products as a function of energy applied

It was possible to release compounds into the gas phase and subsequently ionize them using VUV radiation at all levels of energy input (0.05-1.84 $MWcm^{-2}$). Total ion counts from mineral and protein phases generally increased with higher energy application, with some exceptions (Table 2.3). Unique signals from protein containing birnessite samples were not detected at energies below 0.20 $MWcm^{-2}$ (Figure S4). Application of 1.28 $MWcm^{-2}$ to BG samples at pH 7 did not generate unique signals from protein samples. When the laser energy was increased from 1.28 $MWcm^{-2}$ to 1.84 $MWcm^{-2}$, unique signals at 408.31 m/z and 707.22 m/z appeared from BG at pH 7 (Figure 2.3F). For BG-birnessite samples at pH 5, increasing the energy level did increase the signal abundance of unique masses arising from protein containing samples (Figure 2.3G-H). The mass spectrum generated after applying 1.28 MW cm-2 to BSA adsorbed onto birnessite at pH 7 contained unique signals between 233.09 to 700.9 m/z (Figure 2.3A). When the energy was increased to 1.84 $MWcm^{-2}$, new signals between 602.21 to 786.33 m/z appeared in BSA-birnessite samples adsorbed at pH 7 (Figure 2.3B). The BSA-birnessite-pH5 combination returned unique signals at 244.26 m/z and 429.47 m/z when 1.28 $MWcm^{-2}$ of energy was applied (Figure 2.3C). Higher energy applications increased the unique signal abundance of the BSA-birnessite-pH 5 combination (Figure 2.3D). In general, increasing the energy application to BG- and BSA-birnessite samples adsorbed at pH 5 increased the signal abundance detected and

the signal intensity of some peaks.

2.4.4 Protein fragmentation patterns differ between mineral surfaces

Most ionized compounds from protein-mineral samples were detected within a range of 0 to 1500 mass per charge (m/z). Signal intensities returned from protein-birnessite combinations were significantly higher than those obtained from proteins adsorbed to kaolinite or Si wafer surfaces, which did not generate signal intensities above the noise level unless subjected to an energy density of 1.84 $MWcm^{-2}$. For this reason, all comparisons between protein-mineral combinations (Figure S5) were performed at that energy level. The maximum count intensities in the mass spectra generated for Si wafer and kaolinite samples were lower than 100 counts. But, depending on adsorption pH and type of protein, birnessite-protein samples returned ion counts with intensities between 800 to 3600.

2.4.5 Fragmentation does not depend on protein size

Neither signal abundance nor total ion counts were a function of protein size. Mass spectra obtained from protein-birnessite combinations at power densities above 0.20 $MWcm^{-2}$ were the only ones that had unique signals above the noise level. Among samples that had been adsorbed at pH 5, BG (135 kDa)-birnessite specimens generated higher total ion counts (TIC) than BSA (66.5 kDa)-birnessite

Energy Applied	Inverse Energy Applied	Beta Glucosidase		Bovine Serum Albumin	
$(MWcm^2)$	$(1/MWcm^2)$	pH 5	pH 7	pH 5	pH 7
0.05	19.4	6355	1987	4493	472
0.06	16.2	4852	2873	3532	493
0.07	14.0	5320	2318	3515	538
0.08	12.5	5083	2589	3769	670
0.09	11.1	5267	2151	4295	724
0.16	6.3	5728	2862	2289	884
0.20	4.9	6507	2677	2487	921
0.68	1.5	15,200	7684	6580	20,695
1.27	0.8	78,667	80,700	47,871	334,470
1.86	0.5	317,420	315,000	19,916	1,147,200

Table 2.3: Comparison between total ion counts of Beta-Glucosidase and Bovine Serum Albumin samples detected off Birnessite at pH 5 and pH 7 with increasing energy applied.

samples (Table 2.3). At an adsorption pH of 7, BG-Birnessite TIC were higher than BSA-Birnessite at energy levels below 0.68 $MWcm^{-2}$ (Table 2.3). Above this energy, the smaller protein (BSA) generated greater total ion counts than the larger protein (BG). The BSA-birnessite samples showed greater unique signal abundance than BG-birnessite samples at pH 7 (Figure 2.3). Only at the highest energy application did BG-birnessite specimens prepared at pH 5 surpass the unique signal abundance of BSA-Birnessite samples made at the same pH.

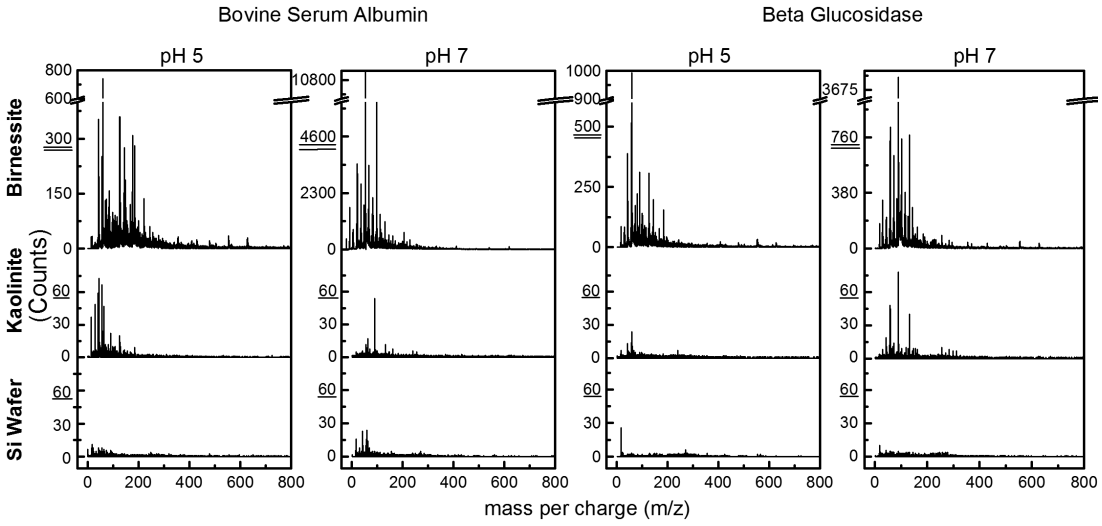

Figure 2.4: Comparison between mass spectra from Beta-Glucosidase (BG) and Bovine Serum Albumin (BSA) desorbed off Birnessite (top), Kaolinite (center) and Si wafer (bottom) at pH 5 and pH 7. Energy applied to all samples was 1.84 $MWcm^{-2}$. Breaks were at added at 85 percent of the scale to focus on peaks not from the buffers. The x-axis includes data from 0-800 m/z.

2.4.6 pH dependence of protein fragmentation

The only samples that had greater signal abundance at an acidic adsorption pH were BG-birnessite; for BSA-birnessite the signal abundance at pH 7 was greater than that at pH 5. BG adsorbed at pH 5 yielded greater TIC than BG adsorbed at pH 7, as energy was held constant (Table 3). We also noticed the presence of unique signals in the BG-birnessite mass spectrum at pH 5 that were not present in spectra from pH 7 specimens (Figure 2.3E-2.3H). In BSA-Birnessite samples, TIC was higher for samples prepared at pH 5 than for those made at pH 7 when the energy levels were below 0.20 $MWcm^{-2}$, but these total ion counts were primarily made up of signals from the buffer and birnessite. The TIC from BSA-birnessite samples at pH 7 surpassed TIC from samples at pH 5 when energy levels reached 0.20 $MWcm^{-2}$. At 1.28 and 1.84 $MWcm^{-2}$, BSA-birnessite specimens produced higher unique signal intensities at pH 7 than pH 5 (Figure 2.3A-3D).

2.4.7 Total ion counts as a function of power density

On all three surface types, adsorbed protein generated largely similar total ion counts (TIC) as long as power densities were below 0.20 $MWcm^{-2}$. Protein-birnessite combinations showed an exponential increase in total ion counts when power density was increased beyond 0.20 $MWcm^{-2}$. Once energy applications surpassed that threshold, TIC from birnessite was generally higher than from kaolinite samples or Si wafer samples within the same energy level (Figure 2.5). In samples containing only birnessite with buffer added, we observed an exponential increase

of TIC with increasing energy (Figure 2.5). The TIC from kaolinite controls (mineral plus buffer, no protein) were much lower than the TIC from birnessite controls. For protein-birnessite at pH 5, higher TIC was detected than from birnessite controls. At pH 7, TIC from the birnessite control was mostly higher than TIC from protein-birnessite TIC with the exception of the birnessite-BSA combination at pH 7. Once an energy threshold of 0.20 $MWcm^{-2}$ was reached, TIC from BSA birnessite samples at pH 7 was higher than the TIC from the birnessite control and the TIC from the BG-Birnessite combination at pH 7. Adsorption of proteins on the surface of kaolinite samples and subsequent exposure to a gradient of laser energies actually decreased the TIC in comparison to the TIC from the kaolinite control. This occurred regardless of pH or energy applied. The TIC detected from proteins added to polished Si wafers increased with application of laser energy. The TIC for protein-Si wafer combinations was similar between proteins and pH with the exception of BSA at pH 5. There was a decrease in TIC when laser energy went below 0.20 $MWcm^{-2}$ for the BSA-Si wafer combination for pH 5 samples. TIC from Si wafer combinations were similar in magnitude to TIC from kaolinite samples. Overall, protein-birnessite combinations had much higher TIC than protein-kaolinite or protein-Si wafer combinations when applying energy above the 0.20 $MWcm^{-2}$ threshold.

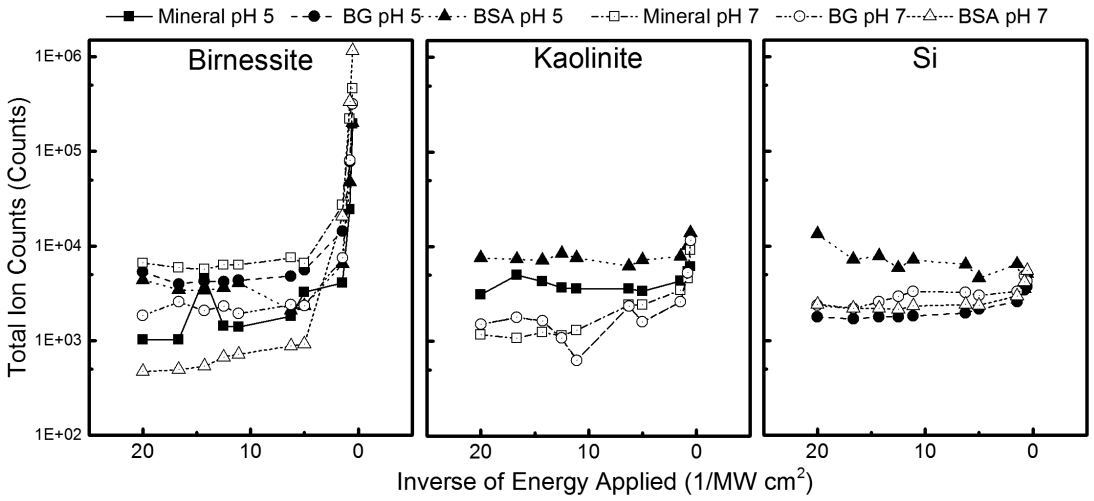

Figure 2.5: Total Ion counts of samples on birnessite (left), kaolinite (middle), and Si wafer (right). Mineral samples (square) indicate either birnessite, or kaolinite with only buffer at pH 5 (closed) and pH 7 (open). X-axis arranged to show increasing application of energy towards the right. TIC below energy threshold show linear trend on log10 y-axis. After 0.2 $MWcm^{-2}$, exponential increase of TIC observed.

2.5 Discussion

2.5.1 Adsorption mechanisms and protein fragmentation are mineral dependent

The extent of charge overlap predicted protein adsorption in kaolinite and in birnessite. In kaolinite samples, more protein was adsorbed when protein and mineral had like charges, in birnessite, the opposite was observed (Figure 2.2A,B). This apparent contradiction can be rationalized by considering significant differences in surface charge characteristics and the surface area between these minerals (Table

2.1). Birnessites have a larger reservoir of negative charge on their surface, between 63 to 240 $cmol_c\ kg^{-1}$, compared to kaolinites reservoir of 3.0 $cmol_c\ kg^{-1}$ (Golden et al., 1986; Borden and Giese, 2001). Kaolinite contains very little permanent negative charge on its basal siloxane surface. The siloxane surface of kaolinite has greater hydrophobic character than that of other phyllosilicates (Jaynes and Boyd, 1991). This hydrophobic character was found to be responsible for the irreversible adsorption of operationally defined humic substances onto kaolinite (Balcke et al. 2002). We did not expect a significant relationship between (α) and q since the siloxane basal planes of kaolinite should favor hydrophobic interactions. This presumption was corroborated by the observation that, when conditions favor electrostatic attraction, protein adsorption to kaolinite decreases. Birnessite, on the contrary, showed evidence for a positive correlation between q and α, indicating that for this mineral, electrostatic interactions exert greater control on protein adsorption than hydrophobic interactions.

The appearance of unique signals from protein-mineral combinations is interpreted as evidence of protein fragmentation. Such signals were observed in acid birnessite samples but not in kaolinite samples, making protein fragmentation mineral dependent as well. Past research has identified birnessite as a sorbent for protein (Naidja et al., 2002), but more recent evidence has shown birnessite can break apart proteins in acidic aqueous systems (Russo et al. 2009) and generate peptide fragments less than 1000 Da (Reardon et al. 2016). In contrast, kaolinite functions as a sorbent even after energy applications that simulate intense forest fires. Our research emphasizes the importance of both pH (greater mineral reactivity with

lower pH) and energy input (change from passive sorbent to chemical reactant) for the overall reactivity of birnessite.

2.5.2 Birnessite is more susceptible to disintegration than kaolinite

Contrary to kaolinite controls (kaolinite plus buffer, no protein), birnessite controls (birnessite plus buffer, no protein) responded to energy input with the production of signals that were tentatively identified as organomanganese complexes (see Supplemental Information). This phenomenon can be rationalized by considering the significantly lower threshold of birnessite to transform into different minerals. Temperatures must reach 550°C before dehydroxylation occurs in kaolinite and 1000°C until it transforms into the aluminum oxide Mullite (Insley and Ewell, 1935; Glass, 1954). In contrast, the dehydration of the birnessite surface and interlayers occurs between the temperatures of 25-200°C, which can modify the layered structure (Ghodbane et al., 2010). The breakdown of birnessite at higher energies suggests that its role in the high temperature reaction is no longer that of the catalyst it was in low temperature, aqueous environments. We deduce that high laser energies change the effect of the mineral birnessite towards proteins from that of a sorbent surface with some catalytic capabilities in aqueous low temperature systems (Reardon et al. 2016, Russo et al. 2009) to that of a chemical reactant. The energetic threshold for this conversion seems to be in the vicinity of 0.2 $MWcm^{-2}$. The susceptibility of birnessite to disintegrate after applying increasing amounts of energy was muted in the presence of protein, suggesting that association with

organic matter can protect metastable minerals in high-intensity fires.

2.5.3 Energy dependence of fragmentation shows a threshold

The energy range of 0.20-1.84 $MWcm^{-2}$ used in our experiments was chosen to be equivalent to natural energy inputs as they may occur in any fire-prone ecosystem (Table S2.3; (Alexander and Cruz, 2012). The signal abundance and total ion counts of all protein-mineral combinations were dependent on the applied power density. In previous work, the LDPI-MS technique was able to detect fragments from medium-sized molecules such as antibiotics and proteins, and collections of compounds such as biofilms (Gasper et al., 2010; Blaze et al., 2011); even nearly intact DNA and RNA were detected despite the fact that those molecules were subjected to internal temperatures above 397°C (Kostko et al., 2011). This can be taken to indicate that little fragmentation should be expected in a vacuum even at high-energy applications unless the mineral support surface acts as either catalyst or reactant towards the sorbate. We observed an energy threshold at 0.20 $MWcm^{-2}$ where TIC increased exponentially for birnessite samples and the concomitant appearance of unique protein fragmentation products. These products were not observed in kaolinite samples. This indicates that we did not apply enough energy to observe the threshold phenomena in the kaolinite samples. Energy input apparently also controls the reaction mechanism between the protein and birnessite: At low energy/temperature and circumneutral pH, birnessite may just act as a sorbent. With decreasing pH, but still at low energy/temperature, bir-

nessite becomes a catalyst for the hydrolysis of protein. With energy inputs above a threshold value corresponding to 0.2 $MWcm^{-2}$, the birnessite crystal structure begins to break apart and the mineral changes its role again to become a reactant forming Mn-organic compounds. Protein interactions with kaolinite show minor energy dependence but significant variation between individual proteins and as a function of pH.

2.5.4 The dominant protein fragmentation mechanism shifts away from hydrolysis

The unique signals found in the mass spectra of protein-birnessite samples did not match hydrolysis reaction products of BSA and BG. Previous studies have demonstrated birnessites capacity to oxidize biomolecules (Laha and Luthy, 1990) and catalytically cleave proteins through hydrolysis (Reardon et al. 2016). We were interested in determining if hydrolysis was still the mechanism responsible for fragmentation of a sorbed protein under dry conditions. If birnessite breaks apart proteins through hydrolysis, the cleavage would be between the amide bonds, generating recognizable peptides and amino acids. But if birnessite oxidizes proteins, the products would not match the hydrolysis byproducts. Protein oxidation could occur through a multitude of pathways that can generate cross-linked proteins, oxidized side chains, carbonylation and fragmentation products that do not align with hydrolysis products (Berlett and Stadtman, 1997). A list of masses generated by hydrolytic cleavage of BSA and BG by Proteinase K, a broad cleavage

activity enzyme, was compiled to compare them to the unique masses found in Figure 2.3. There were only 4 close matches between the unique signals detected from the dry BSA-birnessite samples and the hydrolysis products. These matches were within a m/z difference of less than 0.11 m/z. The other 14 unique masses did not match hydrolysis products, even after accounting for subsequent oxidation of aromatic side chains (Table S2.5). It is possible that some hydrolyzed peptides found in the supernatant by Reardon et al. (2016) could have been removed when we pipetted out the supernatant. Our inference is thus restricted to the fate of residual protein or peptides on the mineral surfaces and not to the peptides released into solution as detected by Reardon et al. (2016). The addition of energy to protein-birnessite samples may begin to shift the mechanism of fragmentation from hydrolysis in low energy and aqueous systems to an oxidative reactant under dry conditions.

2.5.5 Greater protein size does not lead to more fragmentation products

We found protein size did not control the amount of fragmentation products or total ion counts after interaction with a reactive mineral surface. Based on a known positive linear relationship between protein adsorption and the molecular mass of a protein (Harter and Stotzky, 1971) we initially hypothesized that larger proteins would mean more extensive contact with the mineral surface. The more amino acids in contact with the surface, the greater amounts of fragmentation we

expected to observe. Surprisingly, the combination of the smaller protein BSA with birnessite at pH 7 had the lowest amount of protein adsorbed but the highest TIC and unique fragmentation product signals.

2.5.6 Acidic pH enhances fragmentation of BG by birnessite

A low adsorption pH enhanced unique signal intensity and total ion counts for beta-glucosidase (BG) samples but not for Bovine Serum Albumin (BSA). For BG containing samples, fragmentation by birnessite was greater at pH 5 than at pH 7, which is in line with previous observations (Russo et al. 2009; Reardon et al. 2016). Enhanced reactivity of birnessite at acidic pH may be facilitated by increased positive charge of amide functional groups aiding in electrostatic attraction (Laha et al. 1990). But the detection of greater TIC and unique signal abundances at 1.84 $MWcm^{-2}$ for BSA samples at pH 7 than pH 5 contrasts previous observations in protein-birnessite studies. We have no immediate mechanistic explanation for this phenomenon and suggest that it be examined in future investigations.

2.6 Conclusions

A common view of enzyme-mineral interactions in soil is that of a preserving "immobilization" of the enzyme by the mineral matrix. Probably the most significant outcome of our investigation is the insight that protein behavior at mineral surfaces cannot easily be generalized across different minerals. The fate of two proteins dif-

fering in mass and surface charge properties was observed to vary individually and as a function of pH, mineral type and energy applied. On kaolinite (ubiquitous phyllosilicate in most soils of the planet), both of the proteins investigated here adsorbed largely through mechanisms other than electrostatic interactions and showed little evidence that their overall response to experimental treatments was significantly modified by the sorbent surface. On birnessite, initial adsorption was encouraged by electrostatic interactions. Individual proteins responded differently to the birnessite surface but here their response included fragmentation, whose extent was modified by pH and the magnitude of energy input. Complicating matters further, birnessite appears to change its role in the interaction from sorbent surface over catalyst to chemical reactant, depending on the pH and the energetic status of the system. Proteins adsorbed on kaolinite will remain intact after exposure to energy inputs comparable to natural wildfires, while fragmentation and subsequent loss of protein functionality is expected in surface soils replete with pedogenic manganese oxides. Thus, a 'fire-activated' mineral matrix may contribute to the loss of extracellular enzyme function until microorganisms have recolonized the soil. At the same time, a fire activated matrix containing manganese oxides will be able to abiotically react and so may be responsible for previous observations (Bach et al., 2013; Blankinship et al., 2014) of a significant ability of thermally treated soils to break down organic substrates.

2.7 References

Alexander, M.E., Cruz, M.G., 2012. Interdependencies between flame length and fireline intensity in predicting crown fire initiation and crown scorch height. International Journal of Wildland Fire 21, 95-113. Allison, S.D., 2006. Soil minerals and humic acids alter enzyme stability: implications for ecosystem processes. Biogeochemistry 81, 361-373.

Bach, C.E., Warnock, D.D., Van Horn, D.J., Weintraub, M.N., Sinsabaugh, R.L., Allison, S.D., German, D.P., 2013. Measuring phenol oxidase and peroxidase activities with pyrogallol, L-DOPA, and ABTS: Effect of assay conditions and soil type. Soil Biology and Biochemistry 67, 183-191.

Balcke, G.U., Kulikova, N.A., Hesse, S., Kopinke, F.D., Perminova, I.V., Frimmel, F.H., 2002. Adsorption of humic substances onto kaolin clay related to their structural features. Soil Science Society of America Journal 66, 1805-1812.

Baldock, J.A., Skjemstad, J.O., 2000. Role of the soil matrix and minerals in protecting natural organic materials against biological attack. Organic Geochemistry 31, 697-710.

Basile-Doelsch, I., Amundson, R., Stone, W.E.E., Borschneck, D., Bottero, J.Y., Moustier, S., Masin, F., Colin, F., 2007. Mineral control of carbon pools in a volcanic soil horizon. Geoderma 137, 477-489. Berlett, B.S., Stadtman, E.R., 1997. Protein oxidation in aging, disease, and oxidative stress. Journal of Biological Chemistry 272, 20313-20316.

Blankinship, J.C., Becerra, C.A., Schaeffer, S.M., Schimel, J.P., 2014. Sepa-

rating cellular metabolism from exoenzyme activity in soil organic matter decomposition. Soil Biology and Biochemistry 71, 68-75.

Blaze, M.T.M., Takahashi, L.K., Zhou, J., Ahmed, M., Gasper, G.L., Pleticha, F.D., Hanley, L., 2011. Brominated tyrosine and polyelectrolyte multilayer analysis by laser desorption vacuum ultraviolet postionization and secondary ion mass spectrometry. Analytical chemistry 83, 4962-4969.

Borden, D., Giese, R.F., 2001. Baseline studies of The Clay Minerals Society Source Clays: Cation exchange capacity measurements by the ammonia-electrode method. Clays and Clay Minerals 49, 444-445.

Boyd, S.A., Mortland, M.M., 1990. Enzyme interactions with clays and clay-organic matter complexes. Soil biochemistry 6, 1-128.

Byram, G.M., 1959. Combustion of forest fuels, In: Davis, K.P. (Ed.), Forest Fire: Control and Use. McGraw Hill, New York.

Craig, O.E., Collins, M.J., 2002. The removal of protein from mineral surfaces: Implications for residue analysis of archaeological materials. Journal of Archaeological Science 29, 1077-1082.

Doetterl, S., Stevens, A., Six, J., Merckx, R., Van Oost, K., Casanova Pinto, M., Casanova-Katny, A., Munoz, C., Boudin, M., Zagal Venegas, E., Boeckx, P., 2015. Soil carbon storage controlled by interactions between geochemistry and climate. Nature Geoscience 8, 780-783.

Dungait, J.A.J., Hopkins, D.W., Gregory, A.S., Whitmore, A.P., 2012. Soil organic matter turnover is governed by accessibility not recalcitrance. Global Change Biology 18, 1781-1796.

Fiorito, T.M., Icoz, I., Stotzky, G., 2008. Adsorption and binding of the transgenic plant proteins, human serum albumin, -glucuronidase, and Cry3Bb1, on montmorillonite and kaolinite: Microbial utilization and enzymatic activity of free and clay-bound proteins. Applied Clay Science 39, 142-150.

Gasper, G.L., Takahashi, L.K., Zhou, J., Ahmed, M., Moore, J.F., Hanley, L., 2010. Laser desorption postionization mass spectrometry of antibiotic-treated bacterial biofilms using tunable vacuum ultraviolet radiation. Analytical chemistry 82, 7472-7478.

Ghodbane, O., Pascal, J.L., Fraisse, B., Favier, F., 2010. Structural in situ study of the thermal behavior of manganese dioxide materials: toward selected electrode materials for supercapacitors. Applied Materials and Interfaces 2, 3493-3505.

Glass, H.D., 1954. High-temperature phases from kaolinite and halloysite. American Mineralogist 39, 193-207. Golden, D.C., Dixon, J.B., Chen, C.C., 1986. Ion-exchange, thermal transformations, and oxidizing properties of birnessite. Clays and Clay Minerals 34, 511-520.

Grover, A.K., Macmurchie, D.D., Cushley, R.J., 1977. Studies on almond emulsin beta-D-glucosidase. I. Isolation and characterization of a bifunctional isozyme. Biochimica et biophysica acta 482, 98-108.

Harter, R.D., Stotzky, G., 1971. Formation of clay-protein complexes. Soil Science Society of America Proceedings 35, 383.

Hirayama, K., Akashi, S., Furuya, M., Fukuhara, K., 1990. Rapid confirmation and revision of the primary structure of bovine serum albumin by ESIMS and frit-

FAB LC/MS. Biochemical and Biophysical Research Communications 173, 639-646.

Insley, H., Ewell, R.H., 1935. Thermal behavior of the kaolin minerals. Journal of Research of NIST 14, 615-627.

Jaynes, W.F., Boyd, S.A., 1991. Hydrophobicity of siloxane surfaces in smectites as revealed by aromatic hydrocarbon adsorption from water. Clays and Clay Minerals 39, 428-436.

Kemmitt, S.J., Lanyon, C.V., Waite, I.S., Wen, Q., Addiscott, T.M., Bird, N.R.A., O'Donnell, A.G., Brookes, P.C., 2008. Mineralization of native soil organic matter is not regulated by the size, activity or composition of the soil microbial biomass - a new perspective. Soil Biology and Biochemistry 40, 61-73.

Kostko, O., Takahashi, L.K., Ahmed, M., 2011. Desorption dynamics, internal energies, and imaging of organic molecules from surfaces with laser desorption and vacuum ultraviolet (VUV) photoionization. Chemistry, an Asian journal 6, 3066-3076.

Laha, S., Luthy, R.G., 1990. Oxidation of aniline and other primary aromatic-amines by manganese-dioxide. Environmental Science and Technology 24, 363-373.

Liu, S.Y., Kleber, M., Takahashi, L.K., Nico, P., Keiluweit, M., Ahmed, M., 2013. Synchrotron-based mass spectrometry to investigate the molecular properties of mineral-organic associations. Analytical chemistry 85, 6100-6106.

Liu, S.Y., Shawkey, M.D., Parkinson, D., Troy, T.P., Ahmed, M., 2014. Elucidation of the chemical composition of avian melanin. Rsc Advances 4, 40396-40399.

Malamud, D., Drysdale, J.W., 1978. Isoelectric points of proteins: a table.

Analytical Biochemistry 86, 620-647.

Marin-Spiotta, E., Swanston, C.W., Torn, M.S., Silver, W.L., Burton, S.D., 2008. Chemical and mineral control of soil carbon turnover in abandoned tropical pastures. Geoderma 143, 49-62.

Mckenzie, R.M., 1981. The surface-charge on manganese dioxides. Australian Journal of Soil Research 19, 41-50.

Miltner, A., Zech, W., 1999. Microbial degradation and resynthesis of proteins during incubation of beech leaf litter in the presence of mineral phases. Biology and Fertility of Soils 30, 48-51.

Naidja, A., Liu, C., Huang, P.M., 2002. Formation of protein-birnessite complex: XRD, FTIR, and AFM analysis. Journal of Colloid and Interface Science 251, 46-56.

Norde, W., 2008. My voyage of discovery to proteins in flatland ...and beyond. Colloids and Surfaces B: Biointerfaces 61, 1-9.

Putnam, F.W., 1975. The plasma proteins : structure, function, and genetic control, 2d. ed. Academic Press, New York.

Quiquampoix, H., 2008. Interaction with soil constituents determines the environmental impact of proteins. Journal of Soil science and Plant Nutrition 8, 75-83.

Quiquampoix, H., Abadie, J., Baron, M.H., Leprince, F., MatumotoPintro, P.T., Ratcliffe, R.G., Staunton, S., 1995. Mechanisms and consequences of protein adsorption on soil mineral surfaces. Proteins at Interfaces II 602, 321-333.

Rasmussen, C., Southard, R.J., Horwath, W.R., 2006. Mineral control of or-

ganic carbon mineralization in a range of temperate conifer forest soils. Global Change Biology 12, 834-847.

Reardon, P.N., Chacon, S.S., Walter, E.D., Bowden, M.E., Washton, N.M., Kleber, M., 2016. Abiotic protein fragmentation by manganese oxide: implications for a mechanism to supply soil biota with oligopeptides. Environmental Science and Technology 50, 3486-3493.

Russo, F., Johnson, C.J., Johnson, C.J., McKenzie, D., Aiken, J.M., Pedersen, J.A., 2009. Pathogenic prion protein is degraded by a manganese oxide mineral found in soils. Journal of General Virology 90, 275-280.

Sander, M., Madliger, M., Schwarzenbach, R.P., 2010. Adsorption of transgenic insecticidal Cry1Ab protein to SiO2. 1. Forces driving adsorption. Environmental Science and Technology 44, 8870-8876.

Schmidt, M.W., Torn, M.S., Abiven, S., Dittmar, T., Guggenberger, G., Janssens, I.A., Kleber, M., Kogel-Knabner, I., Lehmann, J., Manning, D.A., Nannipieri, P., Rasse, D.P., Weiner, S., Trumbore, S.E., 2011. Persistence of soil organic matter as an ecosystem property. Nature 478, 49-56.

Schroth, B.K., Sposito, G., 1997. Surface charge properties of kaolinite. Clays and Clay Minerals 45, 85-91. Stone, A.T., 1987. Reductive dissolution of manganese(III/IV) oxides by substituted phenols. Environmental Science and Technology 21, 979-988.

Sunda, W.G., Kieber, D.J., 1994. Oxidation of humic substances by manganese oxides yields low-molecular-weight organic substrates. Nature 367, 62-64.

Torn, M.S., Kleber, M., Zavaleta, E.S., Zhu, B., Field, C.B., Trumbore, S.E.,

2013. A dual isotope approach to isolate soil carbon pools of different turnover times. Biogeosciences 10, 8067-8081.

Torrents, A., Stone, A.T., 1993. Catalysis of picolinate ester hydrolysis at the oxide water interface - inhibition by coadsorbed species. Environmental Science and Technology 27, 1060-1067.

Villalobos, M., Toner, B., Bargar, J., Sposito, G., 2003. Characterization of the manganese oxide produced by Pseudomonas putida strain MnB1. Geochimica et Cosmochimica Acta 67, 2649-2662.

Yan, J., Pan, G., Li, L., Quan, G., Ding, C., Luo, A., 2010. Adsorption, immobilization, and activity of beta-glucosidase on different soil colloids. Journal of colloid and interface science 348, 565-570.

2.8 Appendix for Chapter 2

2.8.1 Schematic of LDPI-MS Setup at 9.0.2 Beamline of the Advanced Light Source

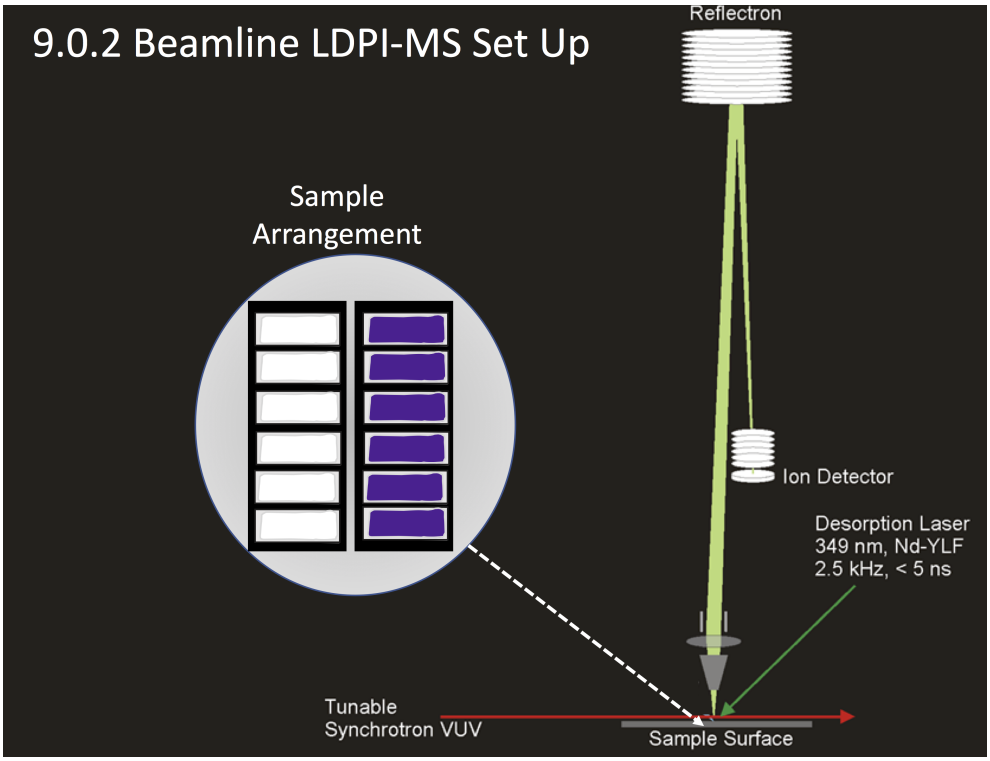

Figure 2.6: The Laser Desorption Post Ionization Set up at the 9.0.2 Beamline uses a laser to desorb a sample from the surface (green arrow). The desorbed sample is ionized using tunable synchrotron vacuum ultraviolet (VUV) radiation and detected with a mass spectrometer.

2.8.2 Laser Application of Protein-Mineral Samples

A 349 nm Nd:YLF laser with a focus spot of 15 m was used to irradiate the sample at 8.5 ns pulses using linear raster scanning over 18 mm at a rate of 2 mms^{-1} with the laser at varying energy levels (Figure S2). The rastering schematic is shown below. The laser rastered over the protein-mineral sample dried on a silicon wafer at 0.05 $MWcm^{-2}$, the desorbed sample was then ionized by VUV radiation. The sample was shifted upward to begin the second energy application, below the first laser scan. This was done for all the ten energy applications

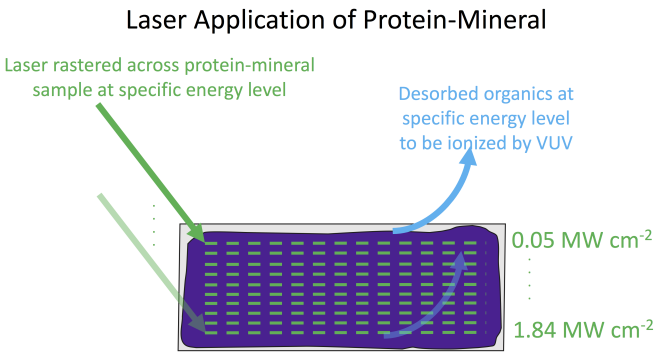

Figure 2.7: Laser energies on the protein-mineral sample was applied by rastering the laser across the sample and ionizing the compounds desorbed. Once the ions were desorbed and detected, the next energy application followed below the previous laser raster. The energy increased from top to bottom

2.8.3 Prolonged Salt Titration (PST) Method for Determining Point of Zero Charge (PZC)

Determination of PZC of acid birnessite and kaolinite was done with the Prolonged Salt Titration method reported by Tan et al. (2008). Birnessite and kaolinite were mixed with MilliQ water at a 0.25 g: 5mL ratio. The acid birnessite samples were adjusted with HCl to a pH range of 0.5 to 2.5, while the kaolinite samples were adjusted to a range of pH 3 to 6. The samples were run in triplicate at every pH value and equilibrated for 72 hours at 25°C and shaken for 1 hour per day. The suspensions were centrifuged at 11,700 rcf and the pH values of the supernatant were measured and denoted as the initial pH (pHi). The suspensions were then amended with 0.25 ml of 2 M KCl. After 24 hrs of shaking (28 h total), samples were centrifuged again and the pH values of the supernatant were measured and denoted as final pH (pHf). The pH values were corrected for changes in the ionic activity coefficient after addition of KCl (0.1 M) and converted to its equivalent pH at no added salt, (pHf*) using the activity coefficient of f0.1 = 0.78, which was derived from the modified Davies equation (Davies, 1962). The PZC was obtained from the plot of pH (pHf* - pHi) against pHi as the point where pH was equal to zero. A polynomial curve was fitted to the data collected. Data for kaolinite was originally published in Reardon et al. (2016).

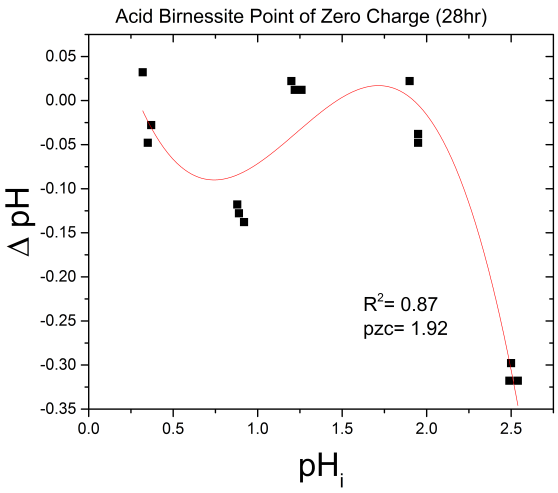

Figure 2.8: Point of zero charge was determined for acid birnessite by fitting a polynomial curve (red) and determining when Delta pH was equal to zero.

2.8.4 Adsorption of proteins on birnessite and kaolinite

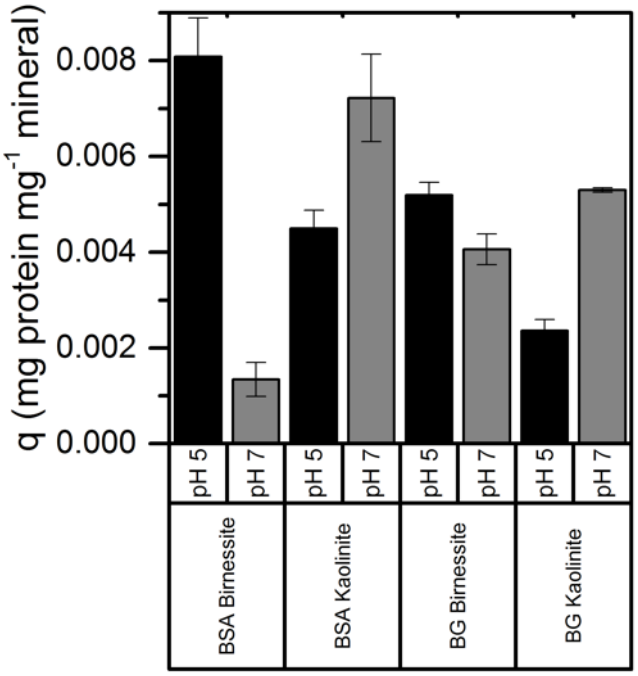

Figure 2.9: Amount of Bovine Serum Albumin (BSA) and Beta-Glucosidase (BG) adsorbed onto Birnessite and Kaolinite. The adsorption conditions were 100 mM sodium acetate pH 5 (black) and 100 mM Tris pH 7 (grey).

2.8.5 Total Ion Counts as a function of energy applied for mineral-buffer samples and protein-mineral samples

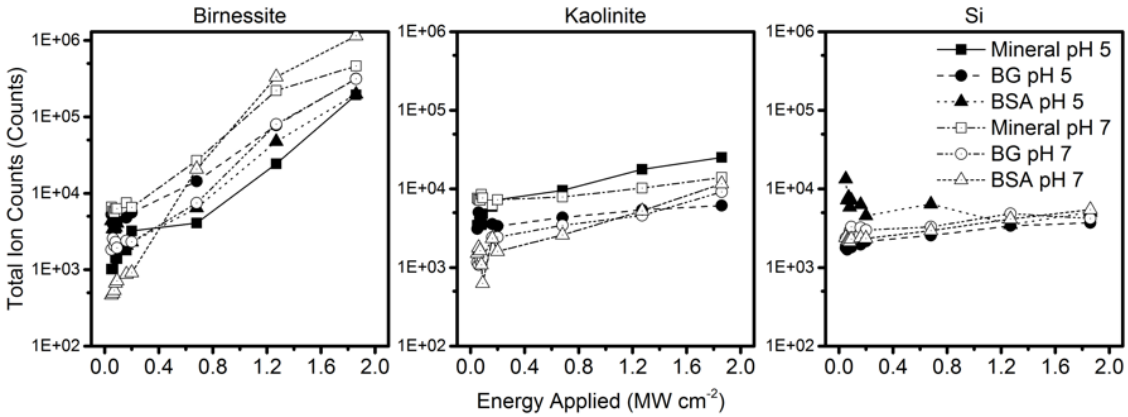

Figure 2.10: Comparison of total ion counts (TIC) as a function of energy. The X-axis was not modified as in Figure 5, which condenses low energy application and emphasizes higher energies. The TIC detected as a function of laser energy applied or power density to Birnessite (left), Kaolinite (middle) and Si wafer (right). Squares represent mineral with just buffer. Samples with BG and buffer are circles, and BSA with buffer is represented with triangles. Closed symbols are pH 5 and open symbols are pH 7.

2.8.6 Multivariable linear regression analysis results for protein adsorption

Results of multivariable linear regression in Table S3.1

Independent Variable:Protein Adsorbed (q)	Parameter	R^2	P-value	Intercept	Slope 1	Slope 2
Kaolinite and Birnessite	α	-0.003	0.3475	5.18E-0.3	-1.12E-05	-
	ν	0.065	0.1207	5.63E-03	-6.85E-04	-
	$\alpha + \nu$	0.070	0.1803	6.9E-03	-1.18E-05	-6.99E-04
Birnessite only	α	-0.045	0.484	3.91E-03	1.43E-05	-
	ν	0.266	0.050	6.54E-03	-1.39E-03	-
	$\alpha + \nu$	0.236	0.121	5.89E-03	1.31E-05	-1.38E-03
Kaolinite only	α	0.693	4.75E-04	6.69E-03	-4.13E-05	-
	ν	-0.097	0.882	4.86E-03	-8.33E-03	-
	$\alpha + \nu$	0.6619	0.003	5.89E-03	1.31E-05	-1.38E-03

Table 2.4: Multivariable linear regression models testing protein adsorption (dependent variable) with independent variables parameterizing electrostatic interactions such as opposite charge overlap (α) and conformational change (ν)

2.8.7 Presence of large masses for birnessite-buffer samples

Signals from birnessite-buffer samples show masses larger than the parent mass signal for the buffers added. In order to elucidate the possible compositions for each signal, we used Formula Finder function in the Molecular Weight Calculator from Pacific Northwest National Laboratory.

Table 2.5: Elemental compositions for signals found in birnessite-buffer samples. Elements used 102 in Formula Finder were chosen based of the composition of birnessite and the buffers used..

Formula	Molecular Weight (Da)	Difference in Mass	Mass per charge (m/z)
355.07 m/z			
C3H21K3MnN91+	355.0211526	-0.0488474	355.021
C11H28Mn3NO1+	355.0312158	-0.0387842	355.031
C2H16K2MnN131+	355.0306176	-0.0393824	355.031
C16H3N8O31+	355.0328108	-0.0371892	355.033
C11H28K51+	355.0376288	-0.0323712	355.038
CH19K4N121+	355.0403874	-0.0296126	355.04
C5H20K2MnN9O1+	355.044535	-0.025465	355.045
C14H17K2N2O41+	355.0462422	-0.0237578	355.046

Continued on next page

Table 2.5 – continued from previous page

Formula	Molecular Weight (Da)	Difference in Mass	Mass per charge (m/z)
C10H23K4N41+	355.0470938	-0.0229062	355.047
C14H19KMnN3O21+	355.0494734	-0.0205266	355.049
C9H26KMn2N4O1+	355.0504506	-0.0195494	355.05
C14H21Mn2N41+	355.0527046	-0.0172954	355.053
C12H32Mn3N1+	355.0675992	-0.0024008	355.068
C17H7N8O21+	355.0691942	-0.0008058	355.069
C7H24K2MnN7O1+	355.0696854	-0.0003146	355.07
C2H18K3N141+	355.0750028	0.0050028	355.075
C10H16KN6O61+	355.0768356	0.0068356	355.077
C15H21K2N2O31+	355.0826256	0.0126256	355.083
C15H23KMnN3O1+	355.0858568	0.0158568	355.086
C10H30KMn2N41+	355.086834	0.016834	355.087
C5H22K3N10O1+	355.0889202	0.0189202	355.089
C9H25Mn2N81+	355.096299	0.026299	355.096
C18H11N8O1+	355.1055776	0.0355776	355.106
C8H28K2MnN71+	355.1060688	0.0360688	355.106
C12H29Mn2N4O1+	355.1102164	0.0402164	355.11
428.98 m/z			
C3H18Mn3N151+	429.0010908	0.0210908	429.001

Continued on next page

Table 2.5 – continued from previous page

Formula	Molecular Weight (Da)	Difference in Mass	Mass per charge (m/z)
C6H22Mn3N11O1+	429.0150082	0.0350082	429.015
C18H9N2O111+	429.0206344	0.0406344	429.021
C17H8MnN7O41+	429.0018208	0.0218208	429.002
C15H26Mn3N3O1+	429.0217146	0.0417146	429.022
C10H33Mn4N41+	429.0226918	0.0426918	429.023
C9H26Mn3N7O21+	429.0289256	0.0489256	429.029
502.96 m/z			
C17H6MnNO141+	502.9168776	-0.0431224	502.917
C14H23Mn4N2O41+	502.9179578	-0.0420422	502.918
C3H19Mn4N14O21+	502.9337174	-0.0262826	502.934
C17H9Mn2N6O61+	502.9344474	-0.0255526	502.934
C7H30Mn5N7O1+	502.941401	-0.018599	502.941
C18H10MnNO131+	502.953261	-0.006739	502.953
C6H23Mn4N10O31+	502.9476348	-0.0123652	502.948
C15H27Mn4N2O31+	502.9543412	-0.0056588	502.954
C18H13Mn2N6O51+	502.9708308	0.0108308	502.971
C8H27Mn4N8O31+	502.9727852	0.0127852	502.973
C8H34Mn5N71+	502.9777844	0.0177844	502.978
C12H27Mn4N81+	502.9880402	0.0280402	502.988

Continued on next page

Table 2.5 – continued from previous page

Formula	Molecular Weight (Da)	Difference in Mass	Mass per charge (m/z)
C19H14MnNO121+	502.9896444	0.0296444	502.99
C16H31Mn4N2O21+	502.9907246	0.0307246	502.991
552.95 m/z			
C14H39Mn6O1+	552.9283504	-0.0216496	552.928
C14H32K5Mn2O31+	552.9297642	-0.0202358	552.93
C17H17K4O111+	552.9319152	-0.0180848	552.932
C15H43Mn61+	552.9647338	0.0147338	552.965
C15H36K5Mn2O21+	552.9661476	0.0161476	552.966
C18H21K4O101+	552.9682986	0.0182986	552.968
626.90 m/z			
C14H35K4Mn4O31+	626.865622	-0.034378	626.866
C14H28K9O51+	626.8670358	-0.0329642	626.867
C17H20K3Mn2O111+	626.867773	-0.032227	626.868
C20H5K2O191+	626.869924	-0.030076	626.87
C15H39K4Mn4O21+	626.9020054	0.0020054	626.902
C15H32K9O41+	626.9034192	0.0034192	626.903
C18H24K3Mn2O101+	626.9041564	0.0041564	626.904
C21H9K2O181+	626.9063074	0.0063074	626.906
C16H43K4Mn4O1+	626.9383888	0.0383888	626.938

Continued on next page

Table 2.5 – continued from previous page

Formula	Molecular Weight (Da)	Difference in Mass	Mass per charge (m/z)
C16H36K9O31+	626.9398026	0.0398026	626.94
C19H28K3Mn2O91+	626.9405398	0.0405398	626.941
C22H13K2O171+	626.9426908	0.0426908	626.943

Chapter 3: Mineral Surfaces As Agents of Environmental Proteolysis: Mechanisms and Controls

Stephany S. Chacon*,

Patrick Reardon, Christopher J. Burgess, Samuel Purvine, Rosalie K Chu, Therese R Clauss, Eric Walter, David D. Myrold, Nancy Washton, Markus Kleber

Submitted to:

Environmental Science and Technology

American Chemical Society

1155 Sixteenth Street N.W. Washington, DC 20036

3.1 Abstract

We investigated the extent to which contact with mineral surfaces affected the molecular integrity of a model protein, with an emphasis on identifying the mechanisms (hydrolysis, oxidation) and conditions leading to protein alteration. To this end, we studied the ability of four mineral surface archetypes (negatively charged, positively charged, neutral, redox-active) to abiotically fragment a well-characterized protein (GB1) as a function of pH and contact time. GB1 was exposed to the soil minerals montmorillonite, goethite, kaolinite, and birnessite at pH 5 and pH 7 for 1, 8, 24, and 168 hours and the supernatant was screened for peptide fragments using Tandem Mass Spectrometry. To distinguish between products of oxidative and hydrolytic cleavage, we combined results from the SEQUEST algorithm, which identifies protein fragments that were cleaved hydrolytically, with the output of a deconvolution algorithm (DECON-Routine) designed to identify oxidation fragments. All four minerals were able to induce protein cleavage. Manganese oxide was effective at both hydrolytic and oxidative cleavage. The fact that phyllosilicates which are not redox active - induced oxidative cleavage indicates that surfaces acted as catalysts and not as reactants. Our results extend previous observations of proteolytic capabilities in soil minerals to the groups of phyllosilicates and Fe-oxides. We identified structural regions of the protein with particularly high susceptibility to cleavage (loops and beta strands) as well as regions that were entirely unaffected (alpha helix).

3.2 Introduction

Proteins are the tools, engines, and catalysts among biomolecules and hence are indispensable elements of a thriving biosphere. For this reason, a mechanistic understanding of the constraints on the functional lifespan of proteinaceous biomolecules is highly desirable. Since protein functionality is tied to its three-dimensional structure and the accessibility of the active site, catalytic proteins in soils and sediments often lose a fraction of their maximum activity as a result of adsorption to mineral surfaces (Lammirato et al., 2010; Schimel et al., 2017). However, this negative effect may be offset by the protective nature of the mineral-protein association, i.e., a loss in efficiency may be balanced or even overcome by a gain in lifespan. The persistence of a protein involved in a mineral association, and, by extension, its functional lifespan, are thought to be constrained by eventual microbial degradation. Previous research (Russo et al., 2009; Reardon et al., 2016; Chacon et al., 2018) demonstrated abiotic fragmentation of protein by manganese oxides, but little is known about the propensity of other relevant surface archetypes (such as negatively charged, positively charged, and predominantly neutral surfaces) to fragment a protein.

Pedogenic oxides can act as oxidants towards reduced organic compounds, i.e., they may accept electrons and become chemically modified in the process. However, phyllosilicates typically contribute most of the reactive surface area in soils and sediments. These minerals vary in specific surface area and surface site density (surface sites = single coordinated hydroxyls (Kleber et al., 2005)) providing three

major options for sorptive interactions: (i) zero charge surfaces; (ii) permanently charged surfaces, and (iii) hydroxylated surfaces. Cleavage of protein by a phyllosilicate has been reported at least once when Johnson et al. (2006) adsorbed prion protein to montmorillonite, encouraging us to investigate the following research questions:

1. How does the susceptibility of a protein proxy to disintegration vary as a function of exposure to the four major mineral surface archetypes in soil (zero-charge, permanent charge, hydroxylated, and redox active)

2. How do the mechanisms of protein fragmentation and disintegration, such as oxidation and hydrolysis, depend on the proton concentration in the solvent??

3. What are the kinetics of protein disintegration by mineral surfaces - how long do proteins need to be in contact with mineral surfaces for disintegration reactions to occur?

4. Are fragmentation patterns random or do they show signs of regularity that may help to constrain mechanisms of mineral induced protein fragmentation?

Our conceptual approach involved exposing a well-characterized and structurally stable model protein to the four mineral surface archetypes mentioned above at two pH levels in an aqueous system while monitoring the eventual production of fragmentation products in the supernatant for one week. Kaolinite is a 1:1 phyllosilicate with little isomorphic substitution, rendering basal planes mostly hydrophobic. Montmorillonite is a 2:1 phyllosilicate with isomorphic substitution

predominantly in the inner octahedral sheet, creating basal planes where hydrophobic microsites alternate with areas of weak permanent charge (Laird and Fleming, 1999; Johnston et al., 2012). The montmorillonite interlayer space can expand and intercalate small organic molecules. It has been posited that unfolded peptide fragments may preferentially associate with broken edges of montmorillonite particles, with amino acid sidechains pointing into expanded interlayer spaces (Gougeon et al., 2003). All phyllosilicates may possess some reactive hydroxyls at the edges of octahedral sheets. Kaolinite and montmorillonite contain similar adsorption sites (zero charge and permanent charge basal surfaces combined with hydroxylated edges), yet at different proportions. Goethite is a pedogenic iron oxide that exhibits positively charged hydroxylated surfaces below a pH of 9. Birnessite is a redox active phyllomanganate known to participate in oxidation reactions with organic matter and to fragment proteins in acidic solutions(Reardon et al., 2018). The model protein (GB1) has an alpha helix, beta strand, and loop regions, the latter being somewhat flexible connections between alpha helices and beta strands. To detect any minute chemical modifications on GB1 after interacting with minerals even at low concentrations, we used liquid chromatography coupled with tandem mass spectrometry (LC-MS/MS). We expected this data-rich technique to provide us with a comprehensive overview of the fragmentation products.

3.3 Materials and Methods

GB1 was produced using the method of Reardon et al. (2016). In short, *Escherichia coli* cells with a plasmid encoding the GB1 gene were grown at 37C in Luria broth until optical densities (OD600 nm) reached 0.6. Protein expression was induced by the addition of Isopropyl β-D-1-thiogalactopyranoside (IPTG) at a final concentration of 1 mM for 6 hours. Cell pellets were lysed, and GB1 was purified using affinity chromatography. GB1 was buffer exchanged into MilliQ water and stored frozen until use.

We obtained montmorillonite (STx-1b) and kaolinite (KGa-1) from the Clay Resource Repository (Purdue University, West Lafayette). Charge balancing cations were exchanged for Na following the procedure of Soukup et al. (2008). Birnessite was synthesized using the acid birnessite protocol in Reardon et al. (2016). Goethite was synthesized following the protocol of Atkinson et al. (1967). The synthesized minerals were dialyzed against Milli-Q water using a membrane rated at 1000 MWCO. All minerals were washed or dialyzed with MilliQ water until the electric conductivity of the filtrate was less than 40 μS cm^{-1}. Minerals were freeze-dried and stored in amber bottles until further use. Mineral properties are reported in Table S2.

General details on the preparation of protein-mineral samples and analysis of the supernatant are provided in the SI. We combined GB1 at 0.4 mg protein mL^{-1} with 20 mg of mineral at a total volume of 1 mL. The pH of the dispersion was adjusted to the desired value (5 or 7) and the sample allowed to react for up to

one week without further adjustment of pH. Sample aliquots were removed at 1, 8, 24, and 168 hours. Our strategy to identify the products of hydrolytic and oxidative protein cleavage consisted of three steps (Figure 1). We first analyzed the supernatants using a reverse phase liquid chromatography separation coupled to a Tandem Mass Spectrometer; details are provided in the SI. The resulting data were then processed using the SEQUEST algorithm (Eng et al., 1994). Because the SEQUEST algorithm makes the inherent assumption of hydrolytic cleavage, we needed an additional step to identify potential oxidation fragments. This was done with the help of a procedure that we developed for the purpose and that we call the DECON - Routine (Figure 1). The details of our analysis are described in the SI.

We used the following metrics to test our hypotheses. The number of cleavage sites (discrete number) informs about how often and where the protein has been cleaved. The signal intensity per fragment (ion count based on the monoisotopic mass of peptide fragment) is used to assess the relative abundance of a given fragment, and the number of unique peptide fragments detected (discrete number) is used to compare the effects of variations in pH and exposure time. To reduce the possibility of false positives, we removed peptides that were observed in the control data from subsequent analysis.

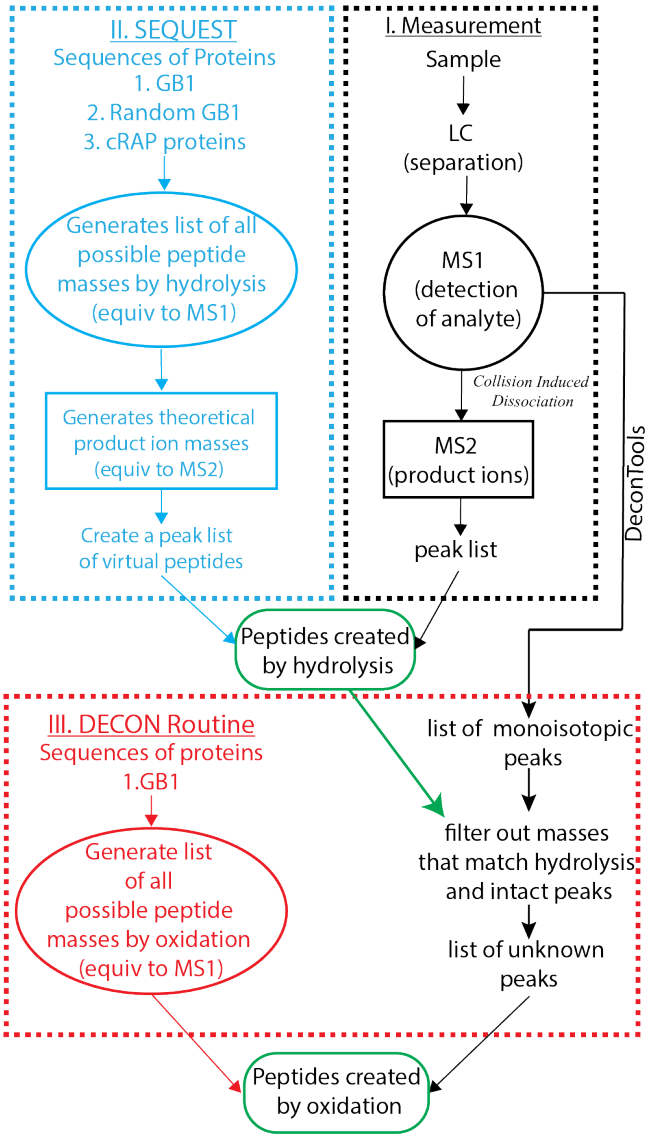

Figure 3.1: The sequence of events leading to the identification of protein fragments generated by hydrolysis and oxidation reactions. Experimental measurements are represented in black, the SEQUEST analysis for the identification of hydrolysis products is represented in blue and the DECON-Routine for the identification of oxidation products in red. Note that the DECON-Routine is applied to MS1 data after filtering out any hydrolysis products identified by the SEQUEST algorithm. Because it does not process MS2 data, the DECON - Routine for the identification of oxidation products does not take full advantage of the MS/MS approach and may return false positives.

3.4 Results and Discussion

3.4.1 All minerals induce protein fragmentation

The susceptibility of our protein GB1 to disintegration was a function of mineral surface type. Overall, the abundance of cleavage sites followed the trend: birnessite > goethite ≅ kaolinite ≅ montmorillonite. When oxidation and hydrolysis mechanisms were considered separately, the trend remained with the qualification that oxidative cleavage occurred about 2.5 times more frequently than hydrolytic cleavage. Oxidative cleavage occurred on 46 instances across all four minerals whereas hydrolytic cleavage was observed on 17 instances across all minerals (Table 1). Goethite did not induce hydrolytic cleavage of GB1 (Figure 3.2; Table 3.1). All four minerals induced oxidative cleavage between residues 38/39 (amino acids glycine and valine, Figure 3.2).

Figure 2 illustrates that exposure to birnessite generated a greater variety of fragments than exposure to phyllosilicate surfaces. We observed variations in the total ion counts for each fragment as indicated by the color code used in Figure 3. The peptides generated after interaction with birnessite tend to have higher ion counts than the ones resulting from interactions with phyllosilicates and goethite indicating more efficient fragmentation. Although this observation is in line with previous reports, the non-quantitative nature of our analytical method prevents us from drawing quantitative inference. We did not recognize an obvious correlation between fragment length and ion count.

Intact protein was detected in the supernatants from birnessite, montmoril-

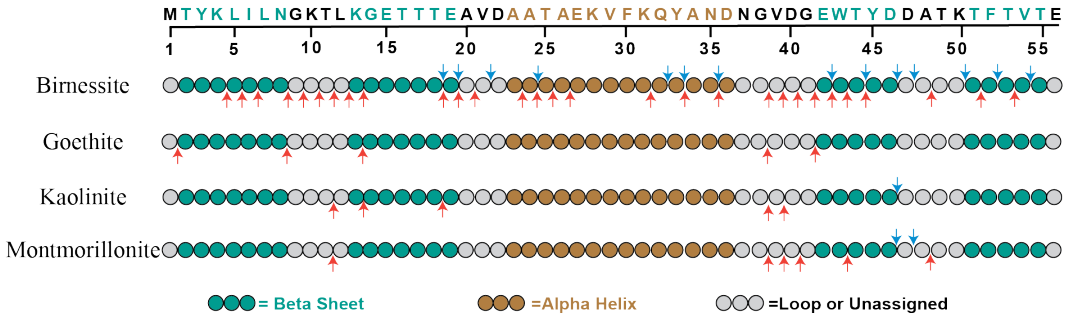

Figure 3.2: The cleavage sites on GB1 as a function of mineral exposure. The minerals tested are identified on the left, next to a schematic of the GB1. The top row has the one letter amino acid sequence of GB1. Below the sequence is the amino acid residue number. Letters and circles colored green designate amino acids within the beta sheets. The brown colored letters and circles designate amino acids within the alpha helix. Letters and circles in black and grey designate amino acids that are unassigned or in a loop region. Blue arrows indicate the location of hydrolytic cleavage sites, red arrows indicate the location of oxidative cleavage.

lonite, and kaolinite samples (Figure 3, row 1). The supernatants of kaolinite and montmorillonite contained two modified versions of GB1 (second and third rows of Panel A, Figure 3, Table S2). The fragment InH2 is GB1 with an oxidized methionine. The fragment InH3 is GB1 with the first methionine cleaved off. Because these modifications were detected in the mineral-free control and are known to be common post-translational modifications of protein expression in E. coli cells (Gupta et al., 2007; Spickett and Pitt, 2012), we do not consider these fragments as products of mineral-induced alteration. The fragment InO1 (first row of Panel B, Figure 3, Table S3) is a GB1 missing the four terminal amino acids. Because it is not detected in control, we consider this fragment as resulting from oxidative cleavage by birnessite.

The SEQUEST algorithm revealed evidence for alteration of aromatic side

chains among hydrolytic fragments, affecting the amino acids phenylalanine (F), tyrosine (Y), and tryptophan (W). The alteration of the side chains involved addition of oxygen or hydrolxyls to the aromatic side chains. This is simply modifying the side chains of the peptides but not resulting in the oxidation of the protein backbone. Modification of amino acid side chains were only seen after exposure to birnessite (Tables S2, Figure 3) and not for the other minerals. Fragments with oxidized amino acid sides chains are H8, H9, H13, H15, H22 (Table S3).

3.4.2 Fragmentation patterns are not entirely random

The propensity of our model protein for cleavage was not constant across minerals, and the positions of the cleavage sites were not random (Figure 3.2 and Table 3.1). For instance, the immediate ends of the alpha helix (residues 22-23 and residues 36-27) were not cleaved by any mineral (Table 3.1). We also point out that the amino acid combination DA occurs twice in the chain, at residues 23-24 at the beginning of the alpha helix, and again at residues 47-48 inside one of the loop regions. Although the latter is a cleavage site for both hydrolysis and oxidation at two surface types (birnessite and montmorillonite), the former is not cleaved by any of the minerals. Some commonality seems to exist between kaolinite and montmorillonite because they share four oxidative cleavage sites (out of 5 and 7 total, respectively) whereas goethite and kaolinite share three oxidative cleavage sites (out of 5 total, Figure 3.2). Between goethite and montmorillonite, only one common oxidative cleavage site was observed.

Oxidation

Cleavage site	Residue #	Birn	Goe	Kao	Mont	SUM
inside alpha helix	24-36	7	0	0	0	7
between helix and loop	22-23;36-37	0	0	0	0	0
inside beta strand	2-8; 13-19;42-46;51-55	10	1	2	2	5
between beta strand and loop	1-2; 8-9; 12-13; 19-20; 41-42; 46-47; 51-52; 55-57	4	2	0	1	7
inside loop	9-12; 20-21; 37-41; 47-50;	8	2	3	4	17
	SUM:	29	5	5	7	46

Hydrolysis

Cleavage site	Residue #	Birn	Goe	Kao	Mont	SUM
inside alpha helix	24-36	4	0	0	0	4
between helix and loop	23-24;36-37	0	0	0	0	0
inside beta strand	2-8; 13-19;42-46;51-55	5	0	0	0	5
between beta strand and loop	1-2; 8-9; 12-13; 19-20; 41-42; 46-47; 51-52; 55-57	3	0	1	1	5
inside loop	9-12; 20-21; 37-41; 47-50;	2	0	0	1	3
	SUM:	14	0	1	2	17
	TOTAL	43	5	6	9	

Table 3.1: The abundance of cleavage sites per structural region of the protein and mineral surface type

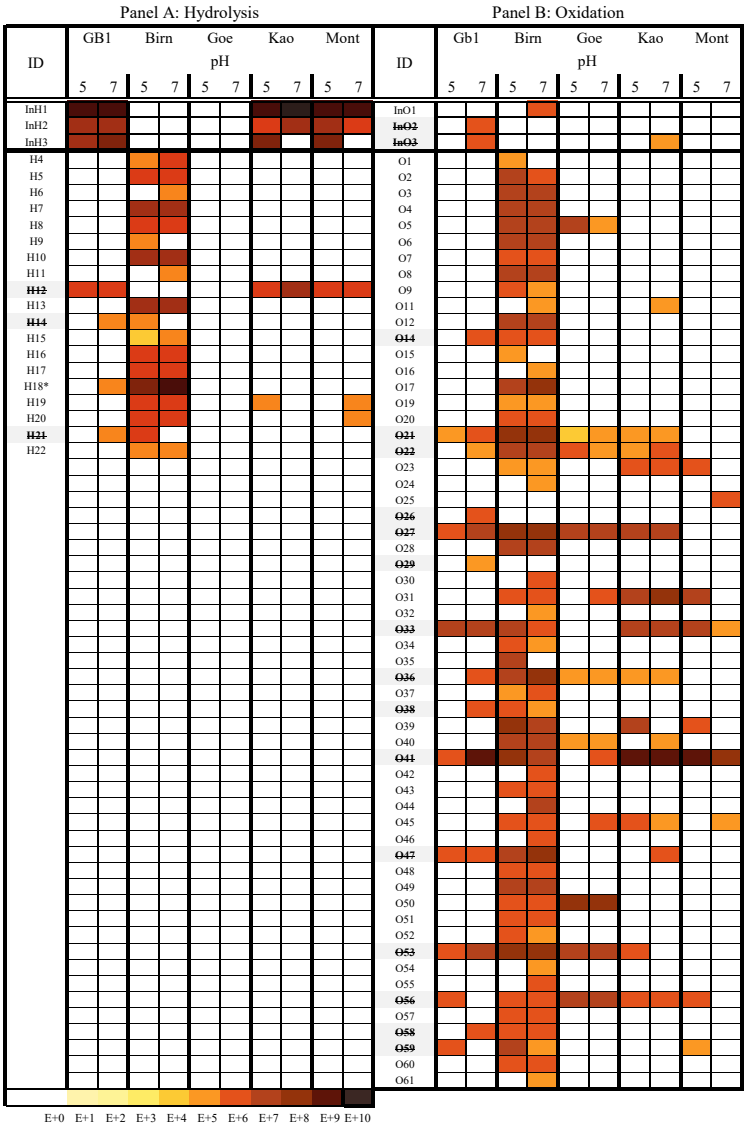

Figure 3.3: Heat map of the sums of ion counts for each mineral treatment (n=12). Fragment numbers refer to table 1 with items below the bold line representing products of fragmentation. Color gradient spans from white to black and covers 10 orders of magnitude.

Looking only at oxidative cleavage, we note that out of the eight peptides that produced intense ion counts in goethite, kaolinite, and montmorillonite samples, five were from cleavage of the 3rd beta-sheet and the 4th loop. The same regions of the protein were susceptible to hydrolytic cleavage in the kaolinite and montmorillonite samples. The other three oxidation-derived peptides found in the phyllosilicate and goethite samples were within the 2nd beta sheet and 1st loop regions. The complete list of peptides that include the sequences of the excluded peptides are provided in Tables S3.2 and S3.3.

3.4.3 Cleavage is not restricted to acidic pH

Previous studies (Russo et al., 2009; Reardon et al., 2016; Chacon et al., 2018) indicated that the propensity of proteins to become cleaved increased with decreasing pH, suggesting the process might be particularly efficient in, and possibly restricted to, acidic soils and environments. When we cumulated the number of unique peptide fragments over all four time points (Figure 3.4), the previously noted pH dependence of protein fragmentation by birnessite disappeared. The phyllosilicates, however, exhibited opposing trends: kaolinite hydrolytically cleaved the protein at pH 5, whereas montmorillonite did so only at pH 7. The number of unique oxidative fragments detected by mass spectrometry did not show an obvious dependency within the pH range considered here.

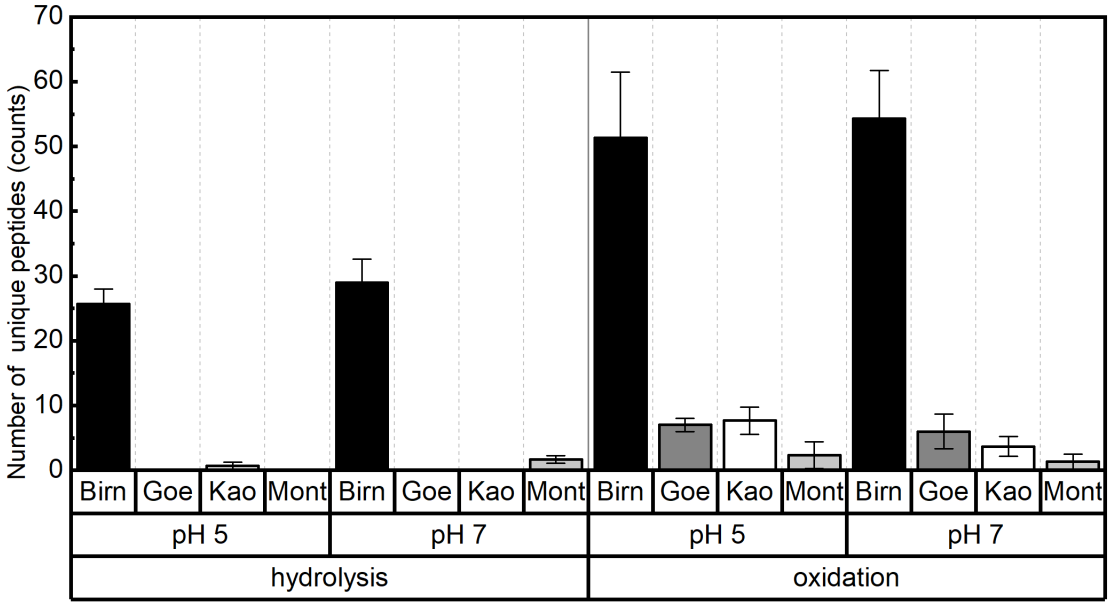

Figure 3.4: The number of unique peptides observed, accumulated over four time points. Error bars indicate variability expressed as standard deviations across replicates and time points (n = 12). Data are organized by cleavage mechanism, pH and mineral surface type.

3.4.4 Protein fragmentation changes with exposure time

Hydrolysis products did not appear in the supernatant from phyllosilicate samples until 24 hours had elapsed. The time course of fragment appearance (number of unique peptides) in phyllosilicate samples differed with pH, with oxidation fragments becoming more prevalent through time in kaolinite samples at pH 5, wherease hydrolytic fragments in the montmorillonite samples increased with time at pH 7. The number of unique peptides generated by oxidation after exposure to goethite did not vary significantly through time or with pH. Slightly higher num-

bers of unique peptides from oxidative cleavage were detected in kaolinite samples at pH 7 than at pH 5 after 8 hours, whereas the abundance of oxidation derived peptides found at pH 7 in montmorillonite diminished after 24 hours of exposure.

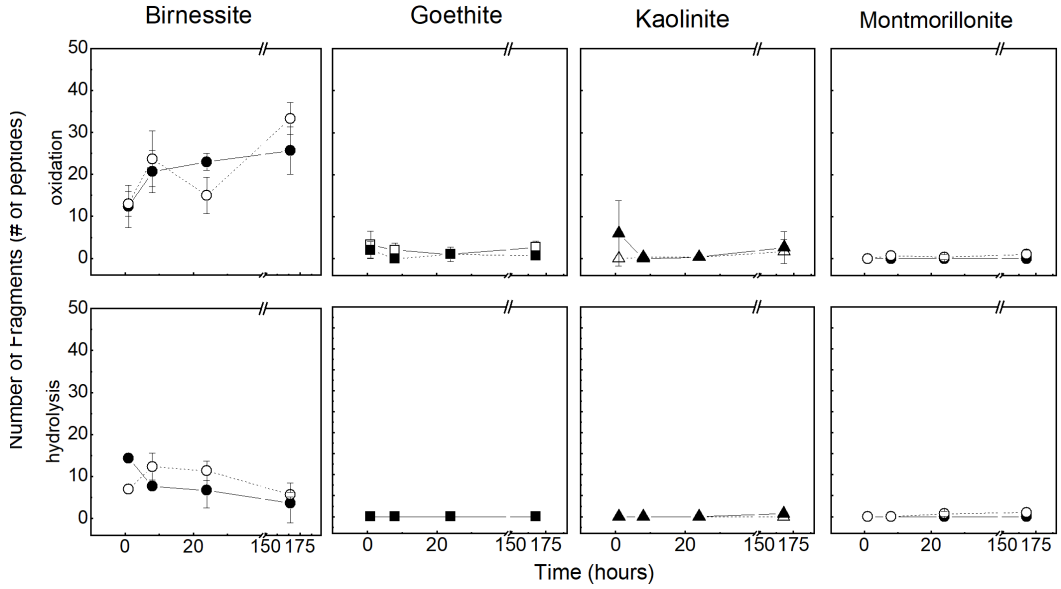

Figure 3.5: The effect of exposure time on the number of unique peptides generated by hydrolysis and oxidation at two pH values. Symbols represent mean values among three replicate samples, with error bars indicating the corresponding standard deviation. Closed symbols and straight lines are pH 5, open signals and dotted lines are respective values at pH 7.

3.5 Discussion

Minerals may have both, a destructive and a protective role in the cycling of organic matter through soils and sediments. Redox active minerals such as manganese oxides are long known as agents of organic matter degradation(Stone and

Morgan, 1984; Sunda and Kieber, 1994). By contrast, poorly crystalline minerals(Torn et al., 1997; Kleber et al., 2005) and phyllosilicate clay minerals(Oades, 1988) are generally viewed as protective towards organic matter. Although there has been conflicting evidence regarding the protective capacity of phyllosilicate clay minerals for soil organic matter (strong correlation with r = 0.86; n = 65 between clay content and OM content reported by Nichols (1984)for warm grassland soils; very weak correlation r = 0.21; n = 83 reported by McDaniel and Munn (1985) for cool grassland soils), there is widespread consensus that proteins have a particular affinity for phyllosilicates (Gianfreda et al., 2011). Such close association is not always conducive to the continued functionality of adsorbed protein, however(Allison, 2006). The main reason for such an impediment in functionality, particularly regarding adsorbed enzymes, has so far been attributed to a) conformational changes to an adsorbed protein and b) in concealment of the active site(Quiquampoix and Burns, 2007; Norde, 2008) (Figure 1 therein 27). Our discovery of protein fragmentation by phyllosilicates adds to this picture by revealing the fact that adsorbed protein will undergo eventual, albeit slow, fragmentation. The resulting peptide fragments may become readsorbed (consistent with some of the time series data presented in Figure 3.5) and hence remain protected against microbial decomposition, which would render fragmented proteinaceous matter still protected but no longer functional.

Both kaolinitic and smectitic minerals are marketed as catalysts in industrial applications (Kodama, 2012), thus it is no surprise that the mechanisms through which they fragment protein involve catalytic hydrolysis and catalytic oxidation.

The fact that the potentially redox-active manganese oxide behaves as a catalyst towards protein at least under the conditions chosen for this experiment, is more difficult to rationalize. When carbohydrate and the GB1 protein were exposed together to a manganese oxide in an aqueous system(Reardon et al., 2018), oxidation of carbohydrate was observed with concomitant reduction of MnO_2 and production of Mn^{2+}. Interestingly, oxidation of carbohydrates and the concomitant production of Mn(II) decreased when the proportion of GB1 in the system increased. These observations support our view that in the systems investigated in the work presented here, MnO2 acts as a catalyst in both protein hydrolysis and protein oxidation, i.e., it fundamentally acts in the same manner as the phyllosilicates and the Fe-oxide. We posit that, unlike standard MnO_2 organic matter reactions, where MnO_2 serves as a reactant that is consumed in the reaction, the MnO_2 protein reactions investigated here follow fundamentally different, namely catalytic reaction schemes. This latter finding seems to be generalizable across the four mineral archetypes investigated.

When comparing abiotic and biotic cleavage patterns we found mineral catalyzed proteolysis to share striking similarities with protease-mediated disassembly of proteins. In biochemistry research, limited proteolysis catalyzed by proteases has been used to determine protein structural domains(Fontana et al., 2004), including work on prion proteins(Sajnani et al., 2008; Sevillano et al., 2018). Proteases preferentially cleave exposed and flexible loop regions of proteins (Fontana et al., 1992). Additional sites of cleavage also occur in areas susceptible to large conformational changes (local unfolding).(Hubbard et al., 1994) An evaluation of

proteolytic events recorded in the CutDB(Igarashi et al., 2007) database showed cleavage to occur in helices and beta sheets as well, but to a lesser degree than in loop regions (Kazanov et al., 2011) Specifically, secondary structures were likely to break apart in such parts of the helices that tended to unfold and in the periphery of the beta strands (Belushkin et al., 2014). Computational models indicated the appearance of a loop within the alpha helix of the protein when GB1 interacted with birnessite but not when it was paired with kaolinite, montmorillonite, or goethite(Andersen et al., 2016). This may explain why we detected fragmentation sites within the alpha helix after interacting with birnessite but not the other soil minerals.

Previous research by Russo et al. (2009) saw a strong pH dependence of prion degradation by birnessite. Our previous NMR-based work (Reardon et al., 2016) also showed faster fragmentation of GB1 at pH 5 than at pH 7, with the number and intensity of signals from fragmentation products increasing over time. However, in the mass spectrometry based data presented here, the number of unique hydrolytic peptides decrease over time. When reconciling this apparent contradiction it is important to keep in mind that mass spectrometry measures the number of unique peptides produced by the mineral interaction and is not a quantitative measure of the concentration of reaction products or reaction efficiency. The mass spectrometry data shows that the number of unique peptides is similar between the two pH values tested, suggesting that the hydrolytic cleavage sites do not change based on the pH range that was used in this study. This again is consistent with our previous NMR data, which indicated that the reaction between birnessite and

GB1 was slowed at pH 7, but that similar reaction products were produced at both pH values. When looking at the peptides resulting from catalytic oxidation by birnessite, we find that the number of unique peptide fragments tends to increase over time, even with our conservative filtering of oxidative fragments to reduce the number of false positives. However, the number of unique peptides remain similar between the two pH conditions for oxidation, suggesting that pH does not significantly alter the abundance of oxidation reaction products. A change in pH will affect the speciation of adsorption sites at hydroxylated surfaces. Low pH conditions below the point of zero charge (pzc) of a mineral surface would generate greater amounts of protonated surface hydroxyls ($M - OH_2^+$) than unprotonated surface hydroxyls ($M - O^{-1}$), which would yield a net positive surface charge. When pH rises above the pzc, a greater proportion of unprotonated hydroxyls will generate a net negative charge. Goethite (pzc 8.43; Table S3.2) is positively charged at both pH conditions investigated here. But birnessite has a very acidic pzc of pH 1.9. Adsorption sites are mostly unprotonated $Mn - O^{-1}$, which may explain why the number of unique peptides is not different between pH 5 and pH 7. The only pH dependent surface charges in phyllosilicates are located at the edges. Deprotonation of the hydroxylated surfaces of kaolinite and montmorillonite only becomes relevant as pH conditions go above pH 5.0 (Liu et al 2013). Although the specific mechanism that catalyzes hydrolysis by kaolinite or montmorillonite is yet unknown, we posit that the sites that catalyze the hydrolysis of GB1 may be different between these two phyllosilicates given the appearance of peptides at different pH.

The time dependence of protein- mineral interactions will require close attention in future work aiming to further elucidate the underlying mechanisms.

Given enough time, even the supposedly protective phyllosilicates eventually fragmented GB1. Protein-mineral interactions have a known kinetic component(Roach et al., 2005), complicating investigations of the outcome of such interactions. This may apply to the adsorption process as well as to subsequent changes in protein conformation, and to the hydrolysis and oxidation reactions eventually leading to fragmentation. Figure 3.5 illustrates how the number of peptides detected evolved during the 168 hours of exposure in our experiment. Time-dependent variation in the presence of fragments in the supernatant was most pronounced in the birnessite treatment, but occurred in the presence of the other minerals as well, raising the possibility that newly generated fragments may find themselves readsorbed quickly. There is also the possibility that products of hydrolytic cleavage might turn out to be particularly susceptible to further oxidative alteration, and vice versa. The extent to which such interactive scenarios contribute to the overall picture seen in Figure 3.5 remains to be explored in future investigations.

3.6 Significance and Implications

Phyllosilicates have traditionally been viewed as sorbents for protein(Gianfreda et al., 2011). Numerous industrial and technical applications take advantage of this sorptive capacity(Gougeon et al., 2003). This understanding has informed a prevailing view of a stabilizing role of phyllosilicate surfaces for soil protein. Our

work extends this view to include the insight that contact times on the order of several days may very well induce fragmentation of a protein that is adsorbed to a phyllosilicate. Awareness of the existence of such a mechanism will be important for assessments of the functional lifespans of extracellular enzymes in soil and should be further investigated as a potential reason for the frequently observed reduction in the catalytic activity of mineral-associated enzymes (Allison, 2006). Hence our work not only expands knowledge about the role of mineral surfaces in determining the functional lifespan of protein in the terrestrial biosphere, but it also suggests that the different elements of the protein secondary structure vary in their susceptibility to abiotic cleavage.

The similarity of cleavage products between proteases and mineral surfaces indicates the abiotic matrix in the soil can supply peptides to microorganisms in the absence of enzymes. Soils containing a significant proportion of reactive mineral surfaces must be considered as able to contribute relevant amounts of abiotically derived peptides to the microbiota for further processing. This property should be accounted for when analyzing fluxes of carbon and nitrogen among soil carbon pools and particularly in work investigating the ecological significance of low molecular weight compounds. Less reactive minerals should not be considered inert. This means the balance between biotic and abiotic pathways for peptide production in the soil will vary as a function of mineralogy.

Finally, the detection of peptide products generated through oxidation of the protein backbone emphasizes the need to reevaluate fundamental assumptions in proteomic analysis of soils. Current tools for analyzing LC-MS/MS data (such as

SEQUEST) typically focus on hydrolytic cleavage of proteins by proteases. Our results suggest that soil protein extracts will also contain oxidatively modified proteins or peptides that could be overlooked by analysis techniques that focus solely on hydrolysis. Expanding our assumptions to include modifications of proteins from mineral interaction could increase the detection and identification of soil proteins during proteomic analysis. Our work emphasizes the necessity to augment existing databases of peptide fragments with information about oxidative fragmentation products and illustrates the need to develop bioinformatics tools that can identify these oxidation products of proteins from secondary ion spectra data. We conclude that our work reveals a previously underappreciated proteolytic functionality of soil minerals. By recognizing this functionality across different mineral groups, such as pedogenic oxides and phyllosilicates, this observation warrants an extension of the paradigm of mineral control of soil carbon stabilization (Torn et al., 1997) to include a more active role of the mineral phase than that of a passive and protective sorbent.

3.6.1 Acknowledgements

This research was performed using EMSL, a DOE Office of Science User Facility sponsored by the Office of Biological and Environmental Research and located at the Pacific Northwest National Laboratory through user proposal # 48183. We gratefully acknowledge the support of the EMSL MS lead scientist, Dr. Mary Lipton. S.S. Chacon would like to acknowledge support through the U.S. Department

of Energy, Office of Science, Office of Workforce Development for Teachers and Scientists, Office of Science Graduate Student Research (SCGSR) program. The SCGSR program is administered by the Oak Ridge Institute for Science and Education for the DOE under contract number DESC001466 and National Science Foundation under grant no. 1456966.

3.7 References

Allison, S.D., 2006. Soil minerals and humic acids alter enzyme stability: implications for ecosystem processes. Biogeochemistry 81, 361-373.

Andersen, A., Reardon, P.N., Chacon, S.S., Qafoku, N.P., Washton, N.M., Kleber, M., 2016. Protein-Mineral Interactions: Molecular Dynamics Simulations Capture Importance of Variations in Mineral Surface Composition and Structure. Langmuir 32, 6194-6209.

Atkinson, R.J., Posner, A.M., Quirk, J.P., 1967. Adsorption of potential-determining ions at the ferric oxide-aqueous electrolyte interface. The Journal of Physical Chemistry 71, 550-558.

Belushkin, A.A., Vinogradov, D.V., Gelfand, M.S., Osterman, A.L., Cieplak, P., Kazanov, M.D., 2014. Sequence-derived structural features driving proteolytic processing. Proteomics 14, 42-50.

Chacon, S.S., Garcia-Jaramillo, M., Liu, S.Y., Ahmed, M., Kleber, M., 2018. Differential capacity of kaolinite and birnessite to protect surface associated proteins against thermal degradation. Soil Biology and Biochemistry 119, 101-109.

Eng, J.K., McCormack, A.L., Yates, J.R., 1994. An approach to correlate tandem mass spectral data of peptides with amino acid sequences in a protein database. J Am Soc Mass Spectrom 5, 976-989.

Fontana, A., De Laureto, P.P., Filippis, V., 1992. Molecular aspects of proteolysis of globular proteins, In: Harder, A., Buitelaar, R.M., Van Den Tweel, W.J.J. (Eds.), Stability and Stabilization of Enzymes: Proceedings of an International Symposium Held in Maastricht, the Netherlands, 22-25 November 1992. Elsevier Science and Technology, Amsterdam.

Fontana, A., de Laureto, P.P., Spolaore, B., Frare, E., Picotti, P., Zambonin, M., 2004. Probing protein structure by limited proteolysis. Acta Biochimica Polonica 51, 299-321.

Gianfreda, L., Rao, M.A., Mora, M., 2011. Enzymatic Activity as Influenced by Soil Mineral and Humic Colloids, In: Huang, P.M., Li, Y., Sumner, M.E. (Eds.), Handbook of soil sciences: resource management and environmental impacts, 2nd ed. CRC press, pp. 5-5.

Gougeon, Rgis D., Soulard, M., Reinholdt, M., Mieh-Brendl, J., Chzeau, J.-M., Dred, Ronan L., Marchal, R., Jeandet, P., 2003. Polypeptide Adsorption on a Synthetic Montmorillonite: A Combined Solid-State NMR Spectroscopy, X-ray Diffraction, Thermal Analysis and N2 Adsorption Study. European Journal of Inorganic Chemistry 2003, 1366-1372.

Gupta, N., Tanner, S., Jaitly, N., Adkins, J.N., Lipton, M., Edwards, R., Romine, M., Osterman, A., Bafna, V., Smith, R.D., Pevzner, P.A., 2007. Whole proteome analysis of post-translational modifications: applications of mass-spectrometry

for proteogenomic annotation. Genome Research 17, 1362-1377.

Hubbard, S.J., Eisenmenger, F., Thornton, J.M., 1994. Modeling studies of the change in conformation required for cleavage of limited proteolytic sites. Protein Science 3, 757-768.

Igarashi, Y., Eroshkin, A., Gramatikova, S., Gramatikoff, K., Zhang, Y., Smith, J.W., Osterman, A.L., Godzik, A., 2007. CutDB: a proteolytic event database. Nucleic Acids Res 35, D546-549.

Johnson, C.J., Phillips, K.E., Schramm, P.T., McKenzie, D., Aiken, J.M., Pedersen, J.A., 2006. Prions adhere to soil minerals and remain infectious. PLoS Pathog 2, e32.

Johnston, C.T., Premachandra, G.S., Szabo, T., Lok, J., Schoonheydt, R.A., 2012. Interaction of biological molecules with clay minerals: a combined spectroscopic and sorption study of lysozyme on saponite. Langmuir : the ACS journal of surfaces and colloids 28, 611-619.

Kazanov, M.D., Igarashi, Y., Eroshkin, A.M., Cieplak, P., Ratnikov, B., Zhang, Y., Li, Z., Godzik, A., Osterman, A.L., Smith, J.W., 2011. Structural determinants of limited proteolysis. J Proteome Res 10, 3642-3651. Kleber, M., Mikutta, R., Torn, M.S., Jahn, R., 2005. Poorly crystalline mineral phases protect organic matter in acid subsoil horizons. European Journal of Soil Science 56, 717-725.

Kodama, H., 2012. Phyllosilicates, In: Huang, P.M., Li, Y., Sumner, M.E. (Eds.), Handbook of Soil Sciences: Properties and Processes, 2nd ed. CRC Press 2011, Boca Raton Fl, pp. 1-44.

Laird, D.A., Fleming, P.D., 1999. Mechanisms for adsorption of organic bases

on hydrated smectite surfaces. Environmental Toxicology and Chemistry 18, 1668-1672.

Lammirato, C., Miltner, A., Wick, L.Y., Kstner, M., 2010. Hydrolysis of cellobiose by -glucosidase in the presence of soil minerals Interactions at solidliquid interfaces and effects on enzyme activity levels. Soil Biology and Biochemistry 42, 2203-2210.

McDaniel, P.A., Munn, L.C., 1985. Effect of Temperature on Organic Carbon-texture Relationships in Mollisols and Aridisols1. Soil Science Society of America Journal 49, 1486-1489.

Nichols, J.D., 1984. Relation of Organic Carbon to Soil Properties and Climate in the Southern Great Plains1. Soil Science Society of America Journal 48, 1382-1384.

Norde, W., 2008. My voyage of discovery to proteins in flatland ...and beyond. Colloids and Surfaces B: Biointerfaces 61, 1-9.

Oades, J.M., 1988. The Retention of Organic Matter in Soils. Biogeochemistry 5, 35-70.

Quiquampoix, H., Burns, R.G., 2007. Interactions between proteins and soil mineral surfaces: Environmental and health consequences. Elements 3, 401-406.

Reardon, P.N., Chacon, S.S., Walter, E.D., Bowden, M.E., Washton, N.M., Kleber, M., 2016. Abiotic Protein Fragmentation by Manganese Oxide: Implications for a Mechanism to Supply Soil Biota with Oligopeptides. Environmental Science and Technology 50, 3486-3493.

Reardon, P.N., Walter, E.D., Marean-Reardon, C.L., Lawrence, C.W., Kleber,

M., Washton, N.M., 2018. Carbohydrates protect protein against abiotic fragmentation by soil minerals. Sci Rep 8, 813.

Roach, P., Farrar, D., Perry, C.C., 2005. Interpretation of protein adsorption: surface-induced conformational changes. J Am Chem Soc 127, 8168-8173.

Russo, F., Johnson, C.J., Johnson, C.J., McKenzie, D., Aiken, J.M., Pedersen, J.A., 2009. Pathogenic prion protein is degraded by a manganese oxide mineral found in soils. Journal of General Virology 90, 275-280.

Sajnani, G., Pastrana, M.A., Dynin, I., Onisko, B., Requena, J.R., 2008. Scrapie prion protein structural constraints obtained by limited proteolysis and mass spectrometry. Journal of molecular biology 382, 88-98.

Schimel, J., Becerra, C.A., Blankinship, J., 2017. Estimating decay dynamics for enzyme activities in soils from different ecosystems. Soil Biology and Biochemistry 114, 5-11.

Sevillano, A.M., Fernandez-Borges, N., Younas, N., Wang, F., S, R.E., Bravo, S., Vazquez-Fernandez, E., Rosa, I., Erana, H., Gil, D., Veiga, S., Vidal, E., Erickson-Beltran, M.L., Guitian, E., Silva, C.J., Nonno, R., Ma, J., Castilla, J., J, R.R., 2018. Recombinant PrPSc shares structural features with brain-derived PrPSc: Insights from limited proteolysis. PLoS Pathog 14, e1006797.

Soukup, D.A., Buck, B.J., Harris, W., 2008. Preparing Soils for Mineralogical Analyses, In: Ulery, A.L., Richard Drees, L. (Eds.), Methods of Soil Analysis Part 5Mineralogical Methods. Soil Science Society of America, Madison, WI.

Spickett, C.M., Pitt, A.R., 2012. Protein oxidation: role in signalling and detection by mass spectrometry. Amino Acids 42, 5-21.

Stone, A.T., Morgan, J.J., 1984. Reduction and dissolution of manganese(III) and manganese(IV) oxides by organics: 2. Survey of the reactivity of organics. Environmental Science and Technology 18, 617-624.

Sunda, W.G., Kieber, D.J., 1994. Oxidation of Humic Substances by Manganese Oxides Yields Low-Molecular-Weight Organic Substrates. Nature 367, 62-64.

Torn, M.S., Trumbore, S.E., Chadwick, O.A., Vitousek, P.M., Hendricks, D.M., 1997. Mineral control of soil organic carbon storage and turnover. Nature 389, 170-173.

Villalobos, M., Toner, B., Bargar, J., Sposito, G., 2003. Characterization of the manganese oxide produced by Pseudomonas putida strain MnB1. Geochimica Et Cosmochimica Acta 67, 2649-2662.

3.8 Appendix for Chapter 3

3.8.1 Preparation of Protein-Mineral Samples

Protein and minerals were mixed at a concentration of 0.4 mg/ml and 20 mg/ml, respectively, in MilliQ purified water. Sample pH was adjusted using 0.1M HCl or 0.1M NaOH. Thimerosal was added to the samples at 0.02% to discourage microbial growth and so ensure any protein alterations detected were abiotic. The protein-mineral mixtures were incubated at room temperature under continuous shaking; aliquots were removed after 1, 8, 24, and 168 hours. For each of the time

points and pH values, we generated control samples by omitting either the protein or the mineral phase. This resulted in 96 control samples (4 time points, 2 pH steps, 4 minerals, 3 replicates) where the protein was omitted and in 24 control samples (4 time points, 2 pH steps, 3 replicates) where the mineral was omitted. The aliquots were centrifuged at 21,000 rcf for 5 minutes to separate the mineral phase from the peptide fragments in solution. The supernatant was centrifuged again to remove any trace of mineral matter and transferred to a new tube. A final filtration step with 0.45 m PVDF nano filter vials (Thomson Instrument Company, Oceanside CA, USA) was then performed to reduce the number of particulates from the solution. The protein concentration in the supernatant was determined using a BCA assay kit (Thermo Fischer Scientific) with a GB1 standard curve.

3.8.2 Differentiation between products of hydrolysis and products of oxidation

3.8.2.1 Mass Spectrometry

Supernatants were stored at -80C until analysis. Thawed samples were diluted to 0.5 ng/L with MilliQ water and transferred to 2mL glass autosampler vials (Microsolv, North Carolina, USA). To detect possible carryover of peptide fragments between samples, blanks were placed between controls every three samples and analyzed for peptides. As an additional measure to minimize the potential of peptide carryover, samples were run in an order of increasing fragmentation probability:

(1) control samples containing no protein; (2) control protein that had not been exposed to mineral surfaces; samples where protein interacted with (3) montmorillonite, (4) kaolinite, (5) goethite, (6) birnessite (Table S1). Samples were analyzed using a Vanquish Ultra-High Performance Liquid Chromatography (UHPLC) system (Thermo Scientific, San Jose, CA) coupled to a LTQ Orbitrap Velos mass spectrometer (Thermo Scientific, San Jose, CA) outfitted with a standard heated electrospray ionization (HESI) source. For LC separation, an Accucore Vanquish c18 column was used (column specifications: 100mm, 2.1 mm o.d. and 1.5 m particle size) and held at 26C. Mobile phases consisted of 0.1% formic acid in water (A), and 0.1% formic acid in acetonitrile (B) operated at a flow rate of 200 L/min. The 15 L injection volume was focused on the analytical column and then eluted with the following gradient profile (minutes : %B); 0:8, 1:8, 2:12, 19:40, 20:95, 21:95, 23:8 over 25 minutes and then held for 12 min at starting conditions to equilibrate the column. The Orbitrap Velos collected mass spectra (auto gain control of 1 x106) from 400-2000 m/z in profile mode at a resolution of 30K m/dm at m/z 400. The resolution of a mass spectrometer is defined as m/dm where m designates the mass of a peak and dm designates the width for separation at mass m. The full width at half maximum for an ion peak is used as dm. The MS2 spectra were collected in centroid mode by selecting the top 3 most abundant ions for subsequent collision-induced dissociation (CID) at a resolution of 7500 with a normalized collision energy set to 35V. A dynamic exclusion time of 30 sec was used to discriminate against previously analyzed ions. The heated capillary temperature and spray voltage were 325C and 2.2 kV, respectively. Charge state

screening was enabled to reject singly charged ions, and the default charge state was set to 5.

Table 3.2: Order of sample injection for tandem mass spectrometry. Sample name abbreviations with no protein samples are designated by sample number, a single letter indicating mineral with a replicate number, pH value, and the time point. M stands for montmorillonite, K for kaolinite, G for goethite and B for birnessite. For example, 180_M3_pH5_T4 is sample number 180 containing the third replicate with montmorillonite at pH 5 taken after 168 hours. Samples containing protein have GB1 in the front, with mineral name, pH, time point and replicate number. For example, $GB1\_Kaolinite\_pH\_5\_T1\_R1$ is the first replicate of a GB1 sample that interacted with kaolinite at pH 5 for 1 hour.

Run Order	Sample	Protein	Mineral	pH	time (hours)
Run Order	Sample	Protein	Mineral	pH	time (hours)
1	Hexa_Floro_Cycle _Blank	None	None	None	None
2	StartBlank	None	None	None	None
3	178_M1_pH5_T4	None	Montmorrilonite	5	168
4	179_M2_pH5_T4	None	Montmorrilonite	5	168
5	180_M3_pH5_T4	None	Montmorrilonite	5	168
6	CycleBlank_180	None	None	None	None

Continued on next page

Table 3.2 – continued from previous page

Run Order	Sample	Protein	Mineral	pH	time (hours)
7	180_M1_pH7_T4	None	Montmorrilonite	7	168
8	181_M2_pH7_T4	None	Montmorrilonite	7	168
9	182_M3_pH7_T4	None	Montmorrilonite	7	168
10	CycleBlank_182	None	None	None	None
11	082_K1_pH5_T4	None	Kaolinite	5	168
12	080_K2_pH5_T4	None	Kaolinite	5	168
13	084_K3_pH5_T4	None	Kaolinite	5	168
14	CycleBlank_082	None	None	None	None
15	094_K1_pH7_T4	None	Kaolinite	7	168
16	095_K2_pH7_T4	None	Kaolinite	7	168
17	096_K3_pH7_T4	None	Kaolinite	7	168
18	132_G2_pH5_T4	None	Goethite	5	168
19	133_G3_pH5_T4	None	Goethite	5	168
20	142_G1_pH7_T4	None	Goethite	7	168

Continued on next page

Table 3.2 – continued from previous page

Run Order	Sample	Protein	Mineral	pH	time (hours)
21	143_G2_pH7_T4	None	Goethite	7	168
22	144_G3_pH7_T4	None	Goethite	7	168
23	CycleBlank_144	None	None	None	None
24	034_G1_pH5_T4	None	Goethite	5	168
25	035_G2_pH5_T4	None	Goethite	5	168
26	036_G3_pH5_T4	None	Goethite	5	168
27	046_G1_pH7_T4	None	Goethite	7	168
28	047_G2_pH7_T4	None	Goethite	7	168
29	048_G3_pH7_T4	None	Goethite	7	168
30	CycleBlank_048	None	None	None	None
31	EndBlank_048	None	None	None	None
32	blank-start_protein_wash	None	None	None	None
33	GB1__pH_5_T4_R1	GB1	None	5	168
34	GB1__pH_5_T4_R2	GB1	None	5	168

Continued on next page

Table 3.2 – continued from previous page

Run Order	Sample	Protein	Mineral	pH	time (hours)
35	GB1__pH_5_T4_R3	GB1	None	5	168
36	blank-wash-2	None	None	None	None
37	GB1__pH_7_T4_R1	GB1	None	7	168
38	GB1__pH_7_T4_R2	GB1	None	7	168
39	GB1__pH_7_T4_R3	GB1	None	7	168
40	blank-end_protein-wash	None	None	None	None
41	blank_GB1-MpH5-start	None	None	None	None
42	GB1_Montmorillonite_pH_5_T1_R1	GB1	Montmorrilonite	5	1
43	blank_GB1-MpH5-wash-1	None	None	None	None
44	GB1_Montmorillonite_pH_5_T2_R1	GB1	Montmorrilonite	5	8
45	blank_GB1-MpH5-wash-2	None	None	None	None
46	GB1_Montmorillonite_pH_5_T3_R1	GB1	Montmorrilonite	5	24
47	blank_GB1-MpH5-wash-3	None	None	None	None
48	GB1_Montmorillonite_pH_5_T4_R1	GB1	Montmorrilonite	5	168

Continued on next page

Table 3.2 – continued from previous page

Run Order	Sample	Protein	Mineral	pH	time (hours)
49	blank_GB1-MpH5-wash-4	None	None	None	None
50	GB1_Montmorillonite_pH_5_T3_R2	GB1	Montmorrilonite	5	24
51	blank_GB1-MpH5-wash-5	None	None	None	None
52	GB1_Montmorillonite_pH_5_T4_R2	GB1	Montmorrilonite	5	168
53	blank_GB1-MpH5-wash-6	None	None	None	None
54	GB1_Montmorillonite_pH_5_T1_R2	GB1	Montmorrilonite	5	1
55	blank_GB1-MpH5-wash-7	None	None	None	None
56	GB1_Montmorillonite_pH_5_T2_R2	GB1	Montmorrilonite	5	8
57	blank_GB1-MpH5-wash-8	None	None	None	None
58	GB1_Montmorillonite_pH_5_T3_R3	GB1	Montmorrilonite	5	24
59	blank_GB1-MpH5-wash-9	None	None	None	None
60	GB1_Montmorillonite_pH_5_T1_R3	GB1	Montmorrilonite	5	1
61	blank_GB1-MpH5-wash-10	None	None	None	None
62	GB1_Montmorillonite_pH_5_T4_R3	GB1	Montmorrilonite	5	168

Continued on next page

Table 3.2 – continued from previous page

Run Order	Sample	Protein	Mineral	pH	time (hours)
63	blank_GB1-MpH5-wash-11	None	None	None	None
64	GB1_Montmorillonite_pH_5_T2_R3	GB1	Montmorrilonite	5	8
65	blank_GB1-MpH5-wash-12	None	None	None	None
66	blank_GB1-MpH7-start	None	None	None	None
67	GB1_Montmorillonite_pH_7_T1_R1	GB1	Montmorrilonite	7	1
68	blank_GB1-MpH7-wash-1	None	None	None	None
69	GB1_Montmorillonite_pH_7_T2_R2	GB1	Montmorrilonite	7	8
70	blank_GB1-MpH7-wash-2	None	None	None	None
71	GB1_Montmorillonite_pH_7_T3_R1	GB1	Montmorrilonite	7	24
72	blank_GB1-MpH7-wash-3	None	None	None	None
73	GB1_Montmorillonite_pH_7_T4_R1	GB1	Montmorrilonite	7	168
74	blank_GB1-MpH7-wash-4	None	None	None	None
75	GB1_Montmorillonite_pH_7_T3_R2	GB1	Montmorrilonite	7	24
76	blank_GB1-MpH7-wash-5	None	None	None	None

Continued on next page

Table 3.2 – continued from previous page

Run Order	Sample	Protein	Mineral	pH	time (hours)
77	GB1_Montmorillonite_pH_7_T4_R2	GB1	Montmorrilonite	7	168
78	blank_GB1-MpH7-wash-6	None	None	None	None
79	GB1_Montmorillonite_pH_7_T1_R2	GB1	Montmorrilonite	7	1
80	blank_GB1-MpH7-wash-7	None	None	None	None
81	GB1_Montmorillonite_pH_7_T2_R1	GB1	Montmorrilonite	7	8
82	blank_GB1-MpH7-wash-8	None	None	None	None
83	GB1_Montmorillonite_pH_7_T3_R3	GB1	Montmorrilonite	7	24
84	blank_GB1-MpH7-wash-9	None	None	None	None
85	GB1_Montmorillonite_pH_7_T1_R3	GB1	Montmorrilonite	7	1
86	blank_GB1-MpH7-wash-10	None	None	None	None
87	GB1_Montmorillonite_pH_7_T4_R3	GB1	Montmorrilonite	7	168
88	blank_GB1-MpH7-wash-11	None	None	None	None
89	GB1_Montmorillonite_pH_7_T2_R3	GB1	Montmorrilonite	7	8
90	blank_GB1-MpH7-end	None	None	None	None

Continued on next page

Table 3.2 – continued from previous page

Run Order	Sample	Protein	Mineral	pH	time (hours)
91	QC_Shew_15_01_500ng	Shewanella Proteins	None	None	None
92	blank_GB1-KpH5-start	None	None	None	None
93	GB1_Kaolinite_pH_5_T1_R1	GB1	Kaolinite	5	1
94	blank_GB1-KpH5-wash-1	None	None	None	None
95	GB1_Kaolinite_pH_5_T2_R1	GB1	Kaolinite	5	8
96	blank_GB1-KpH5-wash-2	None	None	None	None
97	GB1_Kaolinite_pH_5_T3_R1	GB1	Kaolinite	5	24
98	blank_GB1-KpH5-wash-3	None	None	None	None
99	GB1_Kaolinite_pH_5_T4_R1	GB1	Kaolinite	5	168
100	blank_GB1-KpH5-wash-4	None	None	None	None
101	GB1_Kaolinite_pH_5_T3_R2	GB1	Kaolinite	5	24
102	blank_GB1-KpH5-wash-5	None	None	None	None
103	GB1_Kaolinite_pH_5_T4_R2	GB1	Kaolinite	5	168
104	blank_GB1-KpH5-wash-6	None	None	None	None

Continued on next page

Table 3.2 – continued from previous page

Run Order	Sample	Protein	Mineral	pH	time (hours)
105	GB1_Kaolinite_pH_5_T1_R2	GB1	Kaolinite	5	1
106	blank_GB1-KpH5-wash-7	None	None	None	None
107	GB1_Kaolinite_pH_5_T2_R2	GB1	Kaolinite	5	8
108	blank_GB1-KpH5-wash-8	None	None	None	None
109	GB1_Kaolinite_pH_5_T3_R3	GB1	Kaolinite	5	24
110	blank_GB1-KpH5-wash-9	None	None	None	None
111	GB1_Kaolinite_pH_5_T1_R3	GB1	Kaolinite	5	1
112	blank_GB1-KpH5-wash-10	None	None	None	None
113	GB1_Kaolinite_pH_5_T4_R3	GB1	Kaolinite	5	168
114	blank_GB1-KpH5-wash-11	None	None	None	None
115	GB1_Kaolinite_pH_5_T2_R3	GB1	Kaolinite	5	8
116	blank_GB1-KpH7-start	None	None	None	None
117	GB1_Kaolinite_pH_7_T1_R1	GB1	Kaolinite	7	1
118	blank_GB1-KpH7-wash-1	None	None	None	None

Continued on next page

Table 3.2 – continued from previous page

Run Order	Sample	Protein	Mineral	pH	time (hours)
119	GB1_Kaolinite_pH_7_T2_R1	GB1	Kaolinite	7	8
120	blank_GB1-KpH7-wash-2	None	None	None	None
121	GB1_Kaolinite_pH_7_T3_R1	GB1	Kaolinite	7	24
122	blank_GB1-KpH7-wash-3	None	None	None	None
123	GB1_Kaolinite_pH_7_T4_R1	GB1	Kaolinite	7	168
124	blank_GB1-KpH7-wash-4	None	None	None	None
125	GB1_Kaolinite_pH_7_T3_R2	GB1	Kaolinite	7	24
126	blank_GB1-KpH7-wash-5	None	None	None	None
127	GB1_Kaolinite_pH_7_T4_R2	GB1	Kaolinite	7	168
128	blank_GB1-KpH7-wash-6	None	None	None	None
129	GB1_Kaolinite_pH_7_T1_R2	GB1	Kaolinite	7	1
130	blank_GB1-KpH7-wash-7	None	None	None	None
131	GB1_Kaolinite_pH_7_T2_R2	GB1	Kaolinite	7	8
132	blank_GB1-KpH7-wash-8	None	None	None	None

Continued on next page

Table 3.2 – continued from previous page

Run Order	Sample	Protein	Mineral	pH	time (hours)
133	GB1_Kaolinite_pH_7_T3_R3	GB1	Kaolinite	7	24
134	blank_GB1-KpH7-wash-9	None	None	None	None
135	GB1_Kaolinite_pH_7_T1_R3	GB1	Kaolinite	7	1
136	blank_GB1-KpH7-wash-10	None	None	None	None
137	GB1_Kaolinite_pH_7_T4_R3	GB1	Kaolinite	7	168
138	blank_GB1-KpH7-wash-11	None	None	None	None
139	GB1_Kaolinite_pH_7_T2_R3	GB1	Kaolinite	7	8
140	blank_GB1-KpH7-wash-12	None	None	None	None
141	blank_GB1-G1pH5-start	None	None	None	None
142	GB1_Goethite_pH_5_T1_R1	GB1	Goethite	5	1
143	blank_GB1-G1pH5-wash-1	None	None	None	None
144	GB1_Goethite_pH_5_T2_R1	GB1	Goethite	5	8
145	blank_GB1-G1pH5-wash-2	None	None	None	None
146	GB1_Goethite_pH_5_T3_R1	GB1	Goethite	5	24

Continued on next page

Table 3.2 – continued from previous page

Run Order	Sample	Protein	Mineral	pH	time (hours)
147	blank_GB1-G1pH5-wash-3	None	None	None	None
148	GB1_Goethite_pH_5_T4_R1	GB1	Goethite	5	168
149	blank_GB1-G1pH5-wash-4	None	None	None	None
150	GB1_Goethite_pH_5_T3_R2	GB1	Goethite	5	24
151	blank_GB1-G1pH5-wash-5	None	None	None	None
152	GB1_Goethite_pH_5_T4_R2	GB1	Goethite	5	168
153	blank_GB1-G1pH5-wash-6	None	None	None	None
154	GB1_Goethite_pH_5_T1_R2	GB1	Goethite	5	1
155	GB1_Goethite_pH_5_T2_R2	GB1	Goethite	5	8
156	blank_GB1-G1pH5-wash-8	None	None	None	None
157	GB1_Goethite_pH_5_T3_R3	GB1	Goethite	5	24
158	blank_GB1-G1pH5-wash-9	None	None	None	None
159	GB1_Goethite_pH_5_T1_R3	GB1	Goethite	5	1
160	blank_GB1-G1pH5-wash-10	None	None	None	None

Continued on next page

Table 3.2 – continued from previous page

Run Order	Sample	Protein	Mineral	pH	time (hours)
161	GB1_Goethite_pH_5_T4_R3	GB1	Goethite	5	168
162	blank_GB1-G1pH5-wash-11	None	None	None	None
163	GB1_Goethite_pH_5_T2_R3	GB1	Goethite	5	8
164	blank_GB1-G1pH7-start	None	None	None	None
165	GB1_Goethite_pH_7_T1_R1	GB1	Goethite	7	1
166	blank_GB1-G1pH7-wash-1	None	None	None	None
167	GB1_Goethite_pH_7_T2_R2	GB1	Goethite	7	8
168	blank_GB1-G1pH7-wash-2	None	None	None	None
169	GB1_Goethite_pH_7_T3_R1	GB1	Goethite	7	24
170	blank_GB1-G1pH7-wash-3	None	None	None	None
171	GB1_Goethite_pH_7_T4_R1	GB1	Goethite	7	168
172	blank_GB1-G1pH7-wash-4	None	None	None	None
173	GB1_Goethite_pH_7_T3_R2	GB1	Goethite	7	24
174	blank_GB1-G1pH7-wash-5	None	None	None	None

Continued on next page

Table 3.2 – continued from previous page

Run Order	Sample	Protein	Mineral	pH	time (hours)
175	GB1_Goethite_pH_7_T4_R2	GB1	Goethite	7	168
176	blank_GB1-G1pH7-wash-6	None	None	None	None
177	blank_GB1-G1pH7-wash-7	None	None	None	None
178	GB1_Goethite_pH_7_T2_R1	GB1	Goethite	7	8
179	blank_GB1-G1pH7-wash-8	None	None	None	None
180	GB1_Goethite_pH_7_T3_R3	GB1	Goethite	7	24
181	blank_GB1-G1pH7-wash-9	None	None	None	None
182	GB1_Goethite_pH_7_T1_R3	GB1	Goethite	7	1
183	blank_GB1-G1pH7-wash-10	None	None	None	None
184	GB1_Goethite_pH_7_T4_R3	GB1	Goethite	7	168
185	blank_GB1-G1pH7-wash-11	None	None	None	None
186	GB1_Goethite_pH_7_T2_R3	GB1	Goethite	7	8
187	blank_GB1-G1pH7-end	None	None	None	None
188	QC_Shew	Shewanella Proteins	None	None	None

Continued on next page

Table 3.2 – continued from previous page

Run Order	Sample	Protein	Mineral	pH	time (hours)
189	blank_GB1-BpH5-start	None	None	None	None
190	GB1_Birnessite_pH_5_T1_R1	GB1	Birnessite	5	1
191	blank_GB1-BpH5-wash-1	None	None	None	None
192	GB1_Birnessite_pH_5_T1_R1	GB1	Birnessite	5	1
193	blank_GB1-BpH5-wash-2	None	None	None	None
194	GB1_Birnessite_pH_5_T3_R1	GB1	Birnessite	5	24
195	blank_GB1-BpH5-wash-3	None	None	None	None
196	GB1_Birnessite_pH_5_T4_R1	GB1	Birnessite	5	168
197	blank_GB1-BpH5-wash-4	None	None	None	None
198	GB1_Birnessite_pH_5_T4_R2	GB1	Birnessite	5	168
199	blank_GB1-BpH5-wash-5	None	None	None	None
200	GB1_Birnessite_pH_5_T3_R2	GB1	Birnessite	5	24
201	blank_GB1-BpH5-wash-6	None	None	None	None
202	GB1_Birnessite_pH_5_T1_R2	GB1	Birnessite	5	1

Continued on next page

Table 3.2 – continued from previous page

Run Order	Sample	Protein	Mineral	pH	time (hours)
203	blank_GB1-BpH5-wash-7	None	None	None	None
204	GB1_Birnessite_pH_5_T2_R2	GB1	Birnessite	5	8
205	blank_GB1-BpH5-wash-8	None	None	None	None
206	GB1_Birnessite_pH_5_T3_R3	GB1	Birnessite	5	24
207	blank_GB1-BpH5-wash-9	None	None	None	None
208	blank_GB1-BpH5-wash-10	None	None	None	None
209	GB1_Birnessite_pH_5_T4_R3	GB1	Birnessite	5	168
210	blank_GB1-BpH5-wash-11	None	None	None	None
211	GB1_Birnessite_pH_5_T2_R3	GB1	Birnessite	5	8
212	blank_GB1-BpH7-start	None	None	None	None
213	blank_GB1-BpH7-blank-1	None	None	None	None
214	GB1_Birnessite_pH_7_T2_R1	GB1	Birnessite	7	8
215	blank_GB1-BpH7-blank-2	None	None	None	None
216	GB1_Birnessite_pH_7_T3_R1	GB1	Birnessite	7	24

Continued on next page

Table 3.2 – continued from previous page

Run Order	Sample	Protein	Mineral	pH	time (hours)
217	blank_GB1-BpH7-blank-3	None	None	None	None
218	GB1_Birnessite_pH_7_T4_R1	GB1	Birnessite	7	168
219	blank_GB1-BpH7-blank-4	None	None	None	None
220	GB1_Birnessite_pH_7_T3_R2	GB1	Birnessite	7	24
221	blank_GB1-BpH7-blank-5	None	None	None	None
222	GB1_Birnessite_pH_7_T4_R2	GB1	Birnessite	7	168
223	blank_GB1-BpH7-blank-6	None	None	None	None
224	GB1_Birnessite_pH_7_T2_R2	GB1	Birnessite	7	8
225	blank_GB1-BpH7-blank-8	None	None	None	None
226	GB1_Birnessite_pH_7_T3_R3	GB1	Birnessite	7	24
227	blank_GB1-BpH7-blank-end	None	None	None	None

3.8.2.2 Identification of hydrolytic fragments using the SEQUEST algorithm

The SEQUEST program is a tool to identify protein and peptide sequences from tandem mass spectra. The program can generate a list of possible peptide masses (analyte masses) when supplied with known protein or peptide sequences. These masses correspond to the masses observed in first stage mass spectra (MS1). The software uses information from the observed MS1 spectra to select the analytes for further processing. It then virtually replicates the effects of the collision induced dissociation (CID) procedure to generate hypothetical product ion spectra, which can be compared to or matched with the actual MS2 spectra. The matching process involves a correlation analysis that uses a cross correlation score to identify highly probable matches. The SEQUEST algorithm was developed with peptides derived from proteolytic digestion of proteins in mind. This is a hydrolytic process, for that reason, the SEQUEST program is not able to predict the results of oxidative breakup of the peptide backbone. It is, however, able to account for the presence of oxidized amino acid side chains within hydrolytic fragments. Side chains susceptible to oxidation are predominantly those carrying aromatic functional groups such as tyrosine (Y), phenylalanine (F), tryptophan (W), and others such as histidine (H). Lysine (K), glutamic acid (E), and methionine (M) are non-aromatic amino acids whose side chains are also susceptible to oxidation (Berlett and Stadtman 1997). Thus, the SEQUEST program can be run to consider monoxidation of side chains in K, E, H, W, Y, and F in hydrolyzed fragments. Dioxidation of F and W

were also considered during the analysis.

The SEQUEST output was manually filtered using cross correlation scores (Xcorr). Correlation scores were applied as suggested by Smith et al. (2002) . At a correlation score above 1.9, peptides with charge states of +1 were considered above background noise. For a charge state of +2; Xcorr needed to be at 3.0, for charge states > +3, scores had to be higher than 3.75. To detect false readings, we used a decoy sequence generated through randomization of the amino acid sequence of GB1 and ran the SEQUEST analysis along with the actual sequence of GB1.

At this stage, we knew which fragments had actually been created by the hydrolytic protein mineral interaction and were able to constrain their amino acid sequences. To distinguish signal from noise, we used a tool called the "MS/MS Automated Selected Ion Chromatogram Generator" (MASIC) (Monroe et al. 2008). Briefly, this tool quantifies the relative abundance of a given peptide based on the prevalence of the corresponding ion across all MS1 spectra obtained for a given sample. As the analyte elutes from the LC column, MS1 spectra are collected every second over 25 minutes. The ion counts associated with a given m/z number are summed over the whole 25 minute period. Peptides whose total ion counts had a signal to noise ratio above 20 were accepted as valid (Wong et al. 2009).

3.8.2.3 Identification of oxidation fragments using the DECON Routine

While able to account for oxidation of amino acid side chains, SEQUEST is unable to identify fragments resulting from oxidative cleavage of the protein backbone. Hence, we needed to develop an independent approach to identify tentative oxidation products in our supernatants. To this end, we first generated a list of theoretical masses as they would result from oxidative cleavage. According to Berlett and Stadtman (1997), the fragmentation of a protein through oxidation occurs in several steps. It is assumed that an oxidant (such as reactive oxygen species) initially reacts with the peptide and results in a radical at an alpha carbon. This radical can accept a further oxygen leading to cleavage of the alpha bond. If cleavage in a short hypothetical peptide were to occur on the left side of the alpha carbon (item A in figure S1), we would observe fragment I with a mass per charge (m/z) of 119.08 and fragment II with 347.15 m/z. If fragmentation would occur on the right side of the alpha carbon (item B in figure S1), fragments III (189.12 m/z) and IV (275.09 m/z) would be created.

To perform corresponding calculations for our GB1 chain of 56 amino acids, we took advantage of a software tool with the ability to calculate the masses of the b and y ions (Roepstorff et al. 1984) of a given amino acid sequence (amounting to 55 b and 55 y ions in our case). These masses were then converted into products of oxidative cleavage by treating each b and y ion to the following mass adjustment:

$$Fragment \quad I : b_{x-1} - O + NH \qquad (1)$$

$$Fragment \quad II : y_{x-1} + O - NH_3 \qquad (2)$$

$$Fragment \quad III : b_x - CH_2O \qquad (3)$$

$$Fragment \quad IV : y_x + CO - H_2 \qquad (4)$$

After establishment of the list of theoretical "monoisotopic" masses, we used the program DECONTools to reduce (or "de-isotope") the multiple signals generated by isotopic variations of given fragments in the MS1 spectra into "monoisotopic" masses as well (Jaitly et al. 2009). This was necessary to be able to compare masses detected in the MS1 spectra to masses from our list of theoretical oxidation fragments. The monoisotopic peak list was then filtered to remove any masses known to be hydrolysis products or intact protein. This information came from the preceding SEQUEST analysis. The masses remaining after this clean up step were compared to the theoretical oxidation fragment list, using a mass tolerance at 0.5 Da to be considered a hit.

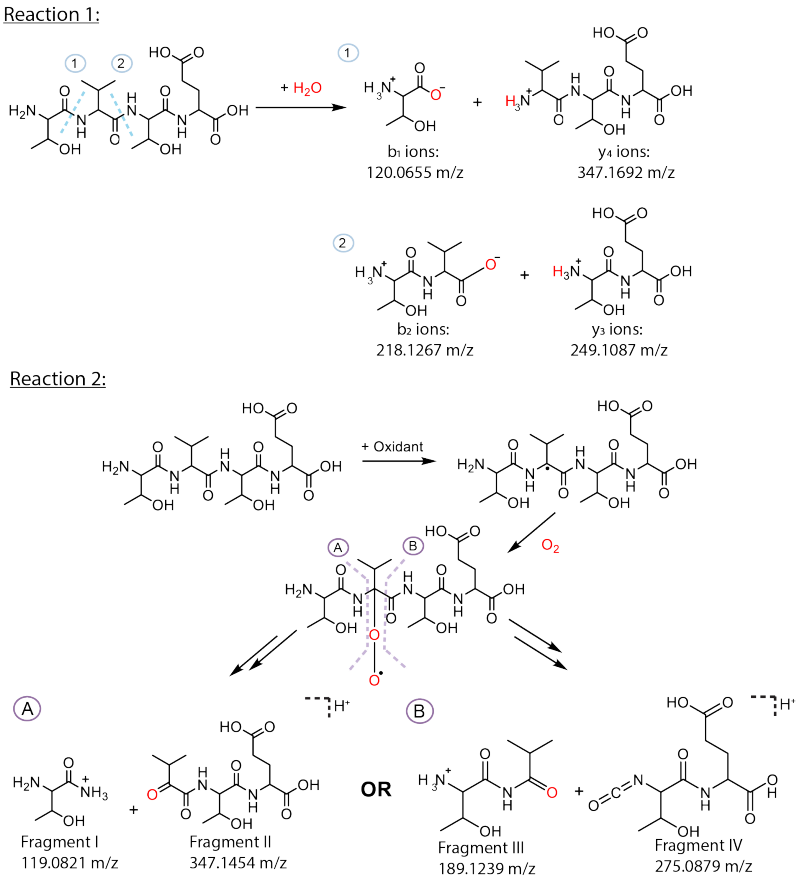

Figure 3.6: Rationale for differentiation between products of hydrolysis and oxidation. For the same hypothetical peptide, reaction pathways involving hydrolysis (Reaction 1) and Oxidation (Reaction 2) are presented, together with the fragmentation products and their corresponding monoisotopic masses. Masses produced (1, 2 for hydrolysis and and I through IV for oxidation) are generally a function of cleavage site indicated by dotted lines. The oxidative cleavage of a peptide (Reaction 2) occurs in several steps according to Berlett and Stadtman (1997). An oxidant (such as reactive oxygen species) reacts with the peptide and transforms the alpha carbon into a radical. Subsequently, an oxygen molecule may attach at this position and cleave the alpha bond. If cleavage were to occur on the left side of the alpha carbon (A), we would observe fragments I and II. If fragmentation occurs on the right side of the alpha carbon (B), fragments III and IV are created

3.8.2.4 Protein adsorption as a function of pH

Adsorption experiments were conducted by adding a stock solution of GB1 to create an initial concentration of 0.40 mg/mL (C_i) for the samples. Protein-mineral samples were made by adding protein stock solution and mixed to a 1mL: 20 mg ratio of protein solution: mineral powder. Thimerosal was also added to the samples at a final concentration of 0.02% to discourage microbial growth and ensure any protein alterations detected were abiotic. To quantify the effect of pH on protein adsorption, samples were made at pH 4, 5, 6, and 7 by adjusting the pH with NaOH and HCl. The pH samples were allowed to interact at room temperature under continuous shaking for 24 hours. All samples were then centrifuged at 21,000 rcf for 5 minutes to remove unadsorbed protein from the mineral phase. The protein supernatant was centrifuged again to pellet any excess mineral phase in solution. The sample was then filtered with a Thompson nanofilter. The concentration of GB1 was determined with absorbance of UV light at 280 nm. Protein concentration of the supernatant (C_e) was determined by absorbance at 280 nm. The amount of protein adsorbed per mass of mineral (q) was calculated with equation 1. All samples were run in triplicate.

$$q = \frac{volume(C_i - C_e q)}{m_m ineral} \qquad (5)$$

3.8.3 Parameterizing electrostatic attraction and conformational change

Although protein adsorption can be controlled by a multitude of mechanisms, the most amendable mechanisms for adsorption are coulombic interactions and con-

formational changes. Coulombic interactions occur when opposite charges on the surface interact to yield electrostatic attraction. Like charges result in electrostatic repulsion. We wanted to test whether conditions favoring electrostatic attraction between GB1 and the minerals controlled adsorption. To do so, we developed a parameter (α) that expresses the extent to which opposing charges overlap, or, in other words, the extent to which negative charges on the sorbate surface are met by positive charges on the sorbent surface at a specific pH (Chacon et al. 2018).For instance, an α value of 100% means that one adsorption partner is entirely negatively charged while the other is entirely positively charged. An α of 0% would mean that one adsorption partner is entirely negatively charged while the other is entirely positively charged. The fraction of positive charge on the protein (Y_B) and the fraction of positive charge on the mineral (Y_A) were determined from the point of zero charge for minerals (PZC) and isoelectric point (pI) for proteins at a specific pH. The fraction of negative charge on the mineral (X_A) and the fraction of negative charge of the protein (X_B) were calculated using equations 7 and 8. The overlap of opposite charge (α) was calculated with equation 9.

$$Y_B = Total\,Charge \times \frac{1}{1+10^{(pH-pI)}} \qquad (5)$$

$$Y_A = Total\,Charge \times \frac{1}{1+10^{(pH-pzc)}} \qquad (6)$$

$$X_B = Total\,Charge - Y_B \qquad (7)$$

$$X_A = Total\,Charge - Y_A \qquad (8)$$

$$\alpha = |X_B - X_A| = |Y_B - Y_A| \qquad (9)$$

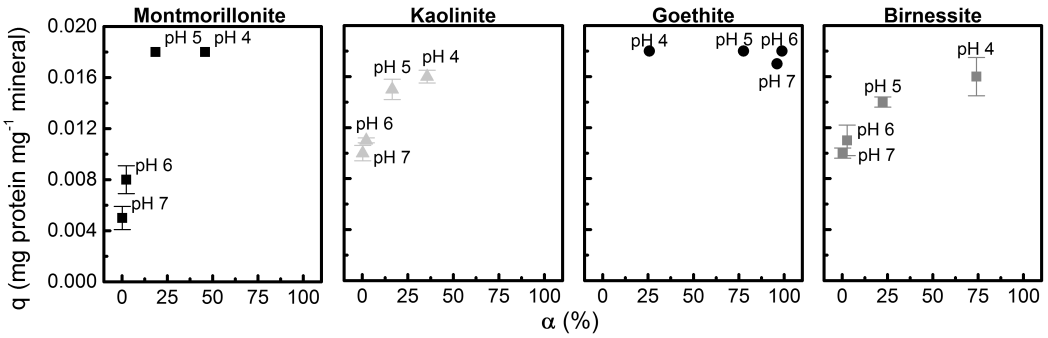

Figure 3.7: Adsorption of Gb1 as a function of potential electrostatic attraction (α, electrostatic attraction increasing with increasing values) for montmorillonite (square), kaolinite (triangle), goethite (circle), and birnessite (gray square). Error bars are standard deviation (n=3). The pH during adsorption is indicated next to the symbol

Table 3.3: Charge Characteristics of Minerals

Mineral	Formula	Point of Zero Charge (pH)	Cation Exchange capacity ($meq100g^{-}1$)	Surface Area ($m^2g^{-}1$)	Surface Archetype
Acid Birnessite	$(Na, Ca, K)x(Mn^{+4}, Mn^{+3})_2O_41.5(H_2O)$	1.9[1]	$63 - 240$[2]	40.5[3]	redox-active, hydroxylated
Goethite	Fe^3OOH	8.43	5[4]	$40.5 - 101$[5]	pH dependent charge, hydroxylated
Kaolinite (KGa-1)	$Al_2Si_2O_5(OH)_4$	3.8[6]	3.0[7]	10.05[8]	zero charged, hydroxylated at the edges
Montmorillonite (Stx-1b)	$(Na, Ca)_0.3(Al, Mg)_2Si_4O_10(OH)_2n(H_2O)$	3.6[9]	89[10]	83.79[11]	permanent negative charged, hydroxylated at the edges

[1] Chacon et. al. 2018
[2] Golden et al. (1986)
[3] Mckenzie (1981)
[4] Weil. Ray R. Brady and Weil
[5] Mckenzie (1981)
[6] Chacon et. al. 2018
[7] Borden and Giese (2001)
[8] Schroth and Sposito (1997)
[9] Thomas et al
[10] Borden and Giese (2001)
[11] Schroth and Sposito (1997)

Table 3.4: Sequences of protein and peptides detected in the supernatants along with their monoisotopic mass and fragment label. Fragment labels will be used throughout the figures and text.Bold sequences indicate the fragment was filtered from further analysis because it was detected in the control. Oxidation of the amino acids is indicated to the right of the letter with # (e.g. M# means oxidized methionine).

Sequence	Fragment	Oxidation	Monoisotopic Mass
MTYKLILNGKTLKGETTTEAVDAATAEKVKQYANDNGVDGEWTYDDATKTFTVTE.	1		6193.012
.M#TYKLILNGKTLKGETTTEAVDAATAEKVKQYANDNGVDGEWTYDDATKTFTVTE.	2	M#	6209.007
M.TYKLILNGKTLKGETTTEAVDAATAEKVKQYANDNGVDGEWTYDDATKTFTVTE.	3		6061.972
T.EAVDAA.T	4		575.267
E.AVDAATAEKVFKQ.Y	5A		1377.737
A.VDAATAEKVFKQ.Y	5B		1306.700
V.DAATAEKVFKQ.Y	5C		1207.632
Y.ANDNGVDGEW#TY#DDATKTFTVTE.	6A	W# Y#	2581.085
Y.ANDNGVDGEW#TYDDATKTFTVTE.	6B	W#	2565.090
Y.ANDNGVDGE.W	7A		890.349
A.NDNGVDGE.W	7B		819.312
D.GEWTYDDATKTFTVTE.	8A		1863.828
W.TY#DDATKTFTVTE.	8B	Y#	1507.680
W.TYDDATKTFTVTE.	8C		1491.685
T.Y#DDATKTFTVTE.	8D	Y#	1227.574
Y.DDATKTF.T	8E		797.368
Y.DDATKTFTV.T	8F		997.484
Y.DDATKTFTVTE.	8G		1227.574
D.DATKTFTVTE.	8H		1112.547
D.ATKTFTVTE.	8I		997.520
A.TKTFTVTE.	8J		926.483
K.TF#TVTE.	8K	F#	926.483

Table 3.5: Sequences of oxidized protein and peptides detected in the supernatants along with their monoisotopic mas and fragment label. Fragment labels will be used throughout the figures and text. Strikeout of a peptide indicates the fragment was filtered from further analysis because it was detected in the controls

Sequence	ID	Monoisotopic Mass
Sequence	ID	Monoisotopic Mass
I_MTYKLILNGKTLKGETTTEAVDAATAEKVFKQYANDNGVDGEWTYDDATKTFT	InO1	5613.745
III_MTYKLILNGKTLKGETTTEAVDAATAEKVFKQYANDNGVDGEWTYDDATKTFTVT	InO2	6032.951
II_KLILNGKTLKGETTTEAVDAATAEKVFKQYANDNGVDGEWTYDDATKTFTVTE	InO3	5795.821
I_MTYKLILNGKTLKGETTTEAVD	O1	2309.266
I_MTYK	O2	412.1775
I_MTYKL	O3	540.2724
I_MTYKLI	O4	653.3565
I_MTYKLILNG	O5	993.5675
I_MTYKLILNGK	O6	1050.589
I_MTYKLILNGKTL	O7	1279.732

Continued on next page

Table 3.5 – continued from previous page

Sequence	ID	Monoisotopic Mass
I_MTYKLILNGKTLK	O8	1392.816
I_MTYKLILNGKTLKG	O9	1520.911
I_MTYKLILNGKTLKGETTT	O11	1909.07
I_MTYKLILNGKTLKGETTTE	O12	2010.118
I_MTYKLILNGKTLKGETTTEAVDA	O14	2424.293
I_MTYKLILNGKTLKGETTTEAVDAA	O15	2495.33
I_MTYKLILNGKTLKGETTTEAVDAAT	O16	2566.367
I_MTYKLILNGKTLKGETTTEAVDAATA	O17	2667.415
I_MTYKLILNGKTLKGETTTEAVDAATAEKVFKQYANDNGVDGEWTYDDA	O19	5212.518
II_ANDNGVDGEWTYDDATKTFTVTE	O20	2547.051
II_ATKTFTVTE	O21	995.4806
II_DATKTFTVTE	O22	1110.511
II_DGEWTYDDATKTFTVTE	O23	1976.811
II_FTVTE	O24	594.2506

Continued on next page

Table 3.5 – continued from previous page

Sequence	ID	Monoisotopic Mass
II_GEWTYDDATKTFTVTE	O25	1861.791
II_KQYANDNGVDGEWTYDDATKTFTVTE	O26	2966.271
II_KTFTVTE	O27	823.3906
II_NDNGVDGEWTYDDATKTFTVTE	O28	2246.951
II_QYANDNGVDGEWTYDDATKTFTVTE	O29	2838.181
II_TKTFTVTE	O30	924.4406
II_VDGEWTYDDATKTFTVTE	O31	2075.881
II_YDDATKTFTVTE	O32	1388.601
III_DGEWTYDDATKTFTVTE	O33	1976.811
III_MTYK	O34	511.2459
III_MTYKL	O35	624.33
III_MTYKLIL	O36	850.4981
III_MTYKLILN	O37	964.541
III_MTYKLILNG	O38	1021.562

Continued on next page

Table 3.5 – continued from previous page

Sequence	ID	Monoisotopic Mass
III_MTYKLILNGKT	O39	1250.705
III_MTYKLILNGKTLK	O40	1491.884
III_MTYKLILNGKTLKG	O41	1548.906
III_MTYKLILNGKTLKGETTTEA	O42	2838.468
III_MTYKLILNGKTLKGETTTEAVDAATA	O43	2709.425
IV_ANDNGVDGEWTYDDATKTFTVTE	O44	2574.061
IV_ATKTFTVTE	O45	1022.491
IV_DATKTFTVTE	O46	1137.521
IV_DDATKTFTVTE	O47	1252.541
IV_DGEWTYDDATKTFTVTE	O48	2003.821
IV_DNGVDGEWTYDDATKTFTVTE	O49	2388.981
IV_EWTYDDATKTFTVTE	O50	1831.781
IV_FTVTE	O51	621.2615
IV_GEWTYDDATKTFTVTE	O52	1888.801

Continued on next page

Table 3.5 – continued from previous page

Sequence	ID	Monoisotopic Mass
IV_GVDGEWTYDDATKTFTVTE	O53	2159.911
IV_NGVDGEWTYDDATKTFTVTE	O54	2273.961
IV_QYANDNGVDGEWTYDDATKTFTVTE	O55	2865.191
IV_TFTVTE	O56	722.3115
IV_TKTFTVTE	O57	951.4515
IV_TVTE	O58	474.1915
IV_TYDDATKTFTVTE	O59	1516.651
IV_WTYDDATKTFTVTE	O60	1702.731
IV_YDDATKTFTVTE	O61	1415.611

Table 3.6: The presence or absence of peptides 8H (D.DATKTFTVTE.-) and 8I (D.ATKTFTVTE.-) in blanks, Kaolinite, and Montmorillonite samples. In order to determine that the presence of peptides was not a function of carryover, the blanks preceding and following the phyllosilicate protein samples were analyzed. The correlation score of the peptide detected Is indicated below. n.d. refers to the peptide not detected in the sample. If the Cross correlation (Xcorr) scores are above the threshold define by Smith et al. (2002a), they are in bold and highlighted in grey. Italicized sample names indicate blank samples. Samples were presented in the order they were run. R indicates replicate number (R1=replicate)

	Fragment #	
Sample	8H	8I
GB1-MpH7-wash-2	n.d.	n.d.
GB1_Montmorillonite_pH_7_24_ hours_R1	2.89	n.d.
GB1-MpH7-wash-3	n.d.	n.d.
GB1_Montmorillonite_pH_7_168 hours_R1	2.94	3.49
blank_GB1-MpH7-wash-4	n.d.	n.d.
GB1_Montmorillonite_pH_7_24 _hours_R2	**3.25**	n.d.
blank_GB1-MpH7-wash-5	n.d.	n.d.
GB1_Montmorillonite_pH_7_168 hours_R2	2.92	**3.37**
blank_GB1-MpH7-wash-6	n.d.	n.d.
blank_GB1-MpH7-wash-8	n.d.	0.54
GB1_Montmorillonite_pH_7_24 _hours_R3	**3.02**	n.d.
blank_GB1-MpH7-wash-9	n.d.	0.42
blank_GB1-MpH7-wash-10	n.d.	n.d.
GB1_Montmorillonite_pH_7_168 hourss_R3	2.87	**3.49**
blank_GB1-MpH7-wash-11	n.d.	n.d.
blank_GB1-KpH5-wash-3	n.d.	n.d.
GB1_Kaolinite_pH_5_168 hours_R1	2.92	n.d.
blank_GB1-KpH5-wash-4	n.d.	n.d.
blank_GB1-KpH5-wash-5	n.d.	n.d.
GB1_Kaolinite_pH_5_168 hours_R2	3.2	n.d.
blank_GB1-KpH5-wash-6	n.d.	0.31
blank_GB1-KpH5-wash-10	n.d.	n.d.
GB1_Kaolinite_pH_5_168 hours_R3	**3.03**	n.d.
GB1-KpH5-wash-11	n.d.	0.39

3.8.3.1 References

1. Berlett, B. S.; Stadtman, E. R., Protein oxidation in aging, disease, and oxidative stress. The Journal of Biological Chemistry 1997, 272 (33), 20313-20316.

2. Smith, R. D.; Anderson, G. A.; Lipton, M. S.; Pasa-Tolic, L.; Shen, Y.; Conrads, T. P.; Veenstra, T. D.; Udseth, H. R., An accurate mass tag strategy for quantitative and high-throughput proteome measurements. Proteomics 2002, 2 (5), 513-23.

3. Monroe, M. E.; Shaw, J. L.; Daly, D. S.; Adkins, J. N.; Smith, R. D., MASIC: a software program for fast quantitation and flexible visualization of chromatographic profiles from detected LC-MS(/MS) features. Comput Biol Chem 2008, 32 (3), 215-7.

4. Wong, C. C.; Cociorva, D.; Venable, J. D.; Xu, T.; Yates, J. R., 3rd, Comparison of different signal thresholds on data dependent sampling in Orbitrap and LTQ mass spectrometry for the identification of peptides and proteins in complex mixtures. Journal of the American Society for Mass Spectrometry 2009, 20 (8), 1405-1414.

5. Roepstorff, P.; Fohlman, J., Proposal for a Common Nomenclature for Sequence Ions in Mass-Spectra of Peptides. Biomed Mass Spectrom 1984, 11 (11), 601-601.

6. Jaitly, N.; Mayampurath, A.; Littlefield, K.; Adkins, J. N.; Anderson, G. A.; Smith, R. D., Decon2LS: An open-source software package for automated processing and visualization of high resolution mass spectrometry data. BMC Bioin-

formatics 2009, 10 (1), 87.

7. Chacon, S. S.; Garcia-Jaramillo, M.; Liu, S. Y.; Ahmed, M.; Kleber, M., Differential capacity of kaolinite and birnessite to protect surface associated proteins against thermal degradation. Soil Biol Biochem 2018, 119, 101-109.

8. Golden, D. C.; Dixon, J. B.; Chen, C. C., Ion-Exchange, Thermal Transformations, and Oxidizing Properties of Birnessite. Clays and Clay Minerals 1986, 34 (5), 511-520.

9. Weil. Ray R. Brady, N. C.; Weil, R. R., The nature and properties of soils. Fifteenth edition. ed.; Pearson: Columbus, 2016; p xvii, 1086 pages.

10. Villacis-Garcia, M.; Ugalde-Arzate, M.; Vaca-Escobar, K.; Villalobos, M.; Zanella, R.; Martinez-Villegas, N., Laboratory synthesis of goethite and ferrihydrite of controlled particle sizes. B Soc Geol Mex 2015, 67 (3), 433-446.

11. Borden, D.; Giese, R. F., Baseline studies of The Clay Minerals Society Source Clays: Cation exchange capacity measurements by the ammonia-electrode method. Clays and Clay Minerals 2001, 49 (5), 444-445.

12. Schroth, B. K.; Sposito, G., Surface charge properties of kaolinite. Clays and Clay Minerals 1997, 45 (1), 85-91.

13. Thomas, F.; Michot, L. J.; Vantelon, D.; Montarges, E.; Prelot, B.; Cruchaudet, M.; Delon, J. F., Layer charge and electrophoretic mobility of smectites. Colloid Surface A 1999, 159 (2-3), 351-358.

14. Smith, J. U.; Smith, P.; Monaghan, R.; MacDonald, A. J., When is a measured soil organic matter fraction equivalent to a model pool? European Journal of Soil Science 2002, 53 (3), 405416.

Chapter 4: Insertion of an amino acid trimer modifies the outcome of protein-mineral interactions

Stephany S. Chacon*,

Expected Co-authors: Patrick Reardon, Christopher J. Burgess, Samuel Purvine, Rosalie K Chu, Therese R Clauss, Eric Walter, David D. Myrold, Nancy Washton, Markus Kleber

4.1 Abstract

In terrestrial and aquatic ecosystems, proteins are often excreted to perform catalytic functions outside the protective cell environment. For instance, extracellular enzymes are proteins that catalyze the depolymerization of soil organic matter (SOM). These enzymes need to operate in contact with a mineral matrix that has the capacity to act as a sorbent, chemical reactant or catalyst towards proteins. It is reasonable to assume that mechanisms of microbial adaptation to environmental conditions include adjustments of the amino acid sequence such that enzyme functionality can be maintained with a minimum investment in physiological resources. To investigate the feasibility of such a hypothetical strategy, we investigated how a slight modification of the amino acid sequence could alter the susceptibility of a model protein to fragmentation by contact with soil minerals. To this end, we modified the sequence of the model protein by inserting amino acid trimers that contained either 3 negatively charged (glutamic acid; EEE), 3 positively charged (lysine, KKK) or 3 neutral amino acids (tryptophan, WWW). These mutants were allowed to interact with four soil minerals (birnessite, goethite, kaolinite, montmorillonite) at pH 5 and pH 7 for 24 hours. We used tandem mass spectrometry (MS/MS) and 1H- 15N HSQC NMR to screen the supernatants for fragmentation products. NMR did not pick up signals indicative of protein fragmentation after interaction with montmorillonite, kaolinite and goethite. Only when our modified proteins interacted with birnessite, did we see an increase in the number of fragmentation products and loss of intact protein signal. However, using a mass

spectrometric technique with inherently higher sensitivity, we found the addition of the trimer in a loop of GB1 did contribute to protein fragmentation after exposure to all minerals tested. Our results confirm the initial assumption that the susceptibility of a protein to mineral adsorption as well as its propensity to undergo fragmentation by contact with a mineral catalyst can be decidedly modified through the insertion of just three amino acids. We posit that minor alterations of the amino acid chain should be considered as a microbial strategy to adjust the functional lifetimes of extracellular enzymes to variations in the composition of the mineral matrix.

4.2 Introduction

Among the major classes of biomacromolecules synthesized by photosynthetic primary production, proteins are the ones that most frequently serve as tools, catalysts, engines or signals (Kleber and Reardon, 2017). This includes numerous tasks and functions, such as catalysis and signaling (Arnosti et al., 2013), that happen outside the controlled biochemical conditions of intracellular space. For instance, extracellular enzymes are proteins that are excreted into the soil environment to catalyze the biotic depolymerization of high molecular weight soil organic matter (SOM). This basic step is necessary because the size of molecular fragments that can be transported across the microbial cell wall for further processing is limited to about 600 Da (Weiss et al., 1991), with recent reports suggesting the existence of occasional exceptions to the rule (Reintjes et al., 2017).

Through their amphoteric nature, proteins are particularly well disposed to interact with surfaces, with consequences for their functionality that may range from total inhibition to an extended functional lifetime (Allison, 2006; Yan et al., 2010). Given the importance of extracellular enzymes in the biogeochemical cycles of C, N, and P, there is significant interest in constraining the determinants of the functional half-life of proteins in soil (Schimel et al., 2017).

Historically, the association of proteins with mineral surfaces has been understood as a protective mechanism extending the persistence of proteins in the terrestrial (Torn et al., 1997; Dungait et al., 2012; Schimel and Schaeffer, 2012) as well as in marine environments (Nagata and Kirchman, 1996). But recent work has shown that soil minerals can as well catalyze the abiotic breakdown of proteins in the absence of microbes by facilitating both hydrolytic and oxidative processes (Johnson et al., 2006; Russo et al., 2009; Chacon et al., 2018; Reardon et al., 2018). Thus, the idea that mineral-organic interactions mainly result in physiochemical protection of OM must be expanded to consider the degradative functionality of minerals. It appears that protein-mineral interactions should be seen as an interplay of protective and destructive mechanisms, with an urgent need to identify the mechanistic constraints on the latter to enable the development of a more comprehensive model of mineral protection of proteinaceous materials in soils and sediments.

For the development of a testable model of protein-mineral interactions it is useful to recollect that mineral surfaces can fundamentally behave in three ways towards a protein: they can act as sorbent (Naidja et al., 2002), catalyst (Naidja et

al., 2000) and reactant (Stone and Morgan, 1984; McBride, 1987), with some minerals such as manganese oxides being able to assume all three roles depending on reaction conditions (Chacon et al., 2018). Protein behavior towards a given surface will largely depend on the distribution of surface charges, which varies with the pH and the ionic composition of the solvent (Norde, 2008; Yu et al., 2013). There is strong evidence that both protective and degradative interactions between proteins and minerals involve an initial adsorption step (Johnson et al., 2006; Reardon et al., 2016; Chacon et al., 2018; Reardon et al., 2018). Given that extracellular enzymes are deliberately released into the environment to perform vital functions for the originating microorganism, it is fair to assume that adaptations may exist that allow a protein to benefit from mineral protection against microbial foraging while maintaining its functionality by avoiding fragmentation. The most obvious way to achieve such environmental adaption of extracellular protein would be a modification of the amino acid sequence. However, physiological economy dictates that any modifications to achieve the purpose of ensuring sufficient functional lifetime of the extracellular protein be kept simple. Also, minor, stochastic mutations are more likely to involve individual amino acid residues rather than entire domains of the protein. *The question then becomes whether small changes of the amino acid sequence will suffice to fundamentally alter protein-mineral interactions without affecting the overall structural integrity that is needed to perform the desired protein function.*

Conceptual approach

Our strategy to answer this research question was to select a model protein

with known structural resilience, induce a set of significant, yet minor changes to its amino acid chain and expose the resulting protein mutants to the four major mineral surface archetypes (negatively charged, positively charged, neutral, redox active) commonly found in terrestrial and aquatic environments. To this end, we chose the Streptococcal B1 immunoglobulin domain of Protein G (GB1), whose overall morphological structure has been shown to be tolerant of loop insertions within amino acid residues 39-40 (Li et al., 2008). At this position, we inserted short (n=3) patches of amino acids exhibiting positive, negative and neutral electrostatic functionalities. Lysine is a positively charged amino acid that should promote interaction with negatively charged mineral surfaces. Glutamic acid contains a carboxylate functional group, which is negatively charged within pH 5 to 7 and is expected to repel negative domains on mineral surfaces. Tryptophan is a hydrophobic amino acid and is expected to promote interaction with zero charged surfaces; it is also thought to be susceptible to chemical alteration when interacting with redox active mineral surfaces. We exposed the resulting GB1 variants to four minerals (kaolinite, montmorillonite, birnessite, and goethite) at pH 5 and pH 7, the latter to cover proton concentrations that occur frequently in terrestrial and aquatic environments. The creation of fragmentation products was then documented using two independent techniques, namely NMR and LC-MS/MS spectrometry.

Our experimental design allowed us to test the following hypotheses:

Hypothesis 1: Insertion of an amino acid patch with a certain charge characteristic is expected to alter the electrostatic interactions towards charged mineral

surfaces. Insertion of amino acids with positive or negative charge is expected to increase adsorption of proteins to mineral surfaces with opposite charge. Addition of neutral amino acids is expected to encourage adsorption on zero-charged minerals surfaces. To test these assumptions, we hypothesize (Null-hypothesis): *The adsorption of GB1 to mineral surfaces will not be affected by the addition of three amino acids into one of its loop regions.*

Hypothesis 2: If mineral mediated fragmentation can be altered by adding an amino acid trimer, the incidence of cleavage may vary as a function of the kind of trimer (positive, negative, neutral charge characteristic) inserted. We tested this assumption by attempting to falsify the hypothesis: *The incidence of cleavage will remain constant regardless of the specific charge characteristics of the inserted trimers.*

Hypothesis 3: Closely related to H2 is the issue of where breakage occurs in the amino acid chain. The charge characteristics of an insert may not only affect the incidence of cleavage but also the location of cleavage points. It is not known whether cleavage is more likely to occur at or close to the inserted patch, or whether there is significant cleavage at more distant positions of the amino acid chain. We investigate this question by testing the hypothesis *that the location of cleavage points will remain constant regardless of the specific charge characteristics of the inserted trimer*

Hypothesis 4: Another useful metric to assess the relevance of mineral-induced protein fragmentation is the number of different peptides that are actually generated and how this parameter changes as a function of the charge characteristics

of the insert. We investigated this question by hypothesizing: *The number of unique peptides will remain constant independent of the charge characteristics of the inserted trimer.*

4.3 Materials and Methods

To grow 3 modified versions of GB1, we purchased plasmids encoding the building blocks for our modified proteins. Plasmids were inserted into *Escherichia coli* cells and grown under conditions conducive to protein expression. To remove and purify the modified proteins, we picked plasmids that would provide a N-terminus histidine tag (His-tag). This tag serves as a handle that will attach to a Ni-column and so facilitate purification of the protein. However, putting a His-tag on the protein proxy also modifies the three amino acids at the respective terminus of the protein proxy, a fact that needs to be considered when comparing the results of this study to previous work (Reardon et al. (2016); Chacon et al., 2018). Consequently, we use the label cGB1 to distinguish the proxy used in this study from the original GB1.

4.3.1 Expression and purification of the His-tagged loop variants

The model protein chosen was the well-characterized B1 domain of Protein G (GB1, 6.2 kDa, IEP 4.5, $T_m = 85$C). We inserted patches (n=3) of identical amino acids into the third loop of the protein between residues 39 and 40. The amino

acids inserted were glutamic acid (E), lysine (K), or tryptophan (W). Sequences of the proteins are in Table S1. To engineer the modified proteins (mutants), we reverse translated the original protein and the modified protein sequences into DNA sequences. Plasmids encoding the modified GB1 proteins and a control were custom made and ordered from Genescript. The DNA sequences were codon optimized for expression in *E. coli*. The DNA sequence was inserted into pET-15b cloning vectors between the Ndel and Xhol incision sites. This cloning vector also provides ampicillin (antibiotic) resistance to the *E.coli*, thereby facilitating the growth of microbes containing our plasmids when grown in the presence of ampicillin. The pET-15b vector expresses proteins with an N-terminal histidine tag (His-tag) sequence followed by a thrombin enzyme cleavage site. The plasmids were inserted into BL21 *E.coli* cells through the heat shock transformation protocol. Details of the protocol are provided in the supplemental information.

Proteins expressed with isotopes at natural abundance were grown in Luria broth, while ^{13}C and ^{15}N label proteins used minimal media as described in Reardon et al. (2016). The new cells containing the plasmids were grown at $37C$ in media until bacteria reached the growth phase indicated by absorbance readings of 0.6 at 600 nm. Expression of the His-tag proteins was induced with 1mM of isopropyl–D-thiogalactoside (IPTG) for 6 hours. Cell pellets were lysed, and His-tag proteins were purified using a Ni column through affinity chromatography (more details in SI). His-tag proteins were then buffer exchanged into 50 mM Tris-HCl, pH 8.0 buffer to be compatible for a thrombin cleavage reaction. The Thrombin-CleanCleave Kit (cat no. RECOMT) from Sigma-Aldrich was used for

thrombin cleavage of the His-tag. The cleaved proteins were then buffer exchanged to remove any $CaCl_2$ and pass through the Ni column to remove any protein that still contained the His-tag. After cleavage of the His-tag, the proteins did contain an N-terminal made up of the amino acids GSH that was not part of the original GB1 sequence.

4.3.2 Preparation of Minerals

The phyllosilicates montmorillonite (STx-1b) and kaolinite (KGa-1) were bought from the Clay Resource Repository (Purdue University, West Lafayette) and cleaned following the procedure of Soukup et al. (2008) and dialyzed in MilliQ water. The pedogenic oxide birnessite was synthesized using the acid birnessite protocol in Reardon et al. (2016). Goethite was synthesized following the protocol of Atkinson et al. (1967). The synthesized minerals were dialyzed in MilliQ water with a 1000 molecular weight cut-off (MWCO). The minerals were freeze-dried and stored in amber bottles until further use. The properties of the minerals used are reported in the Appendix of Chapter 3 (Table 3.3).

4.3.3 Adsorption of Modified Proteins to Minerals

The cGB1 and the modified proteins were allowed to interact with kaolinite, montmorillonite, goethite, and acid birnessite. Experiments were conducted by combining the proteins and mineral at final concentrations of 0.4 mg/ml and 20 mg/ml

respectively. Sample pH was adjusted using 0.1M HCl or 0.1M NaOH at the beginning of the reaction. Thimerosal was added to the samples at a final concentration of 0.02% to discourage microbial growth and ensure any protein alterations detected were abiotic. The protein-mineral mixtures were incubated at room temperature under continuous shaking for 24 hours. The aliquots were centrifuged at 21,000 rcf for 5 minutes to separate the mineral from the peptide fragments in solution. The supernatant was filtered with 0.45 μm polyvinylidene difluoride (PVDF) nano filter vials (Thomson Instrument Company, Oceanside CA, USA) to remove particulates from the solution. The protein concentration was determined using absorbance of 280 nm using a NanoDrop. Samples were then stored until NMR and tandem MS analysis was conducted.

4.3.4 NMR Analysis of supernatant samples

Solution-state NMR experiments were performed on an 800 MHz Agilent VNMRS spectrometer equipped with a cryogenic HCN triple resonance probe. D_2O and 4,4-dimethyl-4-silapentane-1-sulfonic acid (DSS) was added to each solution state NMR sample to a final concentration of 10% v/v and 0.5 mM respectively. Data were collected at 25C ^{15}N-Heteronuclear Single Quantum Coherence (HSQC) spectra were collected with 1024 complex points in the direct (^1H) dimension and 128 complex points in the indirect (^{15}N) dimension. NMR spectra were processed using NMRPipe and visualized using NMRViewJ.

4.3.5 Tandem Mass Spectrometry Analysis

Protein-mineral supernatants were diluted to 0.05 ng per L concentration and transferred to Microsolv vials. The samples were then injected in a liquid chromatography C4 column coupled to a Velos Orbitrap mass spectrometer. Details on the LC separation and mass spectrometry analysis are the same as in the Appendix of Chapter 3, with a specific difference in that we used a C4 column for this experiment than a C18 column from Chapter 3. The data was processed the same manner as developed in Chapter 3 appendix. In short, we used SEQUEST analysis to determine the sequences of intact loop mutant proteins and peptides generated through hydrolytic cleavage. We then used the DECON routine to determine which detected analytes were within 0.5 Da of peptides cleaved through oxidation. The samples were filtered to remove any possible false readings and sequences detected in the no mineral controls.

We used the following metrics to test our hypotheses. The percent of protein adsorbed informs us how much of the added protein was adsorbed on the surface of the minerals. The NMR spectra provide us information on the adsorption of proteins to the mineral by the presence or absence of intact protein signals. NMR also provides information of whether a mineral fragmented our proteins and released the peptides to the solution. To detect fragmentation products below NMR detect limits we use tandem MS identify the number of unique peptide fragments detected and the location of fragmentation. This is used to compare the effects of variations in the type of amino acid trimer inserted in a loop of our

model protein.

4.4 Results and Discussion

4.4.1 Adsorption of GB1 to mineral surfaces was be affected by the addition of three amino acids into one of its loop regions.

The addition of a trimer in a loop region of GB1 altered adsorption to our four mineral surfaces when compared to cGB1, allowing us to reject hypothesis 1. With a single exception, the addition of a trimer increased adsorption to mineral surfaces regardless of the functional group involved (COO^-, NH_3^+ or aromatic side chain, Figure 4.1). Only one combination resulted in a decrease of protein adsorption. When considering the specific charge characteristics of the three amino acid trimers tested as patches, we found surprising results in the outcomes of protein adsorption to our four minerals.

In the case of the mutant with the negatively charged amino acid trimer (EEE-mutant), we observed an increase in adsorption in 4 out of 8 mineral/pH combinations. Increased adsorption was originally expected to occur primarily on positively charged goethite samples, but adsorption of the EEE-mutant and of the cGB1 protein to goethite turned out to be similar as per UV-VIS data (Figure 4.1). This unexpected result was accompanied by the observation of increased adsorption to the negatively charged phyllosilicates, which was particularly noticeable for montmorillonite. If we considered only electrostatic attraction or repulsion

as the mechanism responsible for protein adsorption, we could mistakenly view higher adsorption of the EEE-mutant to montmorillonite as an error. However, other mechanisms are known to be involved in protein adsorption. For instance, proteins with a net negative charge have been observed to adsorb on to negatively charged, hydrophilic surfaces (Hollmann et al., 2008; de Vos et al., 2010). Adsorption to negatively charged surfaces is thought to occur when a protein has weak internal cohesion and is likely to unfold on the surface (Norde, 2008). Thus, an explanation for the behavior of the EEE-mutant towards montmorillonite could be a weakened internal cohesion occasioned by the insertion of the EEE-trimer, allowing the EEE-mutant to unfold upon adsorption to montmorillonite .

The adsorption behavior of the KKK-mutant with its positively charged amino acid patch held several surprises as well. First, the KKK-mutant overwhelmingly exceeded the two other mutants in adsorption across all four mineral surfaces tested. Second, pronounced adsorption was observed when the KKK-mutant was interacted with the positively charged goethite, where repulsion by like charges should have taken place. Finally, adsorption of the KKK-mutant to goethite exceeded the extent of adsorption for the two other mutants, of which at least the EEE-mutant should have been predisposed for stronger adsorption. A reason for the increased adsorption of the KKK-mutant when compared to cGB1 may be because of strong bonding between the amino group found in lysine and the goethite surface. Atomic force microscopy experiments have shown that the amino functional (R-NH_3) group has a stronger binding force to the surface of goethite even during pH conditions where both subjects have a positive charge than carboxylic

acid groups or phosphate groups (Newcomb et al., 2017). There is a possibility of ligand bonding between the amino group and the surface of goethite that could explain such strong binding in AFM experiments, as observed in batch adsorption experiments of alpha-amino acids to goethite (Norn et al., 2008).

Even in the WWW-mutant with the charge-neutral amino acid patch, we saw unexpected adsorption behavior towards the mineral surfaces. In comparison to cGB1, we observed an increase in WWW-mutant adsorption to the negatively charged montmorillonite at both pH conditions and to the positvely charged goethite at pH 5. The only case in which we observed a decrease in the adsorption of our mutant proteins in relation to cGB1 was in the combination of the WWW-mutant with goethite at pH 7. As expected, the insertion of a neutral patch did increase the adsorption to kaolinite. Montmorillonite is often thought of as a phyllosilicate with permanent negative charge surfaces. But depending on surface charge densities, montmorillonite minerals may exhibit charge-neutral microsites between charged sites. Hydrophobic functional groups have been observed to adsorb on the surfaces of montmorillonite, providing evidence of these zero charged microsites (Laird and Fleming, 1999). This may explain why we observed an increase in adsorption of WWW-mutants relative to cGB1 on montmorillonite. The neutral/aromatic amino acids may adsorb on these zero charged microsites located within montmorillonite.

In 20 out of 24 cases, the somewhat less sensitive NMR method generally supported the trends apparent from the UV-VIS results. In three instances we observed only small differences between the NMR and UV-VIS results that were

not pronounced enough to be considered significant . But we did observe one case where the contrast was so strong between the two methods that it warrants to be pointed out. When the EEE-mutant was paired with goethite at pH 7, the UV-VIS method showed no difference between the adsorption of cGB1 and the adsorption of EEE-mutant, while the NMR method returns a full spectrum of cGB1 in the supernatant (suggesting little if no adsorption at all), but no spectrum at all (suggesting complete adsorption) for the EEE-mutant. At this point we do not have a robust explanation for this discrepancy.

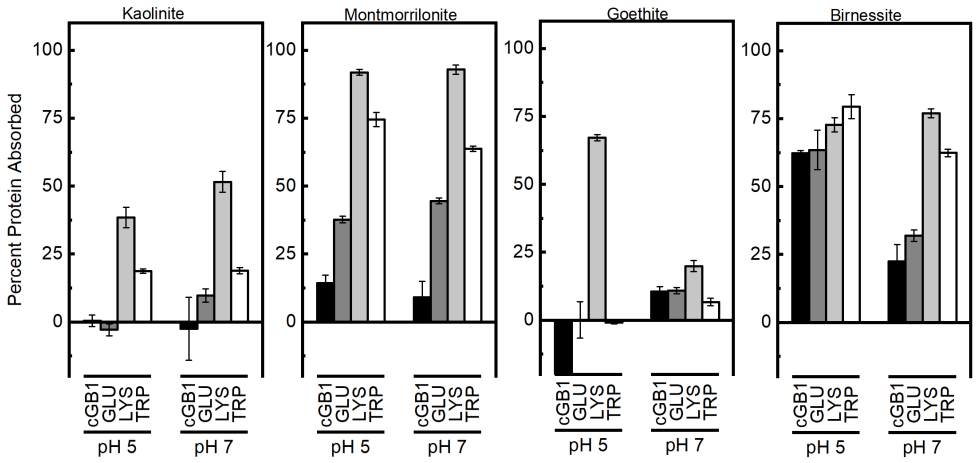

Figure 4.1: The fraction of protein adsorbed to four soil minerals at pH 5 and pH 7 (n=3). The unaltered control is cGb1, GLU stands for the EEE-mutant (- patch), LYS for the KKK-mutant (+ patch) and TRP is the WWW-mutant (neutral patch).

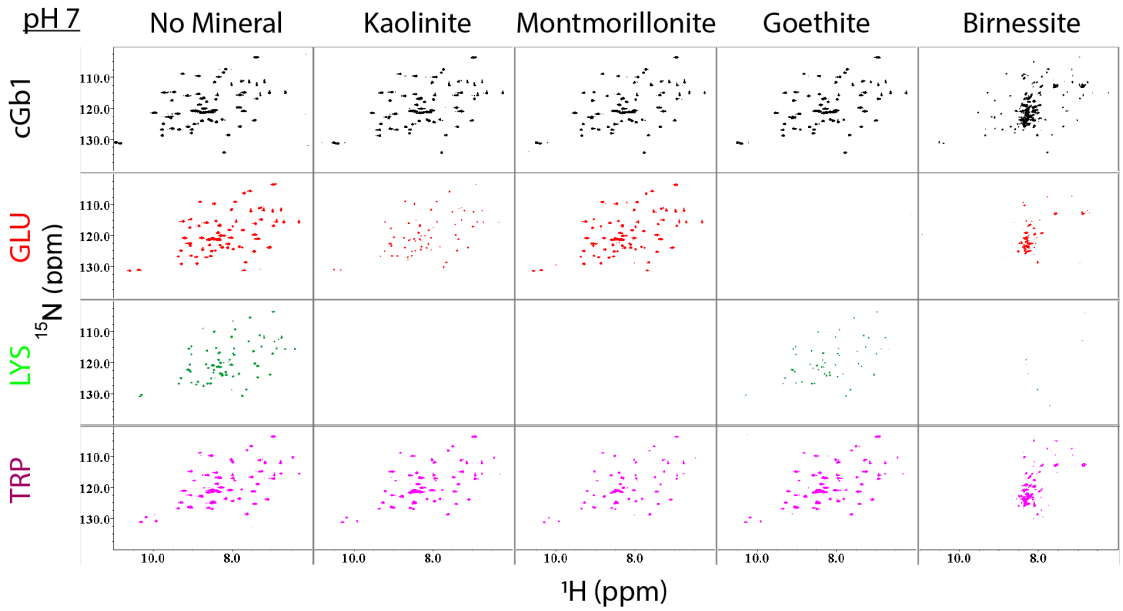

Figure 4.2: Detection of protein at pH 7 by $^{1}H - ^{15}N$ HSQC NMR analysis. Black spectra represent supernatants after reacting the respective mineral with the cGB1 control. Red spectra are from supernatants of adsorption experiments using the mutant with the EEE-trimer (GLU); green spectra are from the KKK-trimer (LYS) and Magenta is the WWW-mutant (TRP).

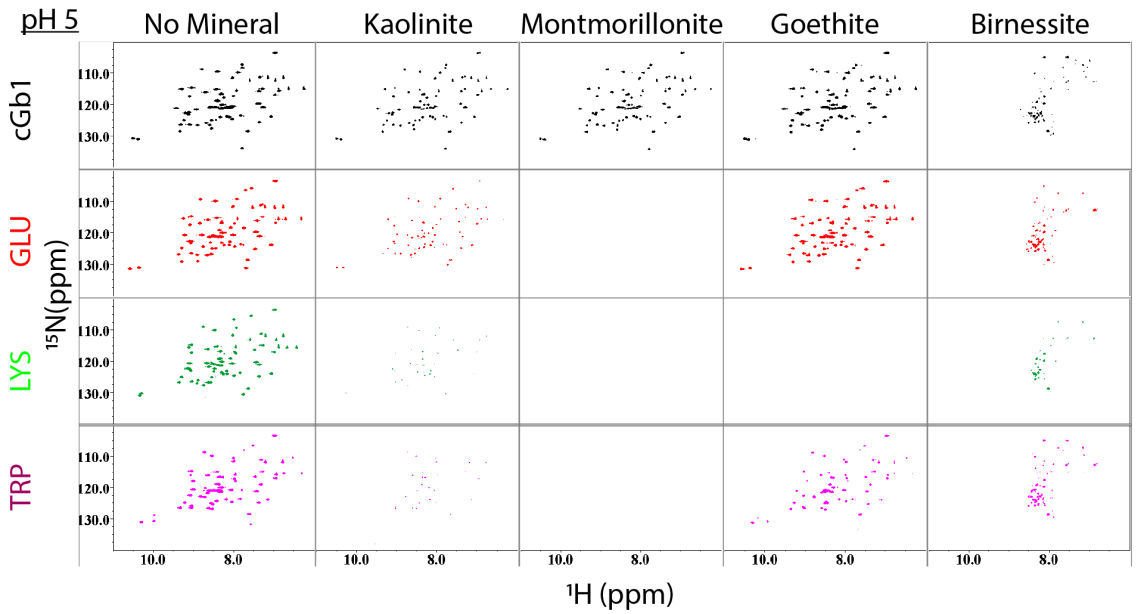

Figure 4.3: Detection of protein at pH 5 by $^{1}H-^{15}N$ HSQC NMR analysis. Black spectra represent supernatants after reacting the respective mineral with the cGB1 control. Red spectra are from supernatants of adsorption experiments using the mutant with the EEE-trimer (GLU); green spectra are from the KKK-trimer (LYS) and Magenta is the WWW-mutant (TRP).

4.4.2 Insertion of three amino acids in the loop region did change the incidence of cleavage through hydrolysis or oxidation by minerals

The incidence of cleavage (number of places where the protein backbone is cleaved) changed as a function of the insertion of an amino acid patch, this allows us to reject hypothesis 2. Owing to the data analysis techniques used (SEQUEST vs DECON routine) we were able to distinguish between cleavage through a hydrolytic mechanism and cleavage through an oxidative mechanism (Table 4.1) Compared to the cGB1 control, the incidence of cleavage by hydrolysis increased for the majority of mutant-mineral interactions with one sole exception (WWW-mutant at montmorillonite). The incidence of cleavage by oxidation, however, decreased for the majority of the mutant-mineral interactions with 3 exceptions (EEE-mutant on kaolinite, EEE-mutant on goethite, KKK-mutant on birnessite).

Changes to the thermal stability of our modified proteins could explain why the incidence of cleavage increased through mineral mediated hydrolysis. It has previously been shown that altering the sequence of a loop region within a protein changed its susceptibility to fragmentation by proteases (Ahmad et al., 2012). These authors found that some mutations to a loop region increased the thermal stability of the modified protein, while other mutations reduced thermal stability. An increase in thermal stability then led to greater resistance to proteolysis by proteases, while decreased thermal stability led to more proteolytic events. Simply mutating a loop region was sufficient in altering the stability of the entire protein.

This may explain why we see new cleavage sites through hydrolysis regardless of the amino acid trimer added. This was surprising because amino acids with aromatic side chains are considered susceptible to oxidation (Berlett and Stadtman, 1997; Stadtman and Berlett, 1997). Yet we did not detect any oxidation of the tryptophan side chains within the samples that interacted with minerals.

Table 4.1: The abundance of cleavage sites as a function of the protein and mineral surface type.

Cleavage Sites on Proteins	Kao	Mont	Goe	Birn	SUM
Hydrolysis					
cGB1	2	21	1	9	33
GLU	4	28	6	12	50
LYS	13	25	18	22	78
TRP	6	18	15	15	54
Oxidation					
cGB1	10	17	10	40	77
GLU	13	11	13	30	72
LYS	0	0	0	57	57
TRP	0	0	0	0	0

4.4.3 The location of cleavage points did not remain constant regardless of the specific charge characteristics of the inserted trimer

The addition of a trimer in a loop region did alter the locations of mineral-mediated cleavage, prompting us to reject hypothesis 3 (Figure 4.4). An alteration in cleavage locations is defined as the appearance of new cleavage sites detected in our mutant proteins that are not detected in our protein control (cGB1). A reduction in the number of cleavage sites is also considered as a change in location of fragmentation sites. We distinguish between cleavage points resulting from hydrolytic fragmentation and cleavage points resulting from oxidative fragmentation.

Compared to cGB1-mineral interactions, we saw a change in the location of cleavage sites for all the mutant-mineral combinations. When considering hydrolytic fragmentation, we find that the mutant proteins tend to be cleaved in more locations than cGB1. The observation of increased fragmentation in such cases where the charge of the mineral surface and the charge of the patch are identical is in line with the previous observation that adsorption (providing the opportunity for catalytic interaction) was stronger in those cases. This picture changes when we consider oxidative fragmentation. In this case only 5 out of 12 mutant-mineral interactions yielded new cleavage locations. The rest of the protein-mineral interactions saw a loss of oxidative cleavage sites. Specific points of interest are the fact that the WWW-mutant was never fragmented oxidatively, even when in contact with the redox-active birnessite. We further notice that

cleavage never occurred inside the added amino acid trimer, with two exceptions. These are the combinations of the EEE-mutant with birnessite and montmorillonite. Finally, we point out that the original GB1 protein that we used in our previous work (Chacon et al in review, Chapter 3) was never cleaved inside the alpha helix by phyllosilicates or goethite. However, the cGB1 with its modified N-terminus shows abundant cleavage inside the alpha helix. The susceptibility of a protein to fragment may increase if there is a greater chance of structural unfolding. Regions of proteins that are more flexible or more likely to unfold have been shown to be more susceptible to proteolytic cleavage by proteases (Fontana et al., 2004). Proteins that interact with non-polar surfaces are likely to unfold when adsorbed (Anand et al., 2010). If protein unfolding is greater for our modified proteins when interacting with kaolinite, that could explain why there is an increase in hydrolytic fragmentation. Computational models revealed that GB1 interacted with birnessite and kaolinite underwent significant conformational changes. In the case of birnessite, the model revealed unfolding within the alpha helix of GB1 (Andersen et al., 2016). If the insertion of an amino acid trimer in a loop region did increase the chances of unfolding during adsorption to mineral surfaces, it also may explain why the locations of fragmentation shifted to supposedly more stable secondary structures. But the absence of oxidation on proteins with the neutral patch (WWW-mutant) is puzzling. Biochemists have noted that aromatic amino acids are not often targets of metal-catalyzed oxidation, but more likely to be oxidized by hydroxyls generated by radiolysis (Giulivi et al., 2003). Since secondary minerals, and specifically phyllosilicates, routinely incorporate metals such as Fe in

their crystalline structure, mineral mediated oxidation may mimic metal-catalyzed oxidation mechanisms with lower reactivity. But a more plausible reason why we may not be detecting peptides from oxidative fragmentation of WWW-mutants may be that they are still adsorbed on the surface of our minerals and hence not detectable in the supernatant. Proteins are known to strongly adhere to mineral surfaces, which has been a major challenge for researchers aiming to extract proteins from soil for proteomic analysis (Keiblinger et al., 2012; Giagnoni et al., 2013). In fact, some researchers have resorted to dissolving the mineral phase in order to extract adsorbed proteins (Craig and Collins, 2000; Oonk et al., 2012)

4.4.4 The number of unique peptides did not remain constant independent of the charge characteristics of the inserted trimer.

The unique number of peptides did not remain constant between cGB1 and the mutant proteins, inducing us to reject hypothesis 4. The maximum number of unique peptides generated by oxidation is greater than the maximum number of peptides generated by hydrolysis. The KKK-mutant always has the highest number of unique peptides when the mechanism of fragmentation is hydrolysis. Higher numbers of unique peptides generated through hydrolysis in the KKK-mutant than cGB1 aligns with the observations of increased adsorption. If adsorption of the KKK-mutant increases in comparison to cGB1, then there are greater opportunities for fragmentation of the protein. A reason why we may see a greater number of unique peptides generated by oxidation than hydrolysis lies in the number of bonds that can break through oxidation. Oxidation on the alpha carbon can lead to fragmentation at the adjacent bonds (refer to Figure 3.6), generating 4 potential fragments (Berlett and Stadtman, 1997; Stadtman and Berlett, 1997). But hydrolysis typically occurs within the peptide bond, generating only two fragments.

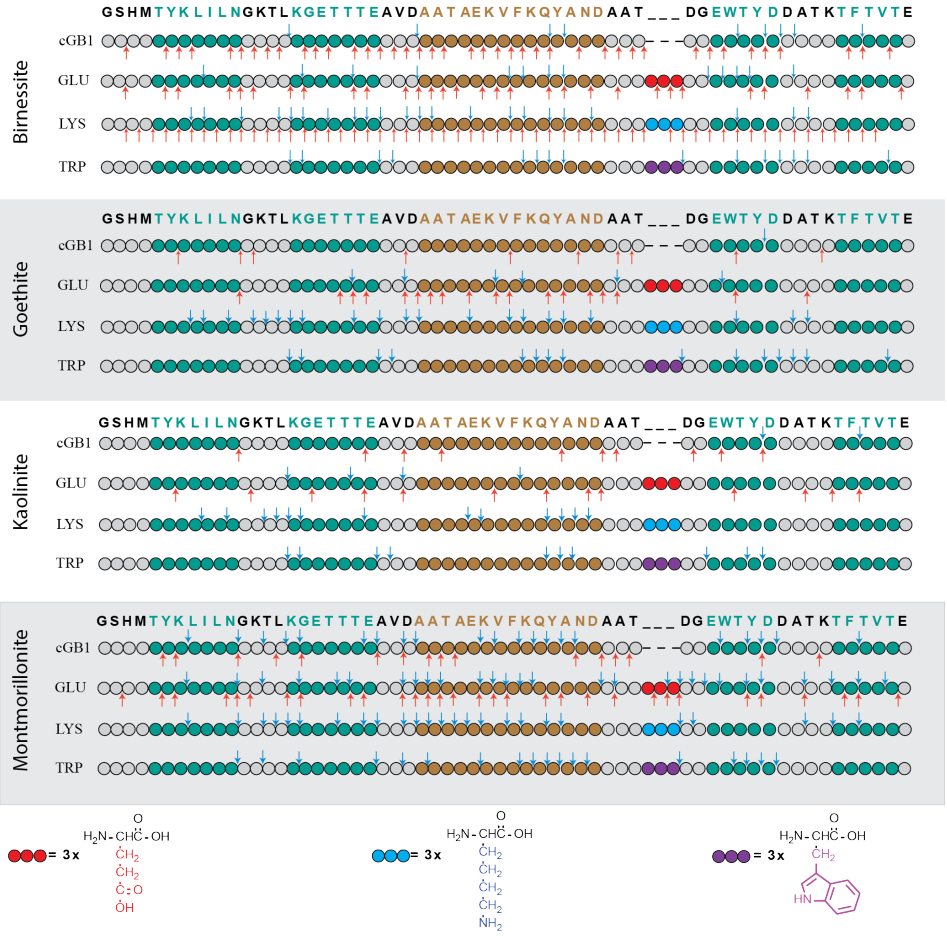

Figure 4.4: The cleavage sites on GB1 and loop mutants as a function of mineral exposure. On the left side are the minerals that proteins interacted with, next to a string of circles that represent a schematic of the loop mutants. The top row has the one letter amino acid sequence of the proteins. Letters and circles colored green designate amino acids within the beta sheets. The brown colored letters and circles designate amino acids within the alpha helix. Red circles indicate the added glutamic acid amino acids. Blue circles indicate the added lysine amino acids in the loop region. Purple circles indicate the added tryptophan amino acids. Letters and circles in black and grey designate amino acids that are unassigned or in the loop region. The blue arrows above the string of circles indicate the location of hydrolytic cleavage after interacting with a mineral on the left. The red arrows below the string of circles indicate the location of oxidative cleavage catalyzed by the mineral on the left side.

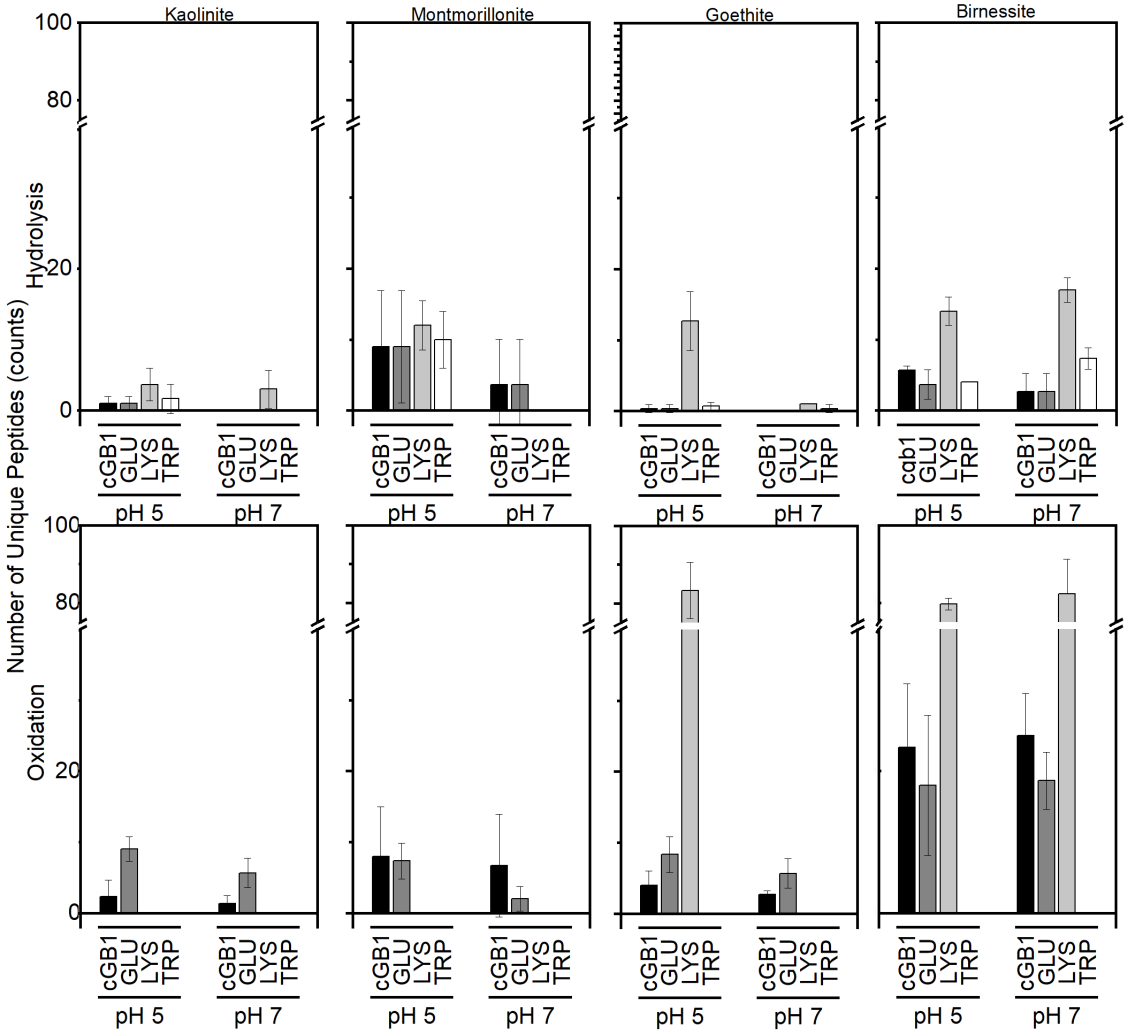

Figure 4.5: The number of unique peptides observed in the supernatant of the protein-mineral samples at pH 5 or pH 7. The error bars indicate variability expresses as standard deviation (n=3). Data are organized by cleavage mechanism, pH, protein and mineral surface type.

4.5 Conclusion

Our experimental results suggest that a protein does not require an entire domain change (20-200 amino acids (Islam et al., 1995; Xu and Nussinov, 1998)) to alter adsorption on mineral surfaces, just having 3 amino acids inserted to a loop region was sufficient. Because the extent of the alteration needed to substantially change the fate of the protein in extracellular space is so small, it becomes possible that these alterations result from stochastic mutations during protein synthesis and are subsequently manifested as protein synthesis pathways following feedback in the form of enhanced extracellular functionality.

If corroborated by further investigation, this mechanism would constitute an evolutionary pathway for soil microbes to adjust extracellular enzymes to the constraints imposed by mineral surfaces whose reactivities change slowly but continuously as a consequence of mineral weathering. The mechanism would also explain why there is such diversity of extracellular enzymes in the soil, especially with regard to enzymes that catalyze the same chemical reactions (Khalili et al., 2011). We posit that minor alterations of the amino acid chain should be considered an evolutionary strategy to adjust the functional lifetimes of extracellular enzymes to variations in the composition of the mineral matrix. We finally suggest that further investigation of the fate of modified proteins while adsorbed on the mineral surface should be undertaken to establish a more complete, mechanistic picture of how small patch modifications can alter the fold of the adsorbed protein.

4.6 Acknowledgements

This research was performed using EMSL, a DOE Office of Science User Facility sponsored by the Office of Biological and Environmental Research and located at the Pacific Northwest National Laboratory through user proposal #48364. We gratefully acknowledge the support of the EMSL MS lead scientist, Dr. Mary Lipton. S.S. Chacon would like to acknowledge support through the U.S. Department of Energy, Office of Science, Office of Workforce Development for Teachers and Scientists, Office of Science Graduate Student Research (SCGSR) program. The SCGSR program is administered by the Oak Ridge Institute for Science and Education for the DOE under contract number DENSC001466 and National Science Foundation under grant 368 no. 1456966.

4.7 References

Ahmad, S., Kumar, V., Ramanand, K.B., Rao, N.M., 2012. Probing protein stability and proteolytic resistance by loop scanning: a comprehensive mutational analysis. Protein Sci 21, 433-446.

Allison, S.D., 2006. Soil minerals and humic acids alter enzyme stability: implications for ecosystem processes. Biogeochemistry 81, 361-373.

Anand, G., Sharma, S., Dutta, A.K., Kumar, S.K., Belfort, G., 2010. Conformational Transitions of Adsorbed Proteins on Surfaces of Varying Polarity. Langmuir 26, 10803-10811.

Andersen, A., Reardon, P.N., Chacon, S.S., Qafoku, N.P., Washton, N.M.,

Kleber, M., 2016. Protein-Mineral Interactions: Molecular Dynamics Simulations Capture Importance of Variations in Mineral Surface Composition and Structure. Langmuir 32, 6194-6209.

Arnosti, C., Bell, C., Moorhead, D.L., Sinsabaugh, R.L., Steen, A.D., Stromberger, M., Wallenstein, M., Weintraub, M.N., 2013. Extracellular enzymes in terrestrial, freshwater, and marine environments: perspectives on system variability and common research needs. Biogeochemistry 117, 5-21.

Atkinson, R.J., Posner, A.M., Quirk, J.P., 1967. Adsorption of potential-determining ions at the ferric oxide-aqueous electrolyte interface. The Journal of Physical Chemistry 71, 550-558. Berlett, B.S., Stadtman, E.R., 1997. Protein oxidation in aging, disease, and oxidative stress. Journal of Biological Chemistry 272, 20313-20316.

Chacon, S.S., Garcia-Jaramillo, M., Liu, S.Y., Ahmed, M., Kleber, M., 2018. Differential capacity of kaolinite and birnessite to protect surface associated proteins against thermal degradation. Soil Biology and Biochemistry 119, 101-109.

Craig, O.E., Collins, M.J., 2000. An improved method for the immunological detection of mineral bound protein using hydrofluoric acid and direct capture. Journal of immunological methods 236, 89-97.

de Vos, W.M., Leermakers, F.A.M., de Keizer, A., Stuart, M.A., Kleijn, M.J., 2010. Field Theoretical Analysis of Driving Forces for the Uptake of Proteins by Like-Charged Polyelectrolyte Brushes: Effects of Charge Regulation and Patchiness. Langmuir 26, 249-259.

Dungait, J.A.J., Hopkins, D.W., Gregory, A.S., Whitmore, A.P., 2012. Soil or-

ganic matter turnover is governed by accessibility not recalcitrance. Global Change Biology 18, 1781-1796.

Fontana, A., de Laureto, P.P., Spolaore, B., Frare, E., Picotti, P., Zambonin, M., 2004. Probing protein structure by limited proteolysis. Acta Biochimica Polonica 51, 299-321.

Giagnoni, L., Migliaccio, A., Nannipieri, P., Renella, G., 2013. High montmorillonite content may affect soil microbial proteomic analysis. Applied Soil Ecology 72, 203-206.

Giulivi, C., Traaseth, N.J., Davies, K.J., 2003. Tyrosine oxidation products: analysis and biological relevance. Amino Acids 25, 227-232.

Hollmann, O., Steitz, R., Czeslik, C., 2008. Structure and dynamics of -lactalbumin adsorbed at a charged brush interface. Physical Chemistry Chemical Physics 10, 1448-1456.

Islam, S.A., Luo, J.C., Sternberg, M.J.E., 1995. Identification and Analysis of Domains in Proteins. Protein Engineering 8, 513-525.

Johnson, C.J., Phillips, K.E., Schramm, P.T., McKenzie, D., Aiken, J.M., Pedersen, J.A., 2006. Prions adhere to soil minerals and remain infectious. PLoS Pathog 2, e32.

Keiblinger, K.M., Wilhartitz, I.C., Schneider, T., Roschitzki, B., Schmid, E., Eberl, L., Riedel, K., Zechmeister-Boltenstern, S., 2012. Soil metaproteomics - Comparative evaluation of protein extraction protocols. Soil Biology and Biochemistry 54, 14-24.

Khalili, B., Nourbakhsh, F., Nili, N., Khademi, H., Sharifnabi, B., 2011. Di-

versity of soil cellulase isoenzymes is associated with soil cellulase kinetic and thermodynamic parameters. Soil Biology and Biochemistry 43, 1639-1648.

Kleber, M., Reardon, P., 2017. Biopolymers and Macromolecules, In: White, W.M. (Ed.), Encyclopedia of Geochemistry. Springer International Publishing, Cham, pp. 1-5.

Laird, D.A., Fleming, P.D., 1999. Mechanisms for adsorption of organic bases on hydrated smectite surfaces. Environmental Toxicology and Chemistry 18, 1668-1672.

Li, H., Wang, H.-C., Cao, Y., Sharma, D., Wang, M., 2008. Configurational entropy modulates the mechanical stability of protein GB1. Journal of molecular biology 379, 871-880.

McBride, M.B., 1987. Adsorption and Oxidation of Phenolic Compounds by Iron and Manganese Oxides1. Soil Science Society of America Journal 51, 1466.

Nagata, T., Kirchman, D.L., 1996. Bacterial degradation of protein adsorbed to model submicron particles in seawater. Marine Ecology Progress Series 132, 241-248.

Naidja, A., Huang, P.M., Bollag, J.M., 2000. Enzyme-clay interactions and their impact on transformations of natural and anthropogenic organic compounds in soil. J Environ Qual 29, 677-691.

Naidja, A., Liu, C., Huang, P.M., 2002. Formation of protein-birnessite complex: XRD, FTIR, and AFM analysis. Journal of Colloid and Interface Science 251, 46-56.

Newcomb, C.J., Qafoku, N.P., Grate, J.W., Bailey, V.L., De Yoreo, J.J., 2017.

Developing a molecular picture of soil organic matter-mineral interactions by quantifying organo-mineral binding. Nat Commun 8, 396.

Norde, W., 2008. My voyage of discovery to proteins in flatland ...and beyond. Colloids and Surfaces B: Biointerfaces 61, 1-9.

Norn, K., Loring, J.S., Persson, P., 2008. Adsorption of alpha amino acids at the water/goethite interface. Journal of Colloid and Interface Science 319, 416-428.

Oonk, S., Cappellini, E., Collins, M.J., 2012. Soil proteomics: An assessment of its potential for archaeological site interpretation. Organic Geochemistry 50.

Reardon, P.N., Chacon, S.S., Walter, E.D., Bowden, M.E., Washton, N.M., Kleber, M., 2016. Abiotic Protein Fragmentation by Manganese Oxide: Implications for a Mechanism to Supply Soil Biota with Oligopeptides. Environmental Science and Technology 50, 3486-3493.

Reardon, P.N., Walter, E.D., Marean-Reardon, C.L., Lawrence, C.W., Kleber, M., Washton, N.M., 2018. Carbohydrates protect protein against abiotic fragmentation by soil minerals. Sci Rep 8, 813.

Reintjes, G., Arnosti, C., Fuchs, B.M., Amann, R., 2017. An alternative polysaccharide uptake mechanism of marine bacteria. ISME J 11, 1640-1650.

Russo, F., Johnson, C.J., Johnson, C.J., McKenzie, D., Aiken, J.M., Pedersen, J.A., 2009. Pathogenic prion protein is degraded by a manganese oxide mineral found in soils. Journal of General Virology 90, 275-280.

Schimel, J., Becerra, C.A., Blankinship, J., 2017. Estimating decay dynamics for enzyme activities in soils from different ecosystems. Soil Biology and Biochemistry 114, 5-11.

Schimel, J., Schaeffer, S., 2012. Microbial control over carbon cycling in soil. Front Microbiol 3, 348.

Soukup, D.A., Buck, B.J., Harris, W., 2008. Preparing Soils for Mineralogical Analyses, In: Ulery, A.L., Richard Drees, L. (Eds.), Methods of Soil Analysis Part 5 Mineralogical Methods. Soil Science Society of America, Madison, WI.

Stadtman, E.R., Berlett, B.S., 1997. Reactive oxygen-mediated protein oxidation in aging and disease. Chemical research in toxicology 10, 485-494.

Stone, A.T., Morgan, J.J., 1984. Reduction and dissolution of manganese(III) and manganese(IV) oxides by organics: 2. Survey of the reactivity of organics. Environmental Science and Technology 18, 617-624.

Torn, M.S., Trumbore, S.E., Chadwick, O.A., Vitousek, P.M., Hendricks, D.M., 1997. Mineral control of soil organic carbon storage and turnover. Nature 389, 170-173.

Weiss, M.S., Abele, U., Weckesser, J., Welte, W., Schiltz, E., Schulz, G.E., 1991. Molecular architecture and electrostatic properties of a bacterial porin. Science 254, 1627-1630.

Xu, D., Nussinov, R., 1998. Favorable domain size in proteins. Fold Des 3, 11-17.

Yan, J., Pan, G., Li, L., Quan, G., Ding, C., Luo, A., 2010. Adsorption, immobilization, and activity of beta-glucosidase on different soil colloids. Journal of Colloid and Interface Science 348, 565-570.

Yu, W.H., Li, N., Tong, D.S., Zhou, C.H., Lin, C.X., Xu, C.Y., 2013. Adsorption of proteins and nucleic acids on clay minerals and their interactions: A

review. Applied Clay Science 80-81, 443-452.

4.8 Appendix Chapter 4

4.8.1 Transformation of E.coli cells with Plasmid DNA encoding Loop Mutants

Plasmids encoding histidine-tagged proteins were ordered from Genescript and stored at -20C until needed. The competent BL21 *E.coli* cells were taken from the -80C freezer and thawed on ice along with the plasmids. The four plasmids were diluted to a concentration of 100ng of DNA L^{-1}. One L of plasmid solution was added to aliquots of competent cells. After waiting for five minutes, the cells were placed on a heating block at 80C for 35 seconds (heat shock). The cells were immediately placed on ice and 250 L of Expression Recovery Medium (Sigma Aldrich) was added to each sample. The cells were then incubated at 37C for one hour. After incubation, aliquots of cells were transferred on sterile ampicillin agar plates and spread evenly. The plates were incubated at 37C overnight.

Colonies from transformed cells were plucked and used to inoculate sterile Luria broth media containing ampicillin. The cultures were grown at 37C until optical densities (at 600 nm) reached 0.6. Aliquots of cultures were vortexed and 800 L of cell solutions was mixed with 200 L of sterile 80% glycerol. The glycerol cell stocks were mixed well and stored at -80C for future use to inoculate media.

4.8.2 Nickel (Ni-NTA) affinity chromatography purification

Histidine-tagged proteins were purified using affinity chromatography with a 5mL HisTrap HP Ni column (GE Healthcare cat no. 17524801) attached to an KTA Fast protein liquid chromatography (FPLC). The Ni column was equilibrated by passing 5 column volumes (25 mL) of wash/binding buffer A1 (50 mM NaPO4, 20 mM Imidazole, 300 mM NaCl pH 8.0) through the column at a flow rate of 1mL min-1. The lysed cells containing histag proteins were injected into an KTA FPLC and loaded onto the Ni column with A1 buffer. The histag proteins were bound to the column and 10 column volumes of A1 buffer were flowed through. This cleaned the cellular debris that did not bind to the Ni column. In order to disrupt the affinity of the Histag proteins to the Ni column, eluding buffer B1(50 mM NaPO4, 250 mM Imidazole, 300 mM NaCl pH 8.0) was passed through the column. The increase concentration of imidazole interfered with the histags affinity to the Ni column, and allowed for the elution of pure histag protein. The fractions containing the histag protein were concentrated with Vivaspin 20 centrifugal concentrators, this also allowed to buffer exchange solution to prepare the proteins for thrombin cleavage reaction.

4.8.3 Thrombin Cleavage Reaction

Purified histidine-tagged proteins were buffer exchanged with 50 mM Tris-HCl, pH 8.0 to be compatible with thrombin enzyme reaction. 400 L aliquots of Thrombin immobilized on agarose beads was transferred to a conical tube for each protein.

The thrombin agarose beads were washed by adding 2.0 mL of 50 mM Tris-HCl, pH 8.0 and the tube was inverted to gently mix the beads. The thrombin agarose beads were centrifuged at 500 g rcf for five minutes, and the supernatant was removed. The washing step was repeated a second time, and the supernatant was discarded. The 2 mL of histidine tag proteins solution was added to the thrombin agarose conical tubes at a concentration of 2 mg mL^{-1}. The sample was diluted to a final volume of 4.0 mL and allowed to react for 4 hours on a rotary shaker at 25 rotations per minute. Once done, the samples were centrifuged for five minutes at 500 g rcf. The supernatant was transferred to a new conical tube. An additional 1 mL of 50 mM Tris-HCl was added to the thrombin agarose beads and gently mixed to retrieve any leftover protein. The samples were centrifuged once more, and the cleaved proteins were transferred. The cleaved proteins were buffer exchanged with Ni-NTA wash buffer (50 mM NaPO4, 20 mM Imidazole, 300 mM NaCl pH 8.0) and run through the Ni column. This was done to bind all proteins still containing a histidine tag to the Ni column and collect the cleaved proteins in the wash through fractions. The final protein samples with the cleaved histidine tag were buffer exchanged into solution conditions chosen for adsorption.

Table 4.2: The sequence of the GB1 and the GB1 Loop Mutant proteins. The proteins expressed by our transformed E. coli were proteins with a histidine tag, shown in blue. The His-tag was at the beginning of the control and the loop mutants (indicated by the asterisk *). After the reaction with the thrombin enzyme, the resulting proteins still contain GSH from the tag.

Protein	Sequence	Isoelectric Point (pI)	Molecular Weight natural abundance	Molar Extinction coefficient ($M^{-1}cm^{-1}$)
Original Sequence				
GB1	MTYKLILNGKTLKGETTTEAVDAATAEKVFKQYANDNGVDGEWTYDDATKTFTVTE	4.46	6195.8	9970
Histidine-Tagged control and Loop Mutants				
His Tag*	HHHHHHSSGLVPRGSH			
His-Gb1	*MTYKLILNGKTLKGETTTEAVDAATAEKVFKQYANDNGVDGEWTYDDATKTFTVTE	6.13	7996.6	9970
His-GLU	*MTYKLILNGKTLKGETTTEAVDAATAEKVFKQYANDNGVEEEDGEWTYDDATKTFTVTE	5.52	8384	9970
His-LYS	*MTYKLILNGKTLKGETTTEAVDAATAEKVFKQYANDNGVKKKDGEWTYDDATKTFTVTE	7.24	8381.2	9970
His-TRP	*MTYKLILNGKTLKGETTTEAVDAATAEKVFKQYANDNGVWWWDGEWTYDDATKTFTVTE	6.13	8555.3	26470
Gb1 control protein and Loop Mutants after thrombin reaction				
cGB1	GSHMTYKLILNGKTLKGETTTEAVDAATAEKVFKQYANDNGVDGEWTYDDATKTFTVTE	4.64	6477	9970
GLU	GSHMTYKLILNGKTLKGETTTEAVDAATAEKVFKQYANDNGVEEEDGEWTYDDATKTFTVTE	4.38	6864.4	9970
LYS	GSHMTYKLILNGKTLKGETTTEAVDAATAEKVFKQYANDNGVKKKDGEWTYDDATKTFTVTE	5.72	6861.5	9970
TRP	GSHMTYKLILNGKTLKGETTTEAVDAATAEKVFKQYANDNGVWWWDGEWTYDDATKTFTVTE	4.64	7035.6	26470

4.8.4 Time series of Modified Proteins interacting with Birnessite

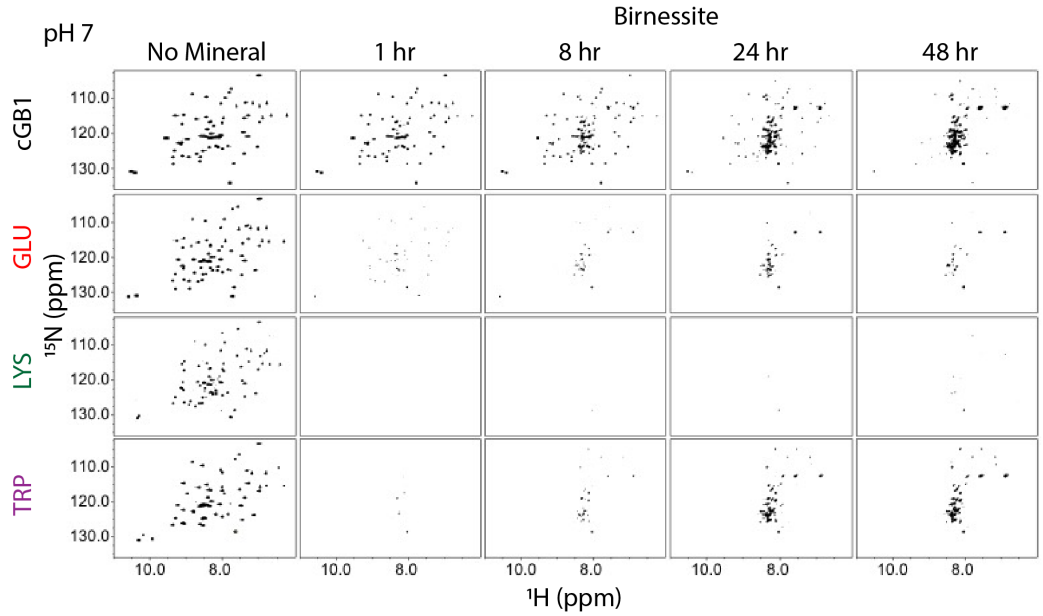

Figure 4.6: The release of peptides from Gb1 control and Gb1 modified proteins varies after interacting with birnessite at pH 7. The $^{1}H-^{15}N$ HSQC NMR spectra indicate the release of peptides into the supernatant. cGb1 indicates the spectra are from Gb1 control. GLU indicates spectra from Gb1 Glutamic acid variant. LYS indicates spectra are from Gb1 lysine mutant. TRP indicates spectra are from Gb1 tryptophan mutant.

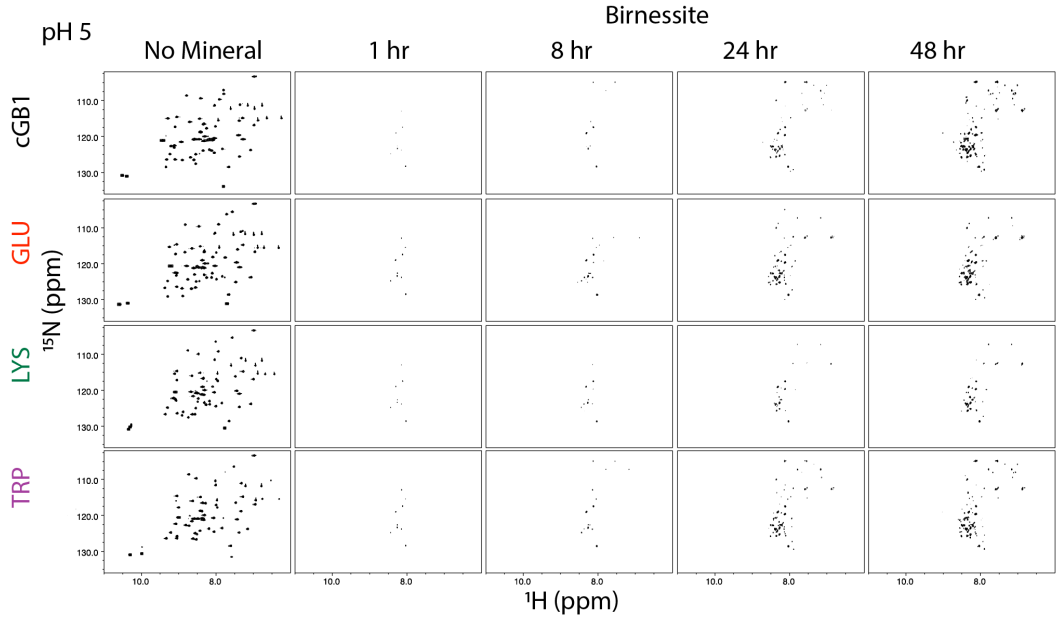

Figure 4.7: The release of peptides from Gb1 control and Gb1 modified proteins varies after interacting with birnessite at pH 5. The $^{1}H-^{15}N$ HSQC NMR spectra indicate the release of peptides into the supernatant. cGb1 indicates the spectra are from Gb1 control. GLU indicates spectra from Gb1 Glutamic acid variant. LYS indicates spectra are from Gb1 lysine mutant. TRP indicates spectra are from Gb1 tryptophan mutant.

Chapter 5: Conclusion

The focus of this dissertation was determining if minerals are capable of chemically modifying or breaking down proteins. My goal was to improve the understanding of how mineral interactions can alter enzyme function and SOM turnover. My objectives were determining under what conditions minerals fragment proteins and the mechanisms responsible for them.

The first chapter revealed that minerals have differential capacities to fragment proteins under dry conditions while experiencing an energy gradient. Thus, we cannot generalize enzyme-mineral interaction outcomes to only result in immobilization. I found that the fate of a protein is tied to the type of mineral to which it adsorbs. Birnessite switches from sorbent to chemical reactant upon reaching energies similar to those detected in fire lines from wildfires. Kaolinite had a much higher energy threshold than birnessite and stayed a sorbent within the energies we applied. My results indicate that proteins immobilized within a mineral matrix containing manganese oxides are more likely to have shorter lifespans than proteins immobilized on kaolinite if the soils experience wildfires. This may be balanced by the increased capacity for "fire activated" soils to react towards organic compounds and could explain the increase in the availability of organic carbon as shown by the higher respiration rates observed in soils after a wildfire (Rutigliano et al., 2002).

In my second research chapter, I found that phyllosilicates have the capacity

hydrolyze proteins, but the reaction takes several days to release peptides to the supernatant. I also detected analytes in the supernatant similar to the fragmentation products generated by oxidative cleavage of the protein backbone. This indicates that mineral mediated proteolysis mechanisms include hydrolysis and oxidation. The locations of mineral mediated cleavage of my model protein also aligned with regions that have been observed as susceptible to protease cleavage. Thus, structural locations within enzymes that are likely to be cleaved by proteases may also be regions that are susceptible to mineral fragmentation. My results establish the need to expand the view of mineral surfaces acting merely as sorbents (Gianfreda et al., 2011) to include their degradative functionality towards proteins (Figure 5.1). My observations provide an incentive to generate databases that can identify oxidation fragments of proteins extracted from soil. It also establishes a need to include mineral-mediated proteolysis as a post-modification option during proteomic analysis of soils extracts.

The third research chapter revealed that adding an amino acid trimer to a loop region of a protein was sufficient in altering adsorption and the degree of fragmentation after interacting with soil minerals. I found that in the majority of the cases, protein adsorption seems to increase, regardless of the functionality of the trimer inserted in the loop region. In general, much of the modified proteins remained intact when interacting with the phyllosilicates or the iron oxide. But modification of a loop region with any amino acid trimer enhanced the susceptibility of the protein to fragmentation by the manganese oxide. I observed low concentrations of peptide fragments, where the addition of a trimer shifted the proportion of hydrolysis and

oxidation of the protein backbones and the locations of the cleavage by minerals. These observations show that small mutations that alter protein properties could change the outcome of protein-mineral interactions, providing evolutionary pressure towards microbes in designing extracellular enzymes that can stay functional during mineral interactions.

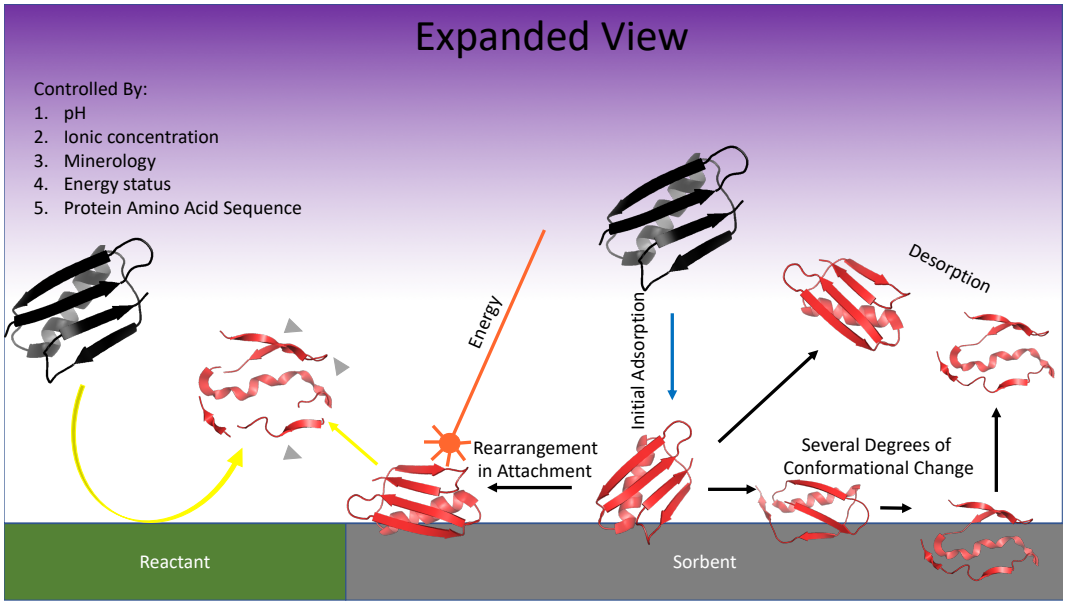

Figure 5.1: An expanded view of the outcomes of protein-mineral interactions with our experimental observations. We expanded to include a protein (black) interacting with a mineral surface that is a reactant. This can generate and release peptides into the soil solution. A protein already attached to a surface of a mineral that experiences a large energy input, such as energies experienced in wildfires, can break the protein and the mineral apart.These interactions are controlled by pH, ionic concentration, mineralogy, energy status, and protein properties, such as amino acid sequence.

Overall, my research shows that minerals are not just agents for protection or immobilization of extracellular enzymes but can be active agents in the degrada-

tion of those enzymes too. The duality of mineral interactions towards enzymes and SOM presents future challenges in determining how these associations affect turnover of SOM. However, recent research shows that incorporating greater details of mineralogy into models (short-range order minerals, Al, Fe oxides) can increase the predictability of SOM content (Rasmussen et al., 2018). Incorporating the reactive nature of mineral surfaces towards extracellular enzymes and SOM may be an additional step to improve the predictive power of SOM turnover models.

Chapter 6: Bibliography For Introduction and Conclusion

Arai, T., Norde, W., 1990. The Behavior of Some Model Proteins at Solid Liquid Interfaces .1. Adsorption from Single Protein Solutions. Colloids and Surfaces 51, 1-15.

Baron, M.H., Revault, M., Servagent-Noinville, S., Abadie, J., Quiquampoix, H., 1999. Chymotrypsin Adsorption on Montmorillonite: Enzymatic Activity and Kinetic FTIR Structural Analysis. J Colloid Interface Sci 214, 319-332.

Barrett, K.A., McBride, M.B., 2005. Oxidative degradation of glyphosate and aminomethylphosphonate by manganese oxide. Environ Sci Technol 39, 9223-9228.

Chang Chien, S.W., Chen, H.L., Wang, M.C., Seshaiah, K., 2009. Oxidative degradation and associated mineralization of catechol, hydroquinone and resorcinol catalyzed by birnessite. Chemosphere 74, 1125-1133.

Chorover, J., Amistadi, M.K., 2001. Reaction of forest floor organic matter at goethite, birnessite and smectite surfaces. Geochimica Et Cosmochimica Acta 65, 95-109.

Conant, R.T., Ryan, M.G., Agren, G.I., Birge, H.E., Davidson, E.A., Eliasson, P.E., Evans, S.E., Frey, S.D., Giardina, C.P., Hopkins, F.M., Hyvonen, R., Kirschbaum, M.U.F., Lavallee, J.M., Leifeld, J., Parton, W.J., Steinweg, J.M., Wallenstein, M.D., Wetterstedt, J.A.M., Bradford, M.A., 2011. Temperature and soil organic matter decomposition rates - synthesis of current knowledge and a way

forward. Global Change Biology 17, 3392-3404.

Craig, O.E., Collins, M.J., 2002. The removal of protein from mineral surfaces: Implications for residue analysis of archaeological materials. Journal of Archaeological Science 29, 1077-1082.

Dec, J., Haider, K., Bollag, J.M., 2001. Decarboxylation and demethoxylation of naturally occurring phenols during coupling reactions and polymerization. Soil Science 166, 660-671.

Dec, J., Haider, K., Bollag, J.M., 2003. Release of substituents from phenolic compounds during oxidative coupling reactions. Chemosphere 52, 549-556. Dungait, J.A.J., Hopkins, D.W., Gregory, A.S., Whitmore, A.P., 2012. Soil organic matter turnover is governed by accessibility not recalcitrance. Global Change Biology 18, 1781-1796.

Filip, Z., Flaig, W., Rietz, E., 1977. Oxidation of some phenolic substances as influenced by clay minerals. Symposium on Soil Organic Matter Studies 2, 91-96.

Gianfreda, L., Rao, M.A., Mora, M., 2011. Enzymatic Activity as Influenced by Soil Mineral and Humic Colloids, In: Huang, P.M., Li, Y., Sumner, M.E. (Eds.), Handbook of soil sciences: resource management and environmental impacts, 2nd ed. CRC press, pp. 5-5.

Li, H., Lee, L.S., Schulze, D.G., Guest, C.A., 2003. Role of soil manganese in the oxidation of aromatic amines. Environ Sci Technol 37, 2686-2693.

Marafatto, F.F., Strader, M.L., Gonzalez-Holguera, J., Schwartzberg, A., Gilbert, B., Pena, J., 2015. Rate and mechanism of the photoreduction of birnessite (MnO2) nanosheets. Proc Natl Acad Sci U S A 112, 4600-4605.

Mario, V., Manuel, C.-C., Richard, G., Lpez-Santiago, N.R., Jimmy, A.M., 2014. The influence of particle size and structure on the sorption and oxidation behaviour of birnessite: II. Adsorption and oxidation of four polycyclic aromatic hydrocarbons. Environmental Chemistry 11.

McBride, M.B., 1989. Oxidation of 1, 2-and 1, 4-dihydroxybenzene by birnessite in acidic aqueous suspension. Clays and Clay Minerals 37, 479-486.

McKenzie, R.M., 1971. The synthesis of birnessite, cryptomelane, and some other oxides and hydroxides of manganese. Mineral. Mag.

Norde, W., Giacomelli, C.E., 2000. BSA structural changes during homomolecular exchange between the adsorbed and the dissolved states. Journal of biotechnology 79, 259-268.

Quiquampoix, H., Ratcliffe, R.G., 1992. A 31P NMR study of the adsorption of bovine serum albumin on montmorillonite using phosphate and the paramagnetic cation Mn2+: modification of conformation with pH. Journal of Colloid and Interface Science 148, 343-352.

Rao, M.A., Iamarino, G., Scelza, R., Russo, F., Gianfreda, L., 2008. Oxidative transformation of aqueous phenolic mixtures by birnessite-mediated catalysis. Science of The Total Environment 407, 438-446.

Rasmussen, C., Heckman, K., Wieder, W.R., Keiluweit, M., Lawrence, C.R., Berhe, A.A., Blankinship, J.C., Crow, S.E., Druhan, J.L., Pries, C.E.H., Marin-Spiotta, E., Plante, A.F., Schadel, C., Schimel, J.P., Sierra, C.A., Thompson, A., Wagai, R., 2018. Beyond clay: towards an improved set of variables for predicting soil organic matter content. Biogeochemistry 137, 297-306.

Russo, F., Johnson, C.J., Johnson, C.J., McKenzie, D., Aiken, J.M., Pedersen, J.A., 2009. Pathogenic prion protein is degraded by a manganese oxide mineral found in soils. Journal of General Virology 90, 275-280.

Rutigliano, F.A., Fierro, A.R., De Pascale, R.A., De Marco, A., Virzo De Santo, A., 2002. Role of fire on soil organic matter turnover and microbial activity in a mediterranean burned area, In: Violante, A., Huang, P.M., Bollag, J.M., Gianfreda, L. (Eds.), Developments in Soil Science. Elsevier, pp. 205-215.

Schmidt, M.W., Torn, M.S., Abiven, S., Dittmar, T., Guggenberger, G., Janssens, I.A., Kleber, M., Kgel-Knabner, I., Lehmann, J., Manning, D.A., Nannipieri, P., Rasse, D.P., Weiner, S., Trumbore, S.E., 2011. Persistence of soil organic matter as an ecosystem property. Nature 478, 49-56.

Servagent-Noinville, S., Revault, M., Quiquampoix, H., Baron, M., 2000. Conformational Changes of Bovine Serum Albumin Induced by Adsorption on Different Clay Surfaces: FTIR Analysis. J Colloid Interface Sci 221, 273-283.

Sinsabaugh, R.L., Antibus, R.K., Linkins, A.E., 1991. An enzymic approach to the analysis of microbial activity during plant litter decomposition. Agriculture, Ecosystems & Environment 34, 43-54.

Stone, A.T., 1987. Reductive Dissolution of Manganese(III/Iv) Oxides by Substituted Phenols. Environmental Science and Technology 21, 979-988. Thompson, T.D., Moll, W.F., 1973. Oxidative Power of Smectites Measured by Hydroquinone. Clays and Clay Minerals 21, 337-350.

Torn, M.S., Kleber, M., Zavaleta, E.S., Zhu, B., Field, C.B., Trumbore, S.E., 2013. A dual isotope approach to isolate soil carbon pools of different turnover

times. Biogeosciences 10, 8067-8081.

van Loosdrecht, M.C., Lyklema, J., Norde, W., Zehnder, A.J., 1990. Influence of interfaces on microbial activity. Microbiological Reviews 54, 75-87.

Zhang, H., Chen, W.R., Huang, C.H., 2008. Kinetic modeling of oxidation of antibacterial agents by manganese oxide. Environ Sci Technol 42, 5548-5554.